LOW TEMPERATURE OXIDATION OF CARBON MONOXIDE USING

MICROFIBROUS ENTRAPED CATALYSTS FOR

FIRE ESCAPE MASK APPLICATION

Except where reference is made to the work of others, the work described in this dissertation is my own or was done in collaboration with my advisory committee. *This dissertation does not include proprietarv or classified information.*

Mukund R Karanjikar

Certificate of Approval:

Christopher B. Roberts
Professor
Chemical Engineering

Bruce J. Tatarchuk, Chair
Professor
Chemical Engineering

James A. Guin
Professor
Chemical Engineering

Daniel K. Harris
Associate Professor
Mechanical Engineering

Stephen L. McFarland
Acting Dean
Graduate School

LOW TEMPERATURE OXIDATION OF CARBON MONOXIDE USING

MICROFIBROUS ENTRAPPED CATALYSTS FOR

FIRE ESCAPE MASK APPLICATION

Mukund R. Karanjikar

A Dissertation

Submitted to

the Graduate Faculty of

Auburn University

in Partial Fulfillment of the

Requirements for the

Degree of

Doctor of Philosophy

Auburn, Alabama

August 8, 2005

VITA

Mukund R Karanjikar, son of Ramchandra Karanjikar and Mangal Karanjikar was born on April 19, 1978. He received his secondary school certificate degree in March 1993 and higher secondary school certificate degree in March 1995. In August 1995 he entered University of Mumbai (formerly University of Bombay) and graduated with a Bachelor of Chemical Engineering in May 1999. In June 1999, he started working for Rallis India Ltd., an agrochemical manufacturing company for a span of two years. In August 2001, he entered Graduate School of Auburn University, Auburn AL for Doctorate of Philosophy.

LOW TEMPERATURE OXIDATION OF CARBON MONOXIDE USING

MICROFIBROUS ENTRAPPED CATALYSTS FOR

FIRE ESCAPE MASK APPLICATION

Mukund R Karanjikar

Doctor of Philosophy, August 8, 2005

(B.Chem. Engg., University of Mumbai 1999)

224 Typed Pages

Directed by Bruce J. Tatarchuk

The prime reason for life casualties in fire is not the fire itself but poisoning caused by presence of carbon monoxide. It has been reported by American Medical Association that CO causes about 2100 deaths per year and about 10000 physical injuries in United States. Carbon monoxide can be lethal at a concentration of more than 400 ppm. Depending upon cases, fire can contain as high as 3600 ppm of carbon monoxide.

This dissertation presents results of R&D efforts to develop a thin, low pressure drop, high face velocity, catalyst substrate capable of meeting various CO reduction standards for Respiratory Protection Applications including CBRN (recently adapted by NIOSH), EN 403 (European Union) and ANSI / ISEA 110-2003 (ANSI).

The goals for this work were set based on performance of current commercial products in the domain and new and emerging standards for testing of fire escape masks. The current products meet well existent EN 403 standards, which corresponds to removal of 2500 ppm CO down to 200 ppm, for a flow rate of 30 LPM for minimum 15 minutes. The new and emerging standards are more stringent and pose a significant challenge for development. Also, current commercial products have been designed based on packed bed configuration of catalyst, hence suffer pressure drop.

The effort here utilizes a unique approach known as Microfibrous Entrapment. Resultant materials are a composite structure wherein a micron sized powder of the catalyst (ca. 10-250 micron in diameter) is entrapped within a sinter-locked mesh of metal, polymer or ceramic fibers (ca. 2 – 20 micron in diameter). These materials are highly advantageous for applications where high contacting efficiency is required. The approach also provides a number of other advantages such as high thermal conductivity, low pressure drop, and high mechanical & structural stability.

In this work, a promoted and proprietary Pt/Al_2O_3 (150 – 250 micron) has been entrapped into a nickel microfibrous mesh consisting of 2-3 vol% of 4 and 8 micron diameter fibers. The catalyst has been tested in a tubular reactor. Various tests were performed according to all the test protocols. Non-linear dynamics of CO oxidation, hysteresis effects, effect of moisture, kinetic oscillations phenomenon are also discussed. Analysis of commercial products was done to compare this technology with existing ones. The results show that this technology utilized 10 times lower quantity of catalyst, has a four-fold lower pressure drop and weighs ten times lighter compared to commercial products. Technology transfer has been detailed to test the scalability of the process.

ACKNOWLEDGEMENTS

I would like to express my sincere gratitude towards Dr. Bruce Tatarchuk for his kind financial and moral support. I would also like to acknowledge Dr. James Guin, Dr. Chris Roberts, and Dr. Daniel Harris for serving on my committee. Special thanks to Dr. Christopher Roy for serving as outside reader for this dissertation. I express my appreciation towards all the members of Center for Microfibrous Materials Manufacturing for their kind help, especially Mr. Dwight Cahela. Many thanks are due to Mr. Joe Aderholdt and Mr. Wendell Sandler for timely help on fabrication.

Special thanks are due to Dr. Amit Mitra for offering great help, while I was making important career decisions. Thanks are due to Dr. Said Elnashaie for special exposure towards chemical engineering and personal help. I shall like to express my deep appreciation to Tamara and other members of LeadershipAU. Special thanks are due to my fellow Auburnites; Rushabh, Bhavin, Nimir, Aziz, BK, Eric, Vitaly, Philip, Ranjit and Dan.

I would like to express my deepest gratitude towards my parents; everything always seemed easy when they explained it. My younger brother, Vikas is always a source of inspiration for me, special thanks to him.

Very many thanks to friends; Lakhan, Prashant, Sanjeev and Shailendra, without whom, it is impossible for me to visualize a life.

Style manual or journal used: *American Chemical Society Style Guide: A Manual for Authors and Editors*

Computer software used: *Microsoft Word*

TABLE OF CONTENTS

LIST OF TABLES

LIST OF FIGURES

CHAPTER I

INTRODUCTION AND LITERATURE REVIEW

I.1 Motivation:

Motivation of the research here is to be able to develop suitable microfibrous entrapped catalysts for low temperature oxidation of carbon monoxide. The research under consideration is applicable for developing respiratory protection systems for military, mining and space devices. It also has applications in orbiting closed cycle CO_2 lasers used for weather monitoring and other remote sensing applications. The catalyst can also be incorporated into fuel cell filter for protecting cathode from CO that can be present in the ambient air. This can be mainly applicable for fuel cell vehicles. The CO content on the roads can be up to 40 ppm. This concentration is sufficient to deactivate the fuel cell catalyst. Hence this catalyst can also be employed to protect the cathode.

A special consideration has been given to the PPE (personal protective equipment) application. This particular catalyst can be incorporated into a fire escape mask to oxidize carbon monoxide generated in fire.

I.2   Introduction:

It has been long known that removal of carbon monoxide is a difficult task. The reason why carbon monoxide removal has been found to be difficult lies in its physical and chemical properties. Due to its low boiling point and critical temperature, adequate adsorption at ordinary temperature is not possible. Due to its very low solubility in all solvents makes it impossible to be removed by physical absorption under any condition. Chemically CO is very inert at room temperature. The only known means so far is to oxidize carbon monoxide by means of a very powerful oxidizing agent such as platinum, palladium etc. Due to many important applications of low temperature carbon monoxide oxidation process, it has received considerable attention over a period of time. Moreover the simplistic appearance of the reaction, yet complex behavior observed in this reaction, became subject of investigations. The reaction has significant applications in control of emission in automotive exhaust gases, environmental clean up and a gamut of industrial applications of significant economic importance. The reaction can be written as follows:

$CO + 0.5O_2 \rightarrow CO_2$
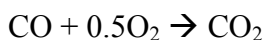
Many catalysts which are active for this process under different conditions are very well known. There still exists a need for developing a better catalyst that would be active for longer time and would be tolerant to moisture and impurities in reacting gases. Moreover effective contacting pattern between the catalyst surface and reacting gases always plays a key role in catalytic reactions. Microfibrous materials are a means of better contacting efficiency as smaller size of catalyst particles can be used at lower pressure drop.

I.3   Importance of Carbon Monoxide Removal for Direct Human Application:

As it is well known, the main cause of life casualties in fire is Carbon monoxide poisoning rather than the fire itself. Carbon monoxide is often referred to as the "Silent Killer". Carbon monoxide causes about 2100 deaths per year and about 10000 physical injuries [1.1]. Carbon monoxide can be lethal at a concentration of more than 400 ppm. Depending upon cases, fire can contain as high as 3600 ppm of carbon monoxide. Other places where it is possible to get poisoned by carbon monoxide are, ship boiler rooms due to defective ventilation, fires below deck in and out, manufacture of power and illuminating gas, coal mining, certain classes of copper mining, wherever explosives are being used in enclosed spaces, leaky flues, exhaust gases from explosive engines and places where coal fires are employed in case of improper ventilation. The catalyst developed here can be very effective to remove CO from the breathing air by incorporating it into gas mask or breathing apparatus.

I.4   History of Breathing Apparatus and Gas Mask Development for Protection from Irrespirable Gases [1.2]:

The history of oxygen breathing apparatus began in 1853 [1.3]. The apparatus was developed by Prof. Schwann as part of an academic competition at Academie Royale Belgique. The machine looked similar to those in use today. In late 1800s Fluess apparatus was developed in England by Prof. H.A. Fleuss. In 1903, an early type of draeger apparatus appeared in Germany. In the United States, mining companies were the first ones to recognize the need of breathing apparatus. Philadelphia & Reading Coal & Iron Co. of Pennsylvania and Anaconda Copper Mining Co. of Montana were the first

ones to provide breathing machines as rescue apparati in their mines in 1907. The United States investigated cause of casualties in mining operations, as a part of which the Bureau of Mines came into being in 1910. The bureau took-up the development of breathing apparatus. Two early American types developed were Gibbs and Paul. The bureau also approved Fleuss-Davis Apparatus developed in England. Due to Bureau's experience with breathing apparatus development, they were called upon in World War I to direct the development of Military Gas Mask. Few years later the research was transferred to Research Division of Chemical Warfare Service. It had long been believed that carbon monoxide could be used as chemical warfare agent. Hence it was important to incorporate materials that would provide protection against carbon monoxide. After World War I, Bureau of Mines carried on investigations to develop gas mask that would be suitable for industrial uses where poisonous gases could be sometimes encountered. The very first escape category mask that bureau of mines came up with was, the 'Universal Gas Mask' [1.4]. The universal gas mask did not supply oxygen and was of the gas purification type. It contained following different adsorbents and catalysts for gas purification purpose:

i.   Activated charcoal for removing organic vapors

ii.   Caustic soda or pumice stones for acid gas removal

iii.   Fused calcium chloride to remove water vapor so that hopcalite catalyst (susceptible to poisoning) does not deactivate

iv.   Hopcalite catalyst for removing carbon monoxide by direct oxidation

v.   Silica gel for removing ammonia

vi.   Filters of cotton wool to remove suspended particulate matter such as dust and

mists

The year after that the Bureau introduced 'The All Service Gas Mask' [1.2]. Figure 1.1 shows the details of this mask.

Heavy wire screen
Absorbent cotton filter .25 in thick between wire screens
Fused calcium chloride 160 cc

Hopcalite 330 CC

Fused calcium chloride 300 CC

Pumice impregnated with anhydrous calcium chloride, 85 cc

Absorbent cotton filter .25 in thick between wire screens

Activated charcoal impregnated with copper sulfate 660 CC

Dome of wire screen covered with Turkish toweling

Figure 1.1: The All Service Gas Mask

As seen in figure this canister does not have the silica gel layer for ammonia removal. Instead of silica, the activated charcoal was impregnated with copper sulfate to remove ammonia. Copper sulfate reacts with ammonia to form ammonium copper sulfate. The canister rested on wearer's chest with a hose connected to the face-piece. The total volume of the canister was 1720-1750 cc.

This development led to different types of masks and breathing apparatus available on the market today.

I.5 Types of Respiratory Protection System:

OSHA (Occupational Safety and Health Administration) Respiratory Protection Standard 29 CFR 1910.134 defines following different classes of respiratory protection systems.

1. Filtering Face-piece (Dust Mask)

A negative pressure particulate respirator with a filter as an integral part of the face-piece or with the entire face-piece composed of the filtering medium.

2. Air-Purifying Respirator (APR)

It is a respirator with an air-purifying filter, cartridge, or canister that removes specific air contaminants by passing ambient air through the air-purifying element.

    a. Powered Air-Purifying Respirator (PAPR)

    It is an air-purifying respirator that uses a blower to force the ambient air through air-purifying elements to the inlet covering.

3. Atmosphere-Supplying Respirator

    a. Self-contained Breathing Apparatus

SCBA is an atmosphere-supplying respirator for which the breathing air source is designed to be carried by the user. These are used in oxygen deficiency type of environments or any situation that is IDLH (Immediately Dangerous to Life or Health) or

can become IDLH or any environment that has unknown environment both in terms of levels and types of contaminants.

b. Supplied Air Respirators

It is an atmosphere-supplying respirator for which the source of breathing air is not designed to be carried by the user. It is also called airline respirator.

4. Escape Only Respirator

A respirator intended to be used only for emergency exit. For example in a building on fire situation escape respirators with appropriate purifying materials in the canister of the mask can be used for escape purpose.

I.6 Testing standards and Test Protocols

For suitability of escape only respirators, European Standards Institute [1.5], NIOSH (National Institute of Occupational Safety and Health) [1.6] and ANSI (American National Standards Institute)/ISEA (International Safety Equipment Association) [1.7] have published different testing standards that these have to comply in order to be suitable for commercial use.

I.6.1 EN 403 Standards for Escape mask application

Table 1.1 shows the details of European EN 403 standards. These standards were proposed and accepted by European Union in 1993. Since then, America also followed the same standards. Recently new standards are being proposed.

Table 1.1: EN 403 Standards Details

Test Agent	Test gas Conc. In air (ppm)	Breakthrough Conc. (ppm)
Propenal (acrolein)	100	10.5
Hydrogen Chloride (HCl)	1000	5
Hydrogen Cyanide	400	10
Carbon Monoxide	2500	200[a]

[a]: Time weighted average over 10 min.

I.6.2   NIOSH Standards

NIOSH standards were published in March 2003 as attachment A to CFR 42.84. Table 1.2 lists the details of NIOSH CBRN (Chemical, Biological, Radioactive and nuclear) with CO standards.

Table 1.2: NIOSH Standards Details

Test Agent	Test gas Conc. In air (ppm)	Breakthrough Conc. (ppm)
Ammonia	1250	25
Cyanogen Chloride	150	2
Cyclohexane	1300	10
Formaldehyde	250	10
Hydrogen Cyanide	470	10
Hydrogen Sulfide	500	30
Nitrogen Dioxide	100	1
Phosgene	125	1.25
Phosphine	150	0.5

Test Agent	Test gas Conc. In air (ppm)	Breakthrough Conc. (ppm)
Sulfur Dioxide	750	5
Carbon Monoxide[c]	3600	402.5[b]

[b]: Time weighed average over the one time use of canister
[c]: For a flow rate of 64 LPM (equivalent to breathing flow rate)

The respirators would be evaluated under following conditions:

a. Three respirators to be tested at 64 ± 10 LPM continuous airflow at 89 to 95% relative humidity at $25 \pm 3\,^0$C.

b. Three respirators to be tested at 64 ± 10 LPM continuous airflow at 89 to 95% relative humidity at $0 \pm 2.5\,^0$C.

Additional Tests for Carbon Monoxide:

Service Life Testing:

- For an inlet concentration of 3600 ppm and flow rate of 110 LPM, the canister should be able to remove CO down to 402.5 ppm average for at least 5 minutes

Inspired Air Temperature:

- For an inlet concentration of 1200 ppm, outlet concentration should always be less than 10 ppm, wherein the temperature does not exceed 46 ^{0}C.

Specific Category Tests:

- The inlet concentration of 6000 ppm of CO to be reduced to 402.5 time weighted over the service period

Service Life Test:

- For an inlet concentration of 6000 ppm and flow rate of 110 LPM, the canister should be able to remove CO down to 402.5 ppm average for at least 5 minutes

I.6.3 ANSI/ISEA 110-2003 Standards

American National Standards Institute, in collaboration with International Safety Equipment Association has proposed a set of standards for fire escape application. There are seven different categories. Category number six and seven are applicable to Carbon Monoxide removal.

I.6.3.1 ANSI/ISEA 110-2003 #6:

The mask should be active minimum for 15 minutes while removing 3090 ppm CO down to less than 200 ppm instantaneous at room temperature and 90% relative humidity of the feed.

I.6.3.2 ANSI/ISEA 110-2003 #7:

The mask should be active minimum for 15 minutes while removing 5150 ppm CO down to less than 200 ppm instantaneous at room temperature as well as zero deg C, and 90% relative humidity of the feed. Table 1.3 shows the details of other gas requirements for ANSI/ISEA 110-2003 standards.

Table 1.3: Other Gas Requirements for ANSI/ISEA 110-2003

Test Agent	Test gas Conc. In air (ppm)	Breakthrough Conc. (ppm)
Propenal (acrolein)	100	0.5
Hydrogen Chloride (HCl)	1000	5
Hydrogen Cyanide	400	10
Cyclohexane	500	5
Sulfur Dioxide	100	3

I.7   Current Status of Escape Respirators:

Major manufacturers like Drager®, Sundstrom® and Essex® amongst others are into manufacturing of escape masks. No manufacturer has a CBRN with CO compliant escape mask as of now.

Schematic appearance of a fire escape mask on a manikin is shown in figure 1.2.
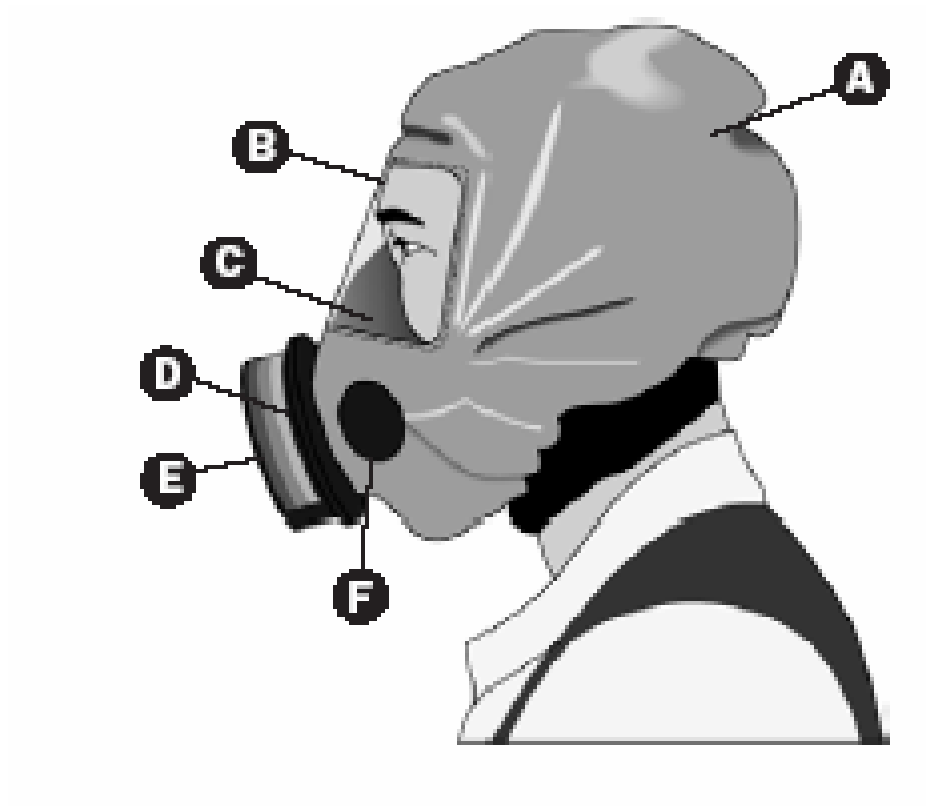
Figure 1.2: Schematic of Fire Escape Mask on a Manikin

(Source: Sundstrom product leaflet)

A: Hood   D: Canister

B: Visor   E: Particulate Filter

C: Half mask   F: Exhalation Valve

The description of the two chosen escape respirators is given in table 1.4.

Table 1.4: Description of Parat C® and SR 77®

Attribute	Parat C®*	SR 77®**
Standards Passed	EN 403	EN 403
Area	71 cm^2	73 cm^2
Total Catalyst Loading	173 gm (Hopcalite)	182 gm (Carbon = 58 gm) (Mol Sieve = 40 gm) (Hopcalite = 84 gm)
Total Bed Depth	4.5 cm	4.5 cm
Pressure Drop thro' the bed	> 40 mm of H_2O	> 40 mm of H_2O
Time	19 min	35 min

(Source: *Product literature, **Personal communications)

12

Figures 1.3 and 1.4 show the product pictures for PARAT C® and SR 77® respectively.

Figure 1.3: SR 77® on a Manikin

(Source: Sundstrom website)

Figure 1.4: Parat C® Done by a Model

(Source: Drager® Website)

As can be seen from the pictures and the numbers in the table, both these products are very big with a high pressure drop, which directly means breathing resistance here. These products are heavy as well. The main reasons for these products to be big are as follows:

- The catalyst loading inside the cartridge is packed bed of approximately 1x3 mm particles. This particular configuration offers very weak contacting efficiency.

- The main component of the cartridge, hopcalite catalyst is very sensitive to moisture poisoning. It deactivates extremely rapidly in presence of moisture. Hence these masks have excess quantities of catalyst.

Moreover, as mentioned earlier, the products on the market so far, can meet only EN 403 standards which are relatively benign when compared to NIOSH or ANSI standards. Due to all these reasons, it is very important to develop a suitable material for respiratory protection that would effectively remove the carbon monoxide before inhalation. The escape mask incorporating the material should be lighter in weight and better in performance. The breathing resistance offered by the material should be extremely low for ease of use.

Microfibrous entrapped Oxidation catalysts offer a promise for research into this arena. This catalyst can be incorporated into the fire escape mask to convert CO to CO_2 thereby reducing the risk of physical injury.

I.8   Carbon Monoxide Oxidation Catalysts:

The development of CO Oxidation catalysts started in the early 1920s. One of the very first developed catalysts was Hopcalite. The development of hopcalite is well known. Lamb, Bray and Frazer and co-workers [1.8] conducted most of the investigations that resulted into the production of this catalyst. Hopcalite is copper and manganese mixed oxide catalysts. Individually manganese oxide and copper oxide are high-temperature active [1.9]. Due to the mixture effect, the mixed oxide becomes low temperature active

14

for CO oxidation. This catalyst suffers due to loss in activity in presence of moisture very rapidly. Same investigators reported much of the later work [1.10, 1.11] on the catalyst oxidation of carbon monoxide related to various factors influencing the catalytic activity of hopcalite and its constituent oxides.

Almquist and Bray [1.9] tested effect of catalyst composition, various operating conditions such as temperature, CO concentration, moisture content and reduction under flowing carbon monoxide. Their findings indicated a strong poisoning by moisture and irreversible activity loss due to reduction of catalysts under carbon monoxide in absence of oxygen.

Lamb and Vail [1.10] studied effect of water on CO oxidation by hopcalite. The different reasons for this deactivation could be, (1) the water can be adsorbed onto the catalyst surface as molecules thereby hindering the access of active sites to reactants or desorption of products from the surface; (2) water might react stoichiometrically with the whole surface or part of it, to form a layer of inactive material that may behave similar to a water layer;(3) water vapor might absorb active radiation of electrons emitted from the catalyst, or it might react with the activated molecules, ion or atoms of the gases near the catalyst surface and so diminish the number of reacting particles; (4) more than one of these effect might happen simultaneously.

Brittan et al [1.12] proposed kinetic model for hopcalite catalyzed carbon monoxide oxidation reaction. The model exhibits significant departure from previously assumed first order kinetics. It follows Langmuir-Hinshelwood type of mechanism.

Veprek et al [1.13] studied the mechanism of deactivation of hopcalite by various analytical techniques. The techniques and characteristics of the catalyst used and

15

observed were EDS (Energy dispersive spectroscopy) for Bulk Composition, SEM (scanning electron microscopy) for Morphology, BET ((Branuer, Emmett, Teller)) for surface area, XRD (X-ray diffraction) for bulk structure, TG/TDA (thermo gravimetric analysis/differential thermal analysis) for thermal properties, XPS (X-ray photoelectron spectroscopy) for surface chemistry, structure and composition and ISS (ion scattering spectroscopy) for depth profile. Phase change induced segregation and impurities and dopants at small levels appearing and blocking sites were observed to be causes of deactivation.

Rogers and co-workers [1.14] investigated mixtures of manganese, cobalt and silver oxides for low temperature CO oxidation. These catalysts exhibited activity similar to that of hopcalite and were found to be moisture sensitive.

Imamura and co-workers [1.15] investigated oxidation of carbon monoxide catalyzed by Manganese-silver composite oxides. The results indicated that composite oxides had much higher activity compared to single oxide of manganese or silver. Silver in the composite catalyst remained in the oxide form for a mol% of less than 50, while it lost lattice oxygen in the presence of manganese at higher temperatures.

Musick and Williams [1.16] compared different catalysts for low temperature carbon monoxide oxidation. The aim of the research program was to be able to reduce CO concentration from 5000 ppm to 50 ppm and be able to maintain it at that level for at least 72 hours in a volume of 4248 m^3. Following catalysts were chosen for study:

- carbon impregnated with copper, chromium and silver (whetlerite),
- hopcalite,
- supported palladium metal

- supported platinum metal.

The catalysts were tested with 3000 to 5000 ppm of CO in air at 2100 Hr^{-1} space velocity, different temperatures and 15% & 50% relative humidity. Their findings indicate, at room temperature and 50% RH, hopcalite and platinum have no catalytic activity. At room temperature and 15% RH, hopcalite is superior to platinum. Hopcalite is more efficient in the temperature range of 52 – 66 ^{0}C compared to all other catalysts for both the humidity levels. At higher temperatures of 113 – 135 ^{0}C, platinum and palladium are superior to hopcalite or whetlerite. Higher humidity affects hopcalite adversely.

Gürdag and Hahn [1.17] studied the synergistic catalytic activity of platinum and metal antimonates and compared that to $Pt/SnO_2/Al_2O_3$. The various catalysts used for this study were $Pt/NiSb_2O_6$, $Pt/CoSb_2O_6$, $Pt/CuSb_2O_6$ and $Pt/SnO_2/Al_2O_3$. Their results indicate that in the zero order region of oxidation reaction when CO concentration is higher, very low degree of synergism is present between platinum and antimonite compared to pt and SnO_2.

Benton and Williams [1.18] studied the oxidation of carbon monoxide in presence of quartz glass. The findings indicated that quartz glass had no effect on the oxidation.

Engelder and Miller [1.19] report the experimental investigation of carbon monoxide oxidation over titania and mixtures of titania with various metallic oxides that included UO_2, Fe_2O_3, NiO, Cr_2O_3, Co_2O_3, CeO_2, CuO, SnO_2, MnO_2, ZnO, ThO_2, Bi_2O_3, HgO, Al_2O_3, Ag_2O, MgO and CdO in different proportions. The best catalysts were obtained from 50:50 mixtures of these oxides. Fe, Cu and Ni oxides exhibited the highest activity

17

at this ratio. All these results were obtained at higher temperatures mainly 150 ^{0}C and 300 ^{0}C. At low temperature of 50 ^{0}C to 60 ^{0}C, the catalysts exhibited lower activities.

Haruta and Co-workers [1.20] discovered that supported gold particles exhibit high catalytic activities for low temperature oxidation of CO. Especially gold supported on TiO_2, α-Fe_2O_3 and Co_3O_4, NiO, $Be(OH)_2$ and $Mg(OH)_2$ is very active even at temperatures below 273 K. Among the gold catalysts supported on TiO_2, α -Fe_2O_3 and Co_3O_4, the turnover frequencies for CO oxidation per surface gold atom are almost independent of the kind of support oxides used and increase sharply with a decrease in diameter for gold particles below 4 nm.

It has been shown that activities of above supported gold catalysts for low-temperature CO oxidation are enhanced by moisture [1.21]. Some of these catalysts are already commercialized to remove odor and CO in air at room temperature. Other commercial applications include selective CO gas sensors [1.22, 1.23]. These catalysts and Au/Fe_2O_3 prepared by other groups have been tested for sealed CO_2 lasers [1.24, 1.25].

These successes were achieved mainly due to method of preparation (achieving very high level of dispersion) because the gold catalysts prepared by conventional impregnation method exhibit no appreciable activity.

It is very difficult to obtain gold in a highly dispersed phase as those of Pt or Pd mainly because of lower melting point of Au (1336 K) compared to 2042 for Pt and 1823 for Pd. It has been reported that melting point of gold particles below 2 nm diameter is lowered to 573 K due to the quantum size effect. Since gold itself is known to be very inactive, the enhancement in activity of gold metal oxide catalyst can be attributed to

18

electronic interactions and/or the active sites on the interfacial perimeter resulting from the gold deposition on a support.

M. Haruta et al [1.26] discussed the low temperature activity of gold based catalysts prepared by co-precipitation method for CO oxidation. The catalysts prepared were Au/MnO_x, $Au/ \alpha -Fe_2O_3$, Au/Co_3O_4, Au/NiO and Au/CuO. Among these $Au/ \alpha -Fe_2O_3$, Au/Co_3O_4 and Au/NiO were highly active for CO oxidation showing appreciable enhancement in catalytic activity due to combined effect of gold and the transition metal oxide. These catalysts were active for CO oxidation even at a temperature as low as 203 K. The high activity of these catalysts is attributed to fine dispersion of gold on the surface of metal oxide giving particle size smaller than 10 nm.

Jia at al [1.27] studied oxidation and adsorption of CO on Au/Al_2O_3 by infra red spectroscopy. The findings include formation of two different species on the surface of gold, reversibly adsorbed CO and irreversibly adsorbed CO. Gold particles catalyzed the CO oxidation process by means of reversibly adsorbed species whereas irreversibly adsorbed species remain untouched. It has also been found that oxidized gold particles have no activity for oxidation also Au/Al_2O_3 calcined at 1273 K had no activity.

Grunwaldt and Baiker [1.28] studied the Au/TiO_2 catalyst for the role of gold-titania interface in CO oxidation. The observed chemisorptive properties of the gold/titania interfaces followed a mechanistic model which is based on oxygen adsorption on vacancy sites of titania and CO adsorption on gold.

Jansson et al [1.29] discussed the low temperature oxidation of CO over cobalt oxide catalyst supported on alumina. The catalyst has been found to be active at low temperature but deactivates rapidly. The deactivation is attributed to carbonate formation

detected by FTIR studies and consumption of surface oxygen that makes the particular site lose its activity.

Costello et al [1.30] studied deactivation behavior of Au/Al_2O_3 catalyst for CO oxidation. The activity is reported to drop very fast for first few minutes. The proposed reaction pathway is insertion of CO into the Au+OH- bond to form a hydroxycarbonyl which, is oxidized to a bicarbonate. Decarboxylation of the bicarbonate completes the reaction. Water addition to the feed is reported to be helpful for enhancing activity.

Date et al [1.31] reported the performance of Au/TiO_2 catalyst for CO oxidation under ambient conditions. The best performance was obtained with a catalyst calcined at 473 K at room temperature. The catalyst maintained activity for few days. Is has also been proposed that there is an optimum moisture level in the feed at around 200 ppm. The catalyst could be effectively regenerated by light irradiation.

Gardner and Hoflund [1.32] prepared and tested MnO_x, Ag/MnO_x, Au/MnO_x, Cu/MnO_x, Pd/MnO_x, Pt/MnO_x, Ru/MnO_x, Au/CeO_x and Au/Fe_2O_3 for low temperature CO oxidation. According to these researchers Pt and Pd based catalysts need to be pre-reduced for better performance. Au/MnO_x catalyst was observed as the best effective catalyst at low temperatures such as room temperature. Also heat treatment in air or oxygen was observed to be beneficial for MnO_x based catalysts.

In a separate study Hoflund, Gardner and co-workers [1.33] reported the influence of promoters on the performance of Au/MnO_x and $Pt/SnO_x/SiO_2$ low temperature CO oxidation catalysts under stoichiometric conditions. The results indicate that, the performance of $Pt/SnO_x/SiO_2$ catalyst is improved by the addition of 5wt% of Fe, 1 wt% Sb, 5 wt% Sb, 1 wt% As and 1.8% P. The performance of Au/MnO_x could be improved

significantly by the addition of 1 at% Ce but reduced by the addition of 1 at% Co. Under the conditions studied, Au/MnO_x is found to be better catalyst compared to $Pt/SnO_x/SiO_2$.

Dong and co-workers [1.34] studied various palladium based catalysts for low temperature CO oxidation. These include Pd/CeO_2, Pd/SnO_2-TiO_2, Pd/ZrO_2-TiO_2, $Pd/Al_2O_3-TiO_2$, Pd/CeO_2-TiO_2 and Pd/TiO_2. Among all the catalysts, Pd/CeO_2-TiO_2 exhibited better catalytic activity. Among various Pd/CeO_2-TiO_2 catalysts the best candidate corresponds to 1wt% Pd loading and Ce/Ti ratio of 1:7 to 1:5. This catalyst showed significant activity at room temperature.

Gulari et al [1.35] discussed use of silver cobalt composite oxide for CO oxidation. The catalyst structure study by XRD, XPS and TGA indicate that silver cobalt oxide is a composite oxide where silver is stabilized in an oxide in the presence of cobalt at temperatures as high as 1073 K. IR spectroscopy study of the reaction shows that, the catalyst is deactivated due to presence of CO_2 and water in the feed stream. This was mainly because of weak adsorption of CO_2 and water on the surface of catalyst thereby physically blocking the sites. This deactivation was not observed at temperatures more than 393 K.

Lin et al [1.36] reported the preparation and testing of Au/Y zeolite, and Au-Fe/Y zeolite. These catalysts exhibited significant activity at lower temperatures. XPS studies done on Au-Fe/Y suggested that formation of carbonate like species that covered the active sites was the main cause for catalyst deactivation. On the other hand TEM studies suggested that the sintering of nano-gold particles was the main reason for the slight deactivation of Au/Y.

Hoflund [1.37] prepared and studied silica supported Pt/SnO_x and Fe promoted Pt/SnO_x. Ion scattering spectroscopy (ISS) has been used to examine the outermost atomic layers of these catalysts. The nonpromoted catalyst exhibits agglomeration of the platinized tin oxide film exposing the inactive silica support. Whereas this does not happen when Fe is present as promoter and active surface area can be maintained.

Torncrona et al [1.38] studied the low temperature activity of cobalt oxide and ceria promoted Pt and Pd catalyst. Results indicate that cobalt containing catalysts are the most effective ones even in the absence of noble metals. These catalysts showed much lower light-off temperature compared to un-promoted Pt and Pd catalysts.

Thormahlen et al [1.39] studied Pt/Al_2O_3, CoO_x/Al_2O_3 and $Pt/CoO_x/Al_2O_3$ in monolith form. Preoxidized $Pt/CoO_x/Al_2O_3$ was found to be active at very low temperatures even at 200K. At these low temperatures the activity of the catalyst is independent of platinum content. The deactivation was also studies here. Presence of moisture leads to formation of OH^- species on the surface of the catalyst thereby blocking the active sites. Carbonate formation is also reported as a cause of catalyst deactivation.

Mergler et al [1.40] reported the activity of $Pt/CoOx/SiO_2$, $Pt/MnOx/SiO_2$ and Pt/SiO_2. Performance of these catalysts was compared with commercially available catalysts viz. $Pt/CeO_x/Al_2O_3$, $Pt/Rh/Al_2O_3$ and Pt/Al_2O_3. $Pt/CoO_x/SiO_2$ and $Pt/MnO_x/SiO_2$ were the most active catalysts for CO oxidation after a pretreatment of reduction. Partially reduced metal oxides are necessary to increase the activity of $Pt/CoOx/SiO_2$, $Pt/MnO_x/SiO_2$ or $Pt/CeO_x/Al_2O_3$. In Pt/CoO_x catalyst, CoO_x acts as an o-supplier thereby affecting the adsorption of CO or O_2 on platinum.

22

Fuller and Warwick [1.41] studied low temperature oxidation of carbon monoxide on SnO2-CuO gels. The catalyst was found to be active after thermal treatment at 450 ^{0}C. This effect has been attributed to the ion-exchange sorption of Cu (II) on the surface of the primary hydrous SnO_2 particles formed during the precipitation process. The best activity was observed at an atomic ratio of 0.55:1 of Cu:Sn.

Imamura and Yoshie [1.42] reported effect of samarium addition on activity and thermal stability of manganese/silver catalysts. The results suggest that manganese oxide serves as oxygen reservoir that helps in maintaining the activity of the catalyst when used in highly oscillating conditions. The lattice oxygen from manganese oxide is readily transferred to and desorbed from Ag. The results further include an addition of small amount of Sm inhibits grain growth of manganese oxides treated at high temperatures in a reducing atmosphere, thus, leading to retention of a large surface area. Due to restricted grain growth of Mn/Ag/Sm catalyst, Ag could be finely and homogeneously dispersed in the matrix of the catalyst. On the other hand Ag aggregated on the surface as large crystals or migrated towards center of Mn/Ag catalyst particle.

OH and Eickel [1.43] studied effects of Cerium addition on CO oxidation kinetics over alumina supported rhodium catalyst. The observed changes in the kinetics include a suppression of the CO inhibition effect, decreased sensitivity of the rate of O_2 concentration and decreased apparent activation energy. The kinetic effects involved here can be best explained by surface oxidation mechanism. Carbon monoxide adsorbed on Rh site reacts with lattice oxygen of neighboring ceria particle. It was also observed that Ce addition has the same effect regardless of sequence of deposition while preparing the catalyst.

I.9   Methods of Catalyst Preparation:

The preparation of catalyst is commonly described as art [1.44]. In some cases relationship between formulation procedures and final catalyst behavior be obscure but an understanding of effects generated with certain components by manipulations such as precipitation, washing, drying, heating etc helps to clarify the reasoning behind certain procedure. This also throws light on possible improvements in catalyst making process. Many of the catalysts are either a finely divided a metal supported on a high surface area carrier such as Alumina, zeolites, or a metal oxide either on a carrier or unsupported. Some other types of catalysts include promoted catalysts, wherein the performance of metallic catalyst is improved by the presence of some other metal oxide. Following two are main methods of catalyst preparation:

i.   Precipitation Method

ii.   Impregnation Method

I.9.1   Precipitation Method

This method involves in its initial stages, mixing of two or more solutions or suspensions of materials causing precipitation. This is followed by filtration, drying, washing, forming and heating. Simple wet mixing without precipitation is also used sometimes, but this fails to generate required degree of contacting between the species involved. If a carrier needs to be incorporated, the precipitation is done in the presence of suspension of a finely divided support or a compound that can be converted to required form of the carrier. Sometimes binders, cements, die-lubricants or thixotropic agents are also added in a later stage if required. The forming process

determines the final characteristics of the catalyst such as pore size distribution, size and shape of the catalyst particles. The catalyst is activated by physical and chemical changes. This typically involves heating to cause decomposition or calcinations. Sometimes pre-treatments such as reduction is used to regain the metal form of the oxidized catalyst.

I.9.2 Impregnation Method

In this method a carrier, normally porous is contacted with a solution, usually aqueous of one or more suitable metallic compounds. Normally this is done by two different procedures, dipping the support completely into excess quantity of solution or incipient wetness where, support is contacted as by spraying with the solution of appropriate concentration. Incipient wetness method allows a better control over the amount of the active ingredient and reproducibility of the results is better. The carrier is then dried and the catalyst is activated as mentioned above under precipitation method. The final size and shape of the catalyst are that of carrier material. This method is preferred for making noble metal catalysts as it is much cheaper to spread finely divided metallic particles.

I.10   Catalyst Treatment Steps:

This section lists the steps involved in conditioning the catalyst to suit a given requirement. The stages discussed are calcination and reduction of catalyst to metallic form by treating at high temperature in reductive environment.

I.10.1 Calcination

Calcination process can have various purposes. The first is to eliminate extraneous material such as binders and die lubricants, also volatile and unstable anions and cations that have been previously introduced but are not desired in the final catalyst. Second, a substantially elevated temperature is usually needed to increase the strength of the final pellet or extrudate by causing incipient sintering. Excessive sintering, however, may reduce the catalyst activity by reducing surface area, and it may also cause diffusion limitations by reduction of pore size, so an optimum is desired.

I.10.2 Reduction to the Metal

Most commonly, a metal is formed by reduction of the oxide at an elevated temperature by contact with flowing hydrogen or hydrogen diluted with nitrogen, the latter for safety reasons [1.44].

It can be observed from thermodynamic calculations that at temperatures in the region of 570 to770 K the reduction of metal oxide to the metal is highly favored for all group VIII elements and copper, silver, gold, and rhenium [1.45]. For the elements chromium, vanadium, tantalum, titanium, and manganese, the oxide form is highly favored.

I.11   Catalyst Characterizations:

The correlation between catalyst behavior and the physical and chemical structure of the catalyst is a basic problem as most practical catalysts are complex materials. As a result very few methods of characterization are standardized. These include determination of total surface area by the Brunauer-Emmett-Teller (BET) method, void fraction, pore size distribution and in some cases specific metal area by selective chemisorption. Other than these many analytical techniques developed in other branches of chemistry are available for studying the catalyst.

I.11.1 Measurement of Surface Area:

The principal method of measuring total surface area of a catalyst is by adsorption of a particular molecular species from a gas or liquid on the surface. If the conditions under which a complete adsorbed layer, averaging one molecular thick, can be established and the area covered per molecule is known, then the quantity of the adsorbed material gives directly the total surface area of the sample.

The most common method of measuring surface area, and used very routinely in catalyst studies is that developed by Brunauer, Emmett and Teller in 1938.

I.11.2 Specific Area by Selective Chemisorption:

For a supported metal catalyst it is frequently desirable to be able to determine the exposed metal area in distinction to the total surface area. This can be achieved by

measuring the uptake of a gas that is chemisorbed on the metal but negligibly on the support, under conditions that allow monolayer coverage. Most useful for this purpose is hydrogen gas but carbon monoxide as well as oxygen are also used for this purpose. Hydrogen has been studies most extensively especially on platinum and nickel.

As a prerequisite, it is necessary to know the chemisorption stoichiometry which is the number of surface atoms covered for each molecule of gas adsorbed, and the surface area occupied per metal atom. For hydrogen this number is almost always be 2, since it dissociates upon adsorption and each hydrogen atom is adsorbed on one metal atom.

I.11.3   Pore Size Distribution:

Pore size distribution is important for prediction of the effective diffusivity in a porous catalyst. Two different methods are used for this purpose: Physical adsorption of a gas, which is applicable to pores less than about 60 nm in diameter, and mercury porosimetry, applicable to pores larger than about 3.5 nm. In method 1, the measurement of adsorption or desorption of a gas as a function of reduced pressure is used to determine the pore size distribution. Method 2 works on the principle of non wetting liquid penetration in a capillary.

I.11.4   Selected Instrumental Methods:

This section describes the details of selected instrumental methods for catalyst characterization.

I.11.4.1 Scanning Electron Microscopy (SEM)/Energy Dispersive Spectrometry (EDS):

SEM has been used primarily for examination of the topology of catalyst surfaces, for example characterization of platinum gauzes before and after use in a reactor and sintering of large supported metal crystallites. EDS can be used for quantification of various elements present in the catalyst. It also gives wt% of various metals.

I.11.4.2 Transmission Electron Microscopy (TEM):

TEM is useful for indicating the size of the supported metal crystallites, change in their size, shape, and position with catalyst use. Replicas are useful for obtaining information on pore structure.

I.11.4.3 X-Ray Diffraction Crystallography (XRD):

XRD can be used to obtain information about the structure and composition of crystallite materials. Common compounds can be identified using tabulations of reference patterns. The minimal limit of detection is approximately 5% for compounds and approximately 1% for elements. With calibration procedures it is possible to obtain quantitative information and thus determine the approximate amount of a particular phase in a sample.

The mean crystallite size of a material can also be determined from the broadening of an X-ray diffraction peak. Small angle scattering may be used to give the particle distribution in the range of 5 to 100 nm.

I.11.4.4 X-Ray Photoelectron Spectroscopy (XPS):

This method is also called as Electron Spectroscopy for Chemical Analysis (ESCA). It is a powerful technique, which can analyze for all the elements except hydrogen. It gives the most accurate and precise atomic electron binding energy and thus it yields the structural data in terms of the valence of the oxidation state as well as atomic charge densities. Also the analysis is chemically non-destructive.

I.11.5 Calorimetry:

Calorimetry may be employed to observe various types of chemical transformations that are accompanied by significant energy changes. A differential scanning calorimeter may be used with small samples.

I.11.6 Gravimetric Methods:

The change in weight of a catalyst with changing experimental conditions can be used for a variety of studies. The method has been applied for adsorption-desorption studies and has been particularly useful for studying the rate of coking, dehydration, sorption of poisons, catalyst regeneration etc as a function of reaction conditions. It is also useful for catalyst characterization, e.g. that of oxidation catalysts in which weight gain or weight loss may reveal the state of oxidation and hence stability as a function of environment.

I.12   Microfiber Based Composite Materials:

This section gives the details of microfibrous entrapped material development and associated literature.

I.12.1 Wet – lay Process/ Sintering Process

Microfibrous materials are very important due to their typical characteristics of offering enhanced heat and mass transfer in chemical processes. A new patented [1.46] class of materials made by wet lay process followed by sintering at high temperatures produce a fine mesh of metal fibers. Figure 1.5 shows an SEM image of 4 microns Ni fiber mesh.
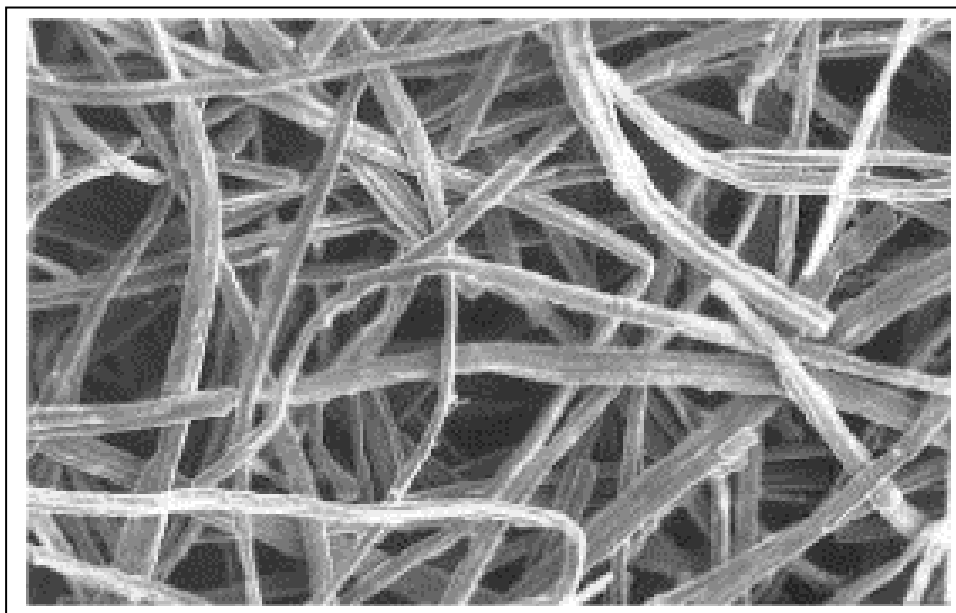
Figure 1.5: SEM Image of 4 μm nickel fiber mesh [1.46]

These materials have the capability to incorporate micron scale particles. Sintered Microfibrous composites using 16% Ni/Al_2O_3 catalyst for toluene hydrogenation have shown 2-6 times higher specific activity than conventional packed bed catalyst on a

weight basis, while volumetric activities of 40 vol.% composite catalysts were 80% higher than conventional pellets [1.47].

Microfibrous materials have various other advantages including high intra bed thermal conductivity, adjustable void volume, higher exposed surface area of catalysts thereby giving higher effectiveness factors, reduced pressure drop and mechanical and structural stability [1.46].

The combination of wet lay and sintering processes allow adjustable void volumes from almost 98% down to those of packed beds [1.48]. This permits the optimization of composite catalysts as per the process requirement.

I.12.2 Alternate Materials of Manufacturing

Microfibrous materials can also be manufactured using various polymer [1.51] and ceramic fibers [1.52] depending upon the type of application. Figures 1.6 and 1.7 show polymeric and ceramic microfibrous entrapped high surface area catalyst supports respectively.
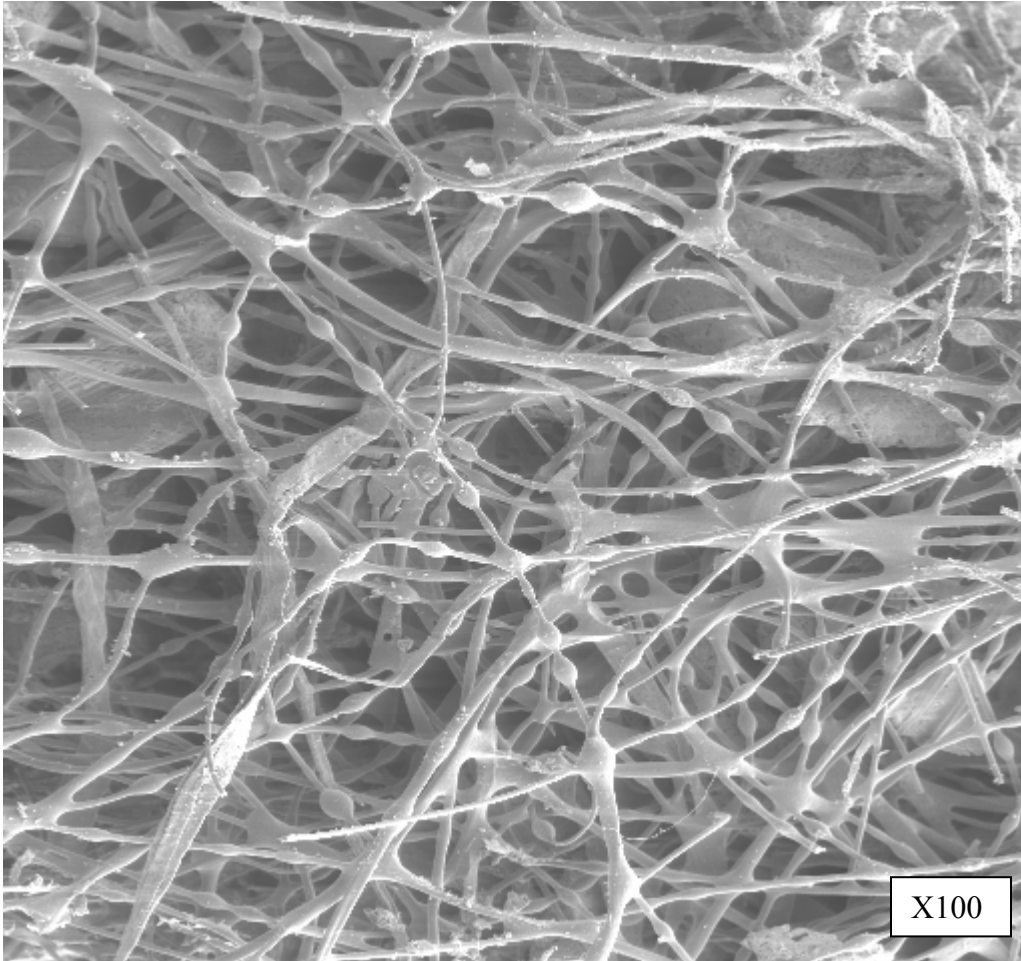
Figure 1.6: Polymer Fiber Entrapped Support [1.51]

Polymer microfibrous materials have substantial cost advantage over metal materials. Hence these materials can be used for high volume low value type of applications such as duct filters. However these materials suffer a major disadvantage in terms of very high temperature instability hence cannot be used for applications such as high temperature catalysis.
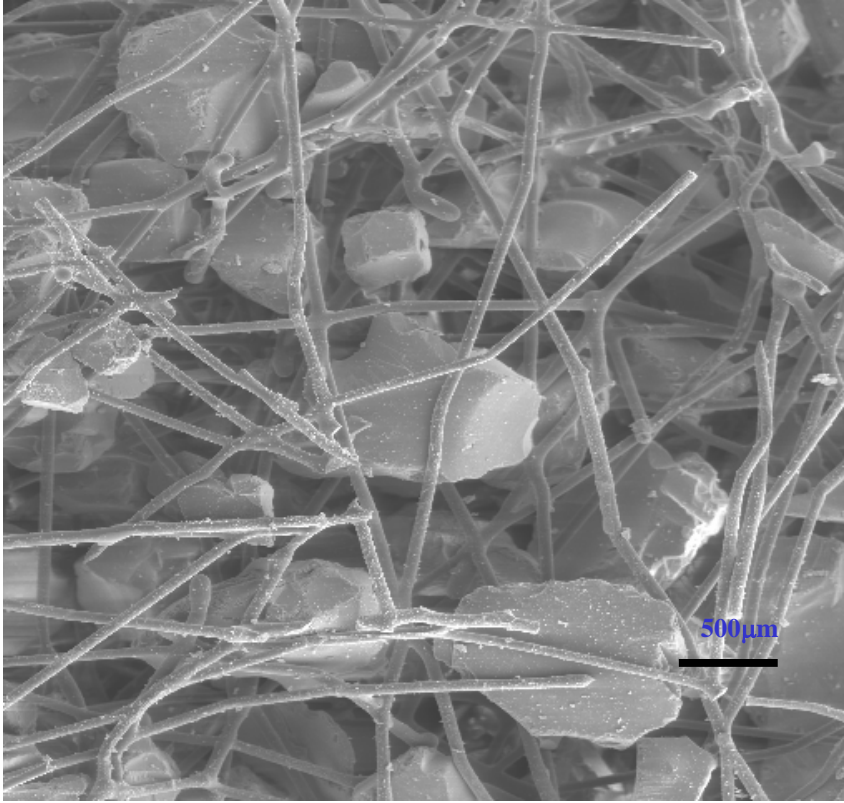
Figure 1.7: Ceramic Fiber Entrapped 150 -250 Micron SiO_2 [1.52]

Ceramic materials find applications in corrosive environment where metal fibers cannot be used. Ceramic microfibrous entrapped materials is a cheaper option to metal fibers.

I.13 Applications of Microfiber Composite Materials:

I.13.1 Microfibrous Entrapped Catalysts and Sorbents:

The application of Microfibrous materials to eliminate hot-spots in a temperature sensitive reactor enables the use of these materials in fuel processing and reforming applications [1.49].

I.13.2 Microfibrous Metallic Filters:

These materials have applications in commercial processes such as polymer filtration, assorted HEPA filter applications and automotive airbags. The relatively low-cost of these media opens the possibility of using regenerable metallic filter elements for automobiles and other low cost applications in place of currently employed disposables. This would result in significant reduction in environmental pollution due to disposables [1.49].

I.13.3 Microfibrous Entrapped Electrocatalysts and Faradaic Materials:

Due to the electrical conductivity of metal mesh, Microfibrous materials are suitable candidates for reducing intra particle and intra electrode resistances and transport limitations experienced in many electrochemical processes and devices such as liquid double layer capacitors and batteries [1.50].

CHAPTER II

EXPERIMENTAL

This chapter presents the experimental apparatus and detailed procedures used in this research. Following various aspects of this research are discussed in this chapter:

II.1　　　Catalyst preparation

II.2　　　Details of chemicals used

II.3　　　Experimental set-up and reactor details

II.4　　　Details of instruments and equipments used for this research work

II.5　　　Pressure drop test set-up

II.6　　　Commercial products testing set-up

II.7　　　Analytical section

II.1　Catalyst Preparation

All the catalysts tested in this study were prepared by either co-precipitation or incipient wetness method. Most noble metal based catalysts supported on a high surface area were prepared by incipient wetness, for example platinum supported on silica. Catalysts such as Cu/CeO_2 were prepared using co-precipitation method.

II.1.1 Incipient Wetness Procedure:

The required support is divided into 150 – 250 μ particle size and dried at about 100^{0}C for 24 hours to make sure that there is no water in the pores of the support. The support was then impregnated with required metal solution until the whole surface was completely wet. The resulting material was then dried at about 100^{0}C for 24 hours. The dried material was then calcined for about 4 hours. For a promoted catalyst, one more step of impregnation, drying and calcinations was added.

II.1.1.1   Preparation of Microfibrous Entrapped Cobalt Promoted Platinum/Alumina Catalysts:

The procedure for preparation of microfibrous entrapped cobalt promoted platinum/alumina catalyst is detailed here.

II.1.1.2   Materials:

- Support: γ - Alumina (220 m^2/gm, 150 – 250 micron)

- Metal: Platinum {Diaminedinitroplatinum (II), 3.4% platinum solution}

- Promoter: Cobalt: {Cobalt (II) Nitrate 99.5% assay, 0.25 M solution}

- Microfibrous Materials:

  3:1 mixture of 4 micron and 2 micron wires

  3:1 ratio of metal to cellulose

  4 gm of alumina entrapped in one 6" disk.

II.1.1.3   Procedure:

1. Entrap 4 gm of 150 -250 micron alumina in one 6" disk. (Composition: 8 micron Ni = 1.5 gm, 4 micron Ni = 0.5 gm, Cellulose = 0.67 gm, Alumina = 4 gm)

2. Dry 3 disks together to make a 2" thick precursor.

37

3. Pre-oxidize the precursor for 30 minutes at 400^0C under controlled air flow.

4. Sinter the material.

5. Dip the precursor in 0.25 M cobalt nitrate solution

6. Apply vacuum to the precursor to remove excess nitrate solution.

7. Dry the precursor in oven at 100^0C for 24 hrs.

8. Calcine the precursor for 4 hrs in air at 400^0C.

9. Impregnate platinum solution drop by drop on the support until wet.*

10. Dry the precursor in oven at 100^0C for 24 hrs.

11. Calcine the precursor for 4 hrs in air at 400^0C.

12. Reduce in flowing hydrogen at 250-300^0C for 2 hrs.

*: Dip and vacuum procedure can also be applied for platinum impregnation and excess solution can be recovered.

II.1.2 Co-precipitation Method:

The required chemicals were mixed in required proportions carefully monitoring the pH of the resulting solution. The solution was then filtered, dried and calcined to yield final catalyst. The catalyst was then crushed to obtain 150 – 250 μ particle size.

II.2   Details of Chemicals Used:

This section details the chemicals used for this research work mainly catalyst preparation along-with source of the material. Table 2.1 gives the list of chemicals used for various catalyst preparations.

Table 2.1: List of Chemicals used for Catalyst Preparation

Sr. No.	Chemical	Purity /Assay (%)	Purpose	Supplier
1.	$Pt(NH_3)_2(NO_2)_2$	3.4% Pt	Metal precursor	Aldrich Chem. Co.
2.	$Mn(NO_3)_2.XH_2O$	99.98	Metal precursor	Alfa Aesar Co
3.	$Co(NO_3)_2.6H_2O$	99.5	Metal precursor	Alfa Aesar Co
4	$Fe(NO_3)_3.9H_2O$	98	Metal precursor	Alfa Aesar Co
5.	$Ce(NO_3)_3.6H_2O$	99.5	Metal precursor	Alfa Aesar Co
6	$HAuCl_4$	49.5 wt% Au	Metal precursor	Alfa Aesar Co
7	$AgNO_3$	99.9	Metal precursor	Alfa Aesar
8	$Pd(NH_2)_2$	5% Pd	Metal precursor	Alfa Aesar Co.
9	$Cu(OH)_2$	56-57 % Cu	Metal precursor	Aldrich Chem. Co.
10	$RuCl_3.3H_2O$	42.71% Ru	Metal precursor	Alfa Aesar
11	SiO_2		Support	Alfa Aesar Co
12	Al_2O_3		Support	Alfa Aesar
13	TiO_2	99.9%	Support	Alfa Aesar Co
14	Na Y Zeolite		Support	
15	BPL Carbon		Support	
16	4A Zeolite		Support	Zeolyst

II.3   Experimental Apparatus:

The apparatus used for catalyst screening tests is shown in figure 2.1. Figure 2.2 shows the reactor for catalyst testing. Figure 2.3 shows the apparatus used for pressure drop measurement.
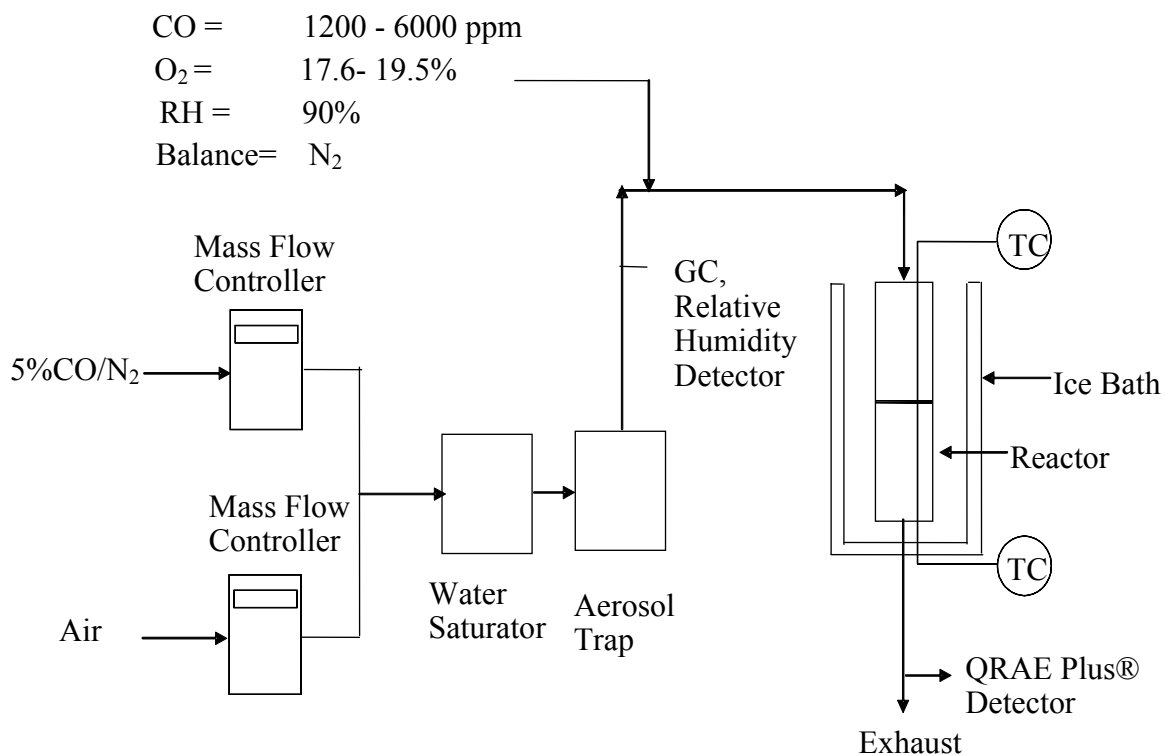
Figure 2.1: Experimental Apparatus for Catalyst Screening
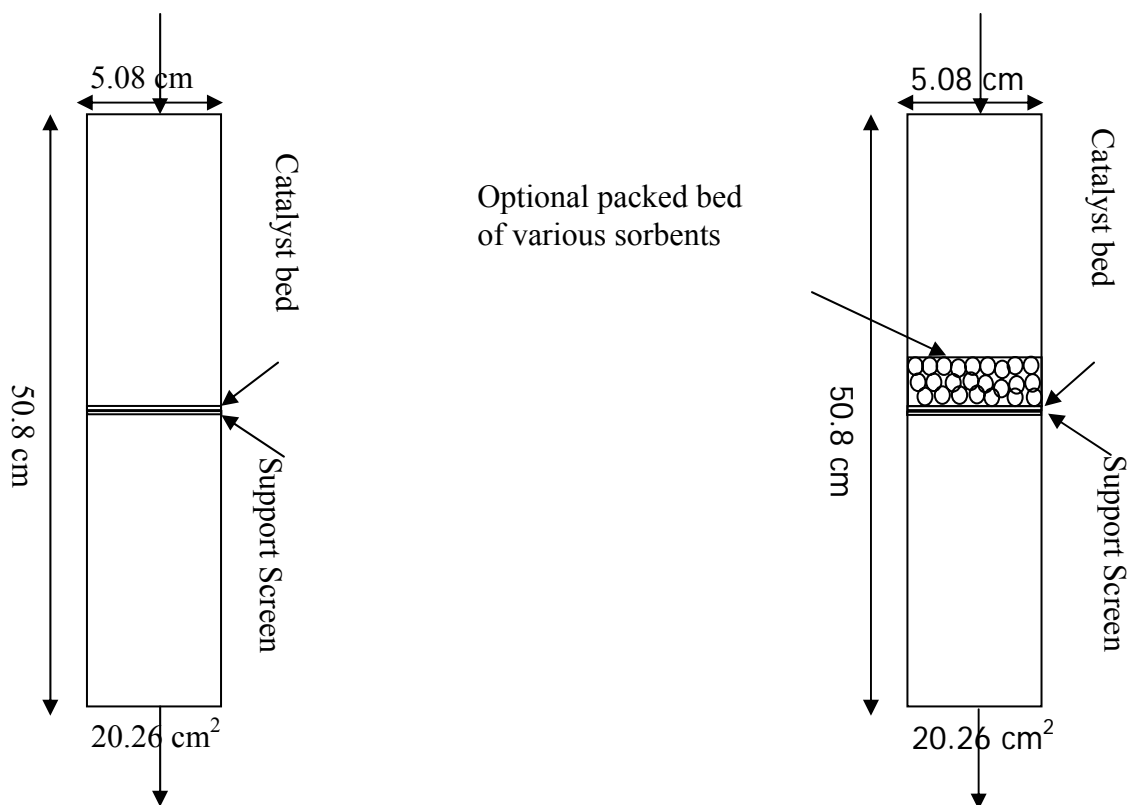
Figure 2.2: Catalyst Testing Reactor

As shown in figure 2.1, a mixture of air and carbon monoxide is passed through a water saturator and fed to the reactor thereafter. The reactor is packed bed tubular reactor. Typically catalyst quantity used for these tests was 0.1 g. After passing through the reactor the gas stream was fed to the gas chromatograph through a moisture trap. The resulting gas mixture was analyzed for carbon monoxide, carbon dioxide, oxygen and nitrogen content. As seen in figure 2.2, the catalyst could be tested in presence of optional packed bed of additional sorbents.
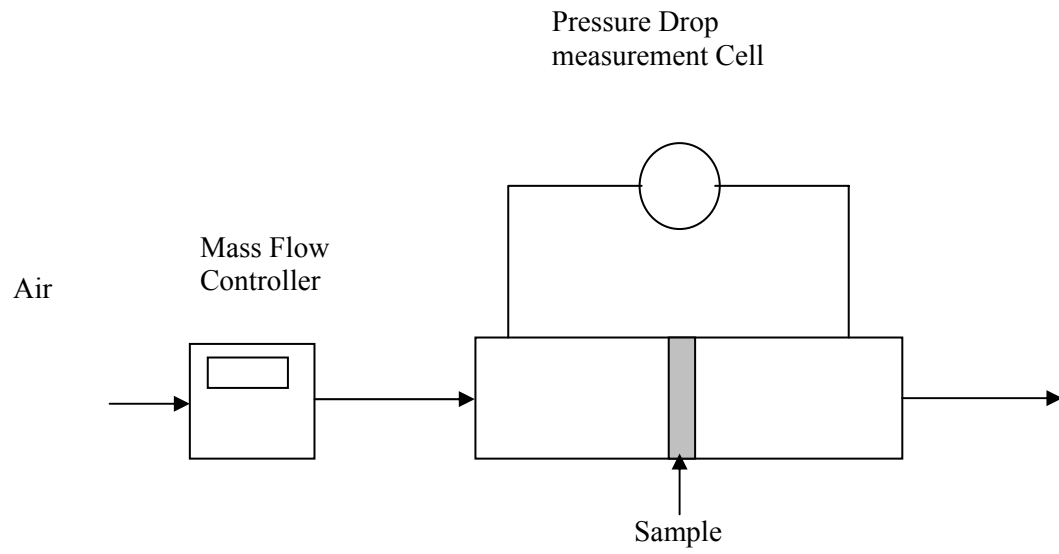
Figure 2.3 Pressure Drop Measurement Apparatus

II.4   Details of Instruments and Equipments used

Table 2.2 gives the list of equipments/instruments used for CO oxidation set up.

Table 2.2: List of Equipments/Instruments used for CO Oxidation Set up

Sr. No.	Item	Description	Range of Operation
1.	Reactor	Glass 0.5 cm dia	
2.	Reactor Furnace	Tube Furnace	$0 - 500\ ^0C$
3.	Air Flow Controller	Make: Omega Co.	$0 - 35$ LPM
4.	CO Flow Controller	Make: Omega Co.	$0 - 2$ LPM
5	Gas Chromatograph	Make: Agilent, Model: 6890, Column: Molecular sieves, Detector: TCD	
6.	CO analyzer	Make: RAE systems model: QRAE plus®	0- 1500 ppm

II.4.1 Experimental Conditions

The experimental conditions for low temperature oxidation were as follows for given sets of experiments:

CO concentration: 0.25 – 2%

Face Velocity: 0.9- 3 cm/sec

Water Content: 3%

Temperature: $20 - 100\ ^0C$

Pressure: 1 atm

II.5 **Pressure Drop Measurements:**

Pressure drop through the Microfibrous material was measured using a sample cell consisting of 0.75 in. Swagelok® Ultratorr fitting with 0.75 in. SS tubing inserted into the ends of the fitting. The cell was equipped fitted with spacers inside the fitting to hold the sample of Microfibrous material properly. The cell was connected to the outlet of a mass flow controller (Omega, 0 – 50 LPM). Pressure drop was measured by a DP cell (Omega, PX154-010DI) and the readings were indicated by a four digit process meter (Omega DP24E). The pressure drop was measured at various values of the inlet flow rate.

Schematic diagram of pressure drop measurement apparatus is shown in figure 2.3.

II.6   Apparatus for Commercial Product Testing:

Schematic diagram of apparatus for testing of commercial products namely canister of Drager® Parat C® and Monolith of Essex® plus 10® are shown in figures 2.4 and 2.5 respectively.

The apparatus were constructed out of PVC pipes with flanges for holding the Drager® canister. For monolith testing, the PVC pipe was fabricated to be able to hold the monolith. The edges of the monolith were sealed using high vacuum silicone sealant. This pipe was then connected via a socket to another pipe which was used for outlet CO measurement section. Air and carbon monoxide mixture at appropriate concentration level passes through moisture saturator and then flows through the canister. QRAE® detector measures the outlet CO concentration.
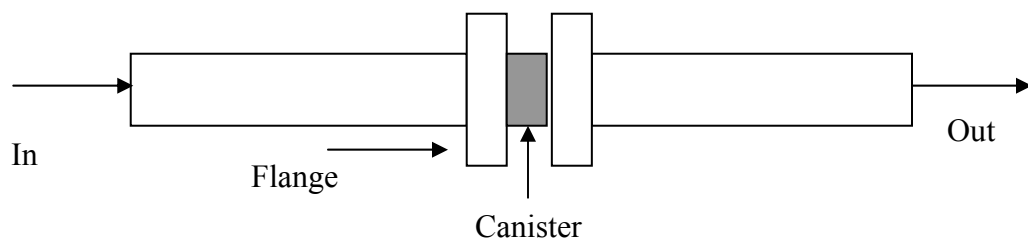
Figure 2.4: Schematic of Drager® Canister Testing Reactor
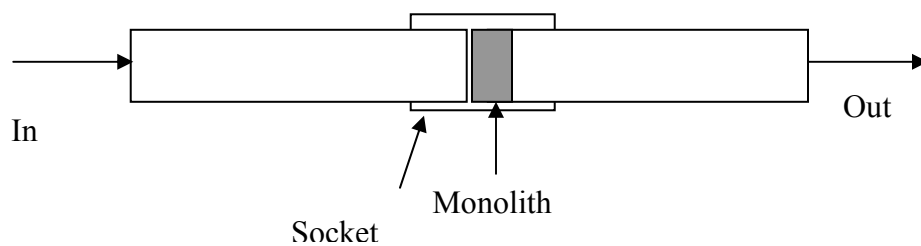
Figure 2.5: Schematic of plus 10® Monolith Test Reactor

II.7   Analytical Section:

This section describes the analytical techniques used for low temperature oxidation of carbon monoxide.

II.7.1 Measurement of Inlet CO Concentration:

For measurement of inlet CO concentration, gas chromatograph has been used (HP 6890). The detector used was of thermal conductivity detector (TCD). The minimum concentration of CO that can be measured using this column was 100 ppm. The gas chromatograph has been equipped with computer to analyze the data and interface software to communicate with computer.

II.7.1.1 GC Calibration:

The gas chromatograph was calibrated using standard gas mixture ordered from BOC/Air products®. It was calibrated in the beginning and end of every experiment.

II.7.2 Measurement of Relative Humidity

Relative humidity was measured using relative humidity detector.

II.7.3 CO Detection and Datalog:

Carbon monoxide can be detected with a sensitivity of 0.1 ppm using the QRAE® plus detector. The detector works on the principal of electrochemical sensor. It is an online type of detector and also logs real time data of carbon monoxide concentration. Once the datalog is over, it can be connected to computer to download the data.

II.7.3.1 Detector Calibration:

The QRAE® detector was calibrated using standard gas ordered from RAE® systems. The calibration was done at least once for each set of experiments.

II.7.3.2 Data Download:

Following procedure should be used to download the data:

1. Make sure the computer has Pro RAEsuite® software that logs the data.

2. Launch the Pro RAEsuite program from the PC

3. Please make sure that the instrument is fully charged before connecting it to PC. If the instrument runs out of power while the downloading process is on, processor may hang up and the unit would need to be returned to factory.

4. Turn on the instrument and connect the computer interface cable between the instrument and the computer

5. Put the instrument into PC communication mode. This can be done by toggling the main menu with the mode key until an option 'communicate with PC?' appears and then press the [Y/+ button].

6. The instrument should display 'Ready to communicate'

7. Under the communications menu in ProRAE Suite, click on 'receive data'. A window will popup reminding to connect the instrument with PC and put it in 'communication with PC' mode.

8. Click 'OK' on the popup window. The download may take few minutes depending upon, how much data is present on the instrument.

9. If communication fails, please check connected cable and the communication/setup port window in ProRAE suite to make sure that the correct

COM port is connected. (COM 1). Also check if the instrument is in 'Ready to communicate' mode.

II.7.3.3 Exporting Data to Excel®:

1. Only data files can be exported, one file at a time.

2. Launch the ProRAE suite ® program from the PC.

3. Display a data file by either by opening a file stored on the computer or by downloading data as described above.

4. Select one of the events and proceed to Option >> Export Text which will bring up the 'Save As' window, save the file. (File type automatically should be 'Tab delimited text files' *.txt)

5. Launch Excel® and go to File >> Open option

6. This will bring up the 'Open' window. At the bottom of the window change file type to 'All Files'.

7. Select the required file to be exported

8. Once the file is opened, the 'Text Import Wizard' window will appear. (3 steps)

9. Click 'Next' to go to step 2, under delimiters click 'Space' in addition to the already selected 'Tab'.

10. Click finish and an excel spreadsheet should appear containing the exported data.

Typical data file as well as exported excel files are shown in Appendix A.

CHAPTER III

RESULTS AND DISCUSSION

III.1 Catalyst Screening Tests

This part contains the activity measurements in terms of CO conversion for various catalysts prepared as a part of this study. Appendix 3.1 lists all the catalysts prepared and tested. The typical conditions used for this catalyst testing were 2% Carbon monoxide in excess air at room temperature.

III.1.1 Gold Based Catalysts

Table 3.1 gives the list of gold based catalysts tested for activity. The activity is stated in terms of initial conversion (IC) and time required for conversion to start dropping from 100% if applicable (t_{drop}). The initial conversion stated here is 100% which can correspond to anywhere from 0 to 100 ppm of CO content in the product stream.

Out of the gold based catalysts prepared, 10% Au/MnO_x is the only catalyst that is capable of removing carbon monoxide completely for first 25 minutes. This is mainly due to higher gold content as well as significant quantity of manganese present in the oxide form. Same metals when loaded on high surface area supports i.e. silica, alumina, zeolite, BPL carbon and titania do not show appreciable conversion due to significant reduction in total metal sites available for oxidation and dispersion might not be as fine as it was observed in Au/MnO_x [1.20]. Gold supported on TiO_2 is another gold based catalyst capable of exhibiting high activity for CO conversion (>80%) for first 15 minutes before it starts deactivating. The metal support boundary here is responsible for catalytic activity [1.29].

But this catalyst is tested without any moisture in the feed. When the catalyst is tested with 3% moisture content in the feed, the conversion drops very fast as water acts as a deactivating agent for the catalyst. When gold/titania is promoted with suitable transition metal such as manganese, the activity drops significantly thereby indicating that promoter affects the reaction adversely.

Table 3.1: Activity Tests of Gold Based Catalysts for Low Temperature CO Oxidation

Sr. No.	Catalyst	IC (%)	t_{drop} (min)	Notes
1.	10% Au/MnO_x	100%	25	(10% Au)
2.	5% Au/MnO_x	44%	NA	(5% Au)
3.	2.5 at% Au/Fe_2O_3	6%	NA	(2.5% Au)
4.	1.3%Au-Fe_2O_3-Al_2O_3	4%	NA	(1.3% Au)
5.	Au - Mn – Alumina	8%	NA	

6.	Au - Mn – Silica	9%	NA	
7.	Au - Mn – Zeolite	7%	NA	
8.	Au - Mn – BPL carbon	7%	NA	
9.	Au - Co – Silica	7%	NA	
10.	Au - Co – Alumina	8%	NA	
11.	Au/TiO$_2$	88%	15	(4% Au)
12.	Au/Mn/TiO$_2$	40%	NA	(4% Au)

III.1.1.1   Au/MnO$_x$ Based Catalysts:
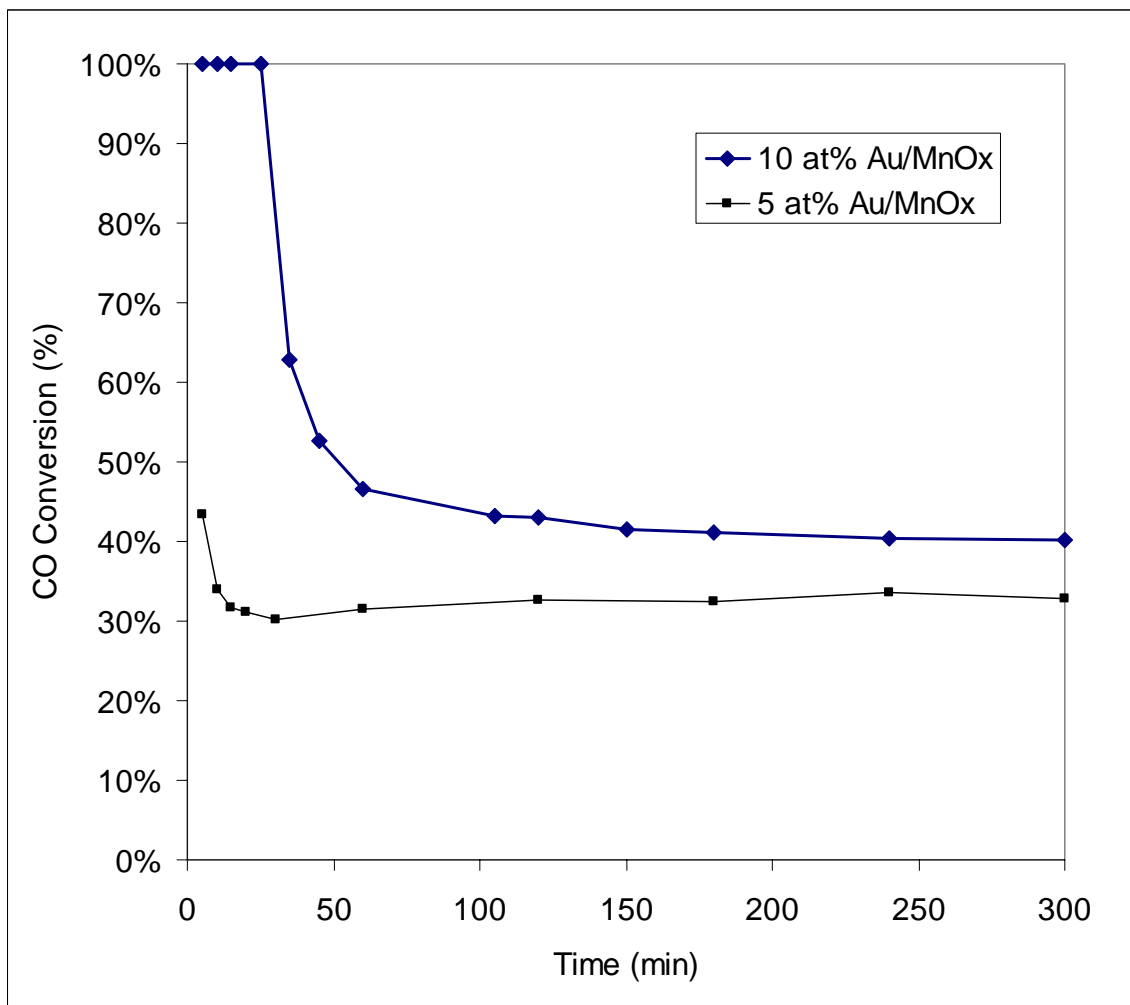
Figure 3.1: Activity Tests of Au/MnO$_x$ Catalysts

Conditions:

Inlet CO Concentration = 2 %

Relative Humidity = 90%

Catalyst loading= 0.1 gm

As shown in figure 3.1, the CO conversion drops to below 50% in one hour. The activity drop can be explained by irreversible adsorption of CO on the surface of gold

which is a pronounced effect for CO oxidation over most metals. Moreover OH⁻ ions from water are adsorbed irreversibly on the surface of gold thereby physically blocking active sites present for CO adsorption [1.30].

III.1.1.2   Activity Tests of Supported Gold Catalysts:

Fig 3.2 and fig 3.3 show the results from activity tests of various supported gold catalysts prepared by method of conventional impregnation.

None of the catalysts show appreciable conversion. This is explained by Haruta et al [1.20]. According to these authors, finely dispersed gold only is responsible for catalysis. Conventional impregnation method of catalyst preparation fails to reach the required particle size of gold on the support.

Figure 3.2: Activity Tests of Supported Gold Catalysts

Conditions:

Inlet CO Concentration = 2 %

Relative Humidity = 90%

Catalyst loading= 0.1 gm

Reactor configuration: Packed Bed

III.1.1.3   Activity Test of Au/TiO$_2$ Catalyst:


Figure 3.3: Activity Test of Au/TiO$_2$ Catalyst

Testing Conditions:

Inlet CO Concentration = 2%

Relative humidity= 90%

Catalyst Loading= 0.1 gm

Reactor Configuration= packed bed

As explained earlier, the initial higher activity of Au/TiO_2 catalyst is due to role played by the metal support interaction. Same observation is reported by Grunwaldt et al [1.28].

III.1.2 Platinum Based Catalysts

Table 3.2 shows the activity measurement studies for Platinum based catalysts.

Table 3.2: Activity Tests of Platinum Based Catalysts

Sr. No.	Catalyst	IC (%)	t_{drop} (min)	Notes
1.	$Pt-Fe_2O_3-Al_2O_3$	7	NA	4% Pt
2.	$4\%Pt-CeO_2-Al_2O_3$	5		
3.	$4\%Pt-Mn_2O_3-Al_2O_3$	4		
4.	$2\%Pt-Al_2O_3$	8%		
5.	$Pt- Co_2O_3 -Al_2O_3$	5		1.1 wt%Pt
6.	$Pt- Co_2O_3 -Al_2O_3$	28		4.7 wt%Pt
7.	$4\% Pt-Co_2O_3-Al_2O_3$	25		4% wt Pt
8.	$4\% Pt- Mn_2O_3-Al_2O_3$	18%		4% wt Pt
9.	$4\% Pt- Co_2O_3-SiO_2$	7%		
10.	$4.7\% Pt- Co_2O_3-Al_2O_3$	70%		Co:Al = 0.04, 4.7wt% Pt
11.	Pt/TiO_2	71%		
12.	$Pt/Co/TiO_2$	75%		
13	$Pt/Mn/SiO_2$	100%	10	5.7 wt% Pt

Among the platinum based catalysts, $Pt/Mn/SiO_2$ is the only catalyst that give100% CO conversion. $Pt/Mn/SiO_2$ gives 100% conversion for first 10 minutes before it starts deactivating. All these catalysts are tested with the presence of 3% moisture in the feed.

III.1.2.1   Activity Tests of Supported Platinum Catalysts:
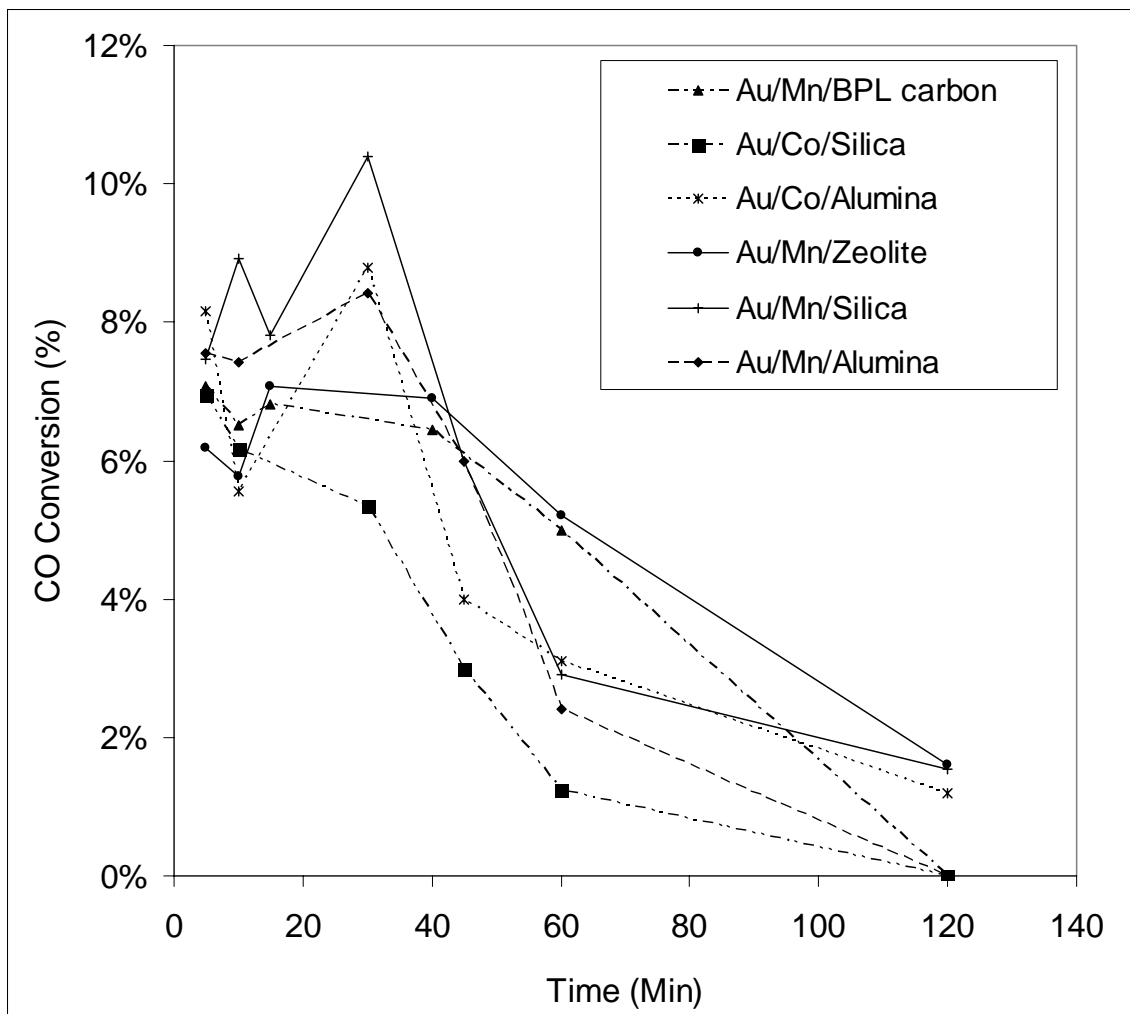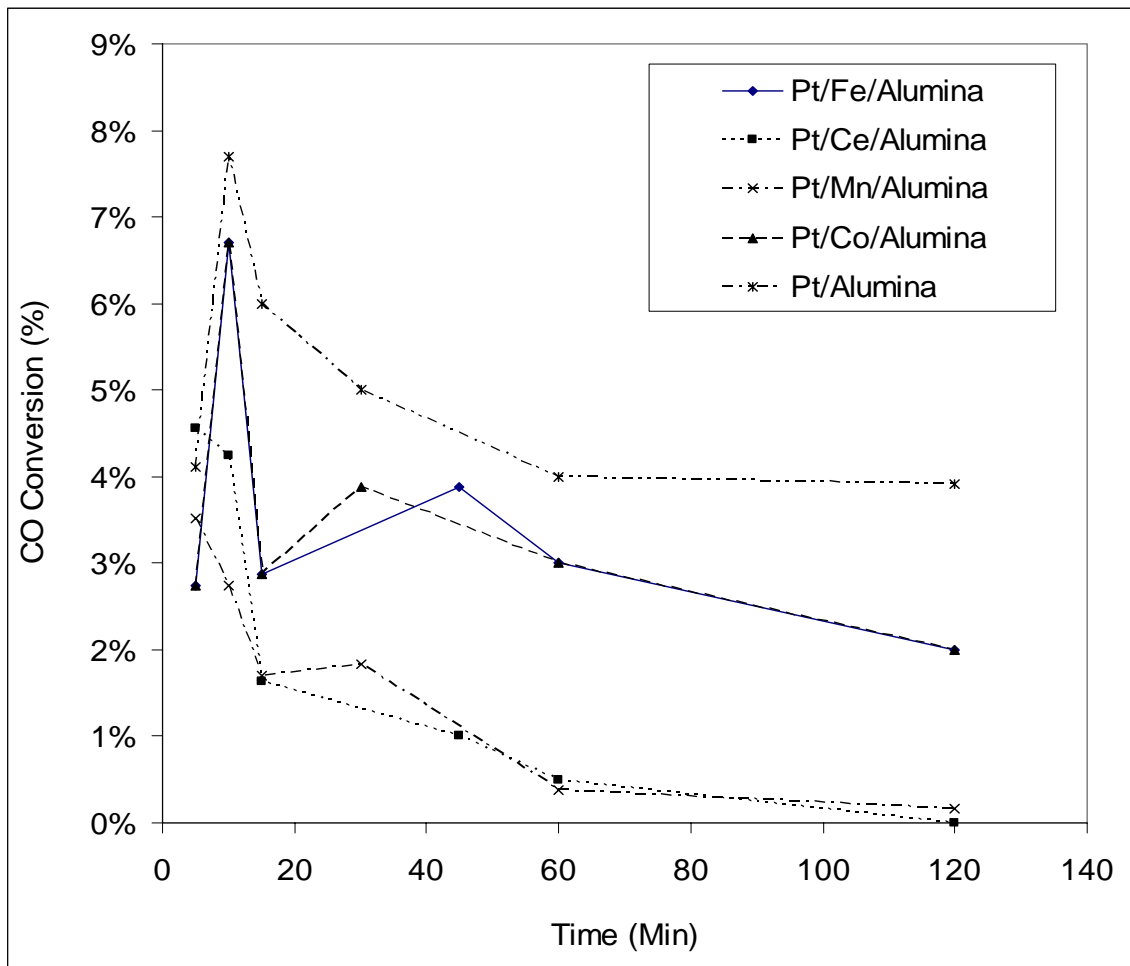

Figure 3.4: Activity Tests of Pt Based Supported Catalysts

Testing Conditions:

Inlet CO Concentration = 2%

Relative humidity= 90%

Catalyst Loading= 0.1 gm

Reactor Configuration= packed bed

Figure 3.4 shows the activity of promoted and unpromoted platinum based catalysts on high surface area alumina. The promoters were chosen from transition metal elements. None of these catalysts showed appreciable conversion for low temperature oxidation.

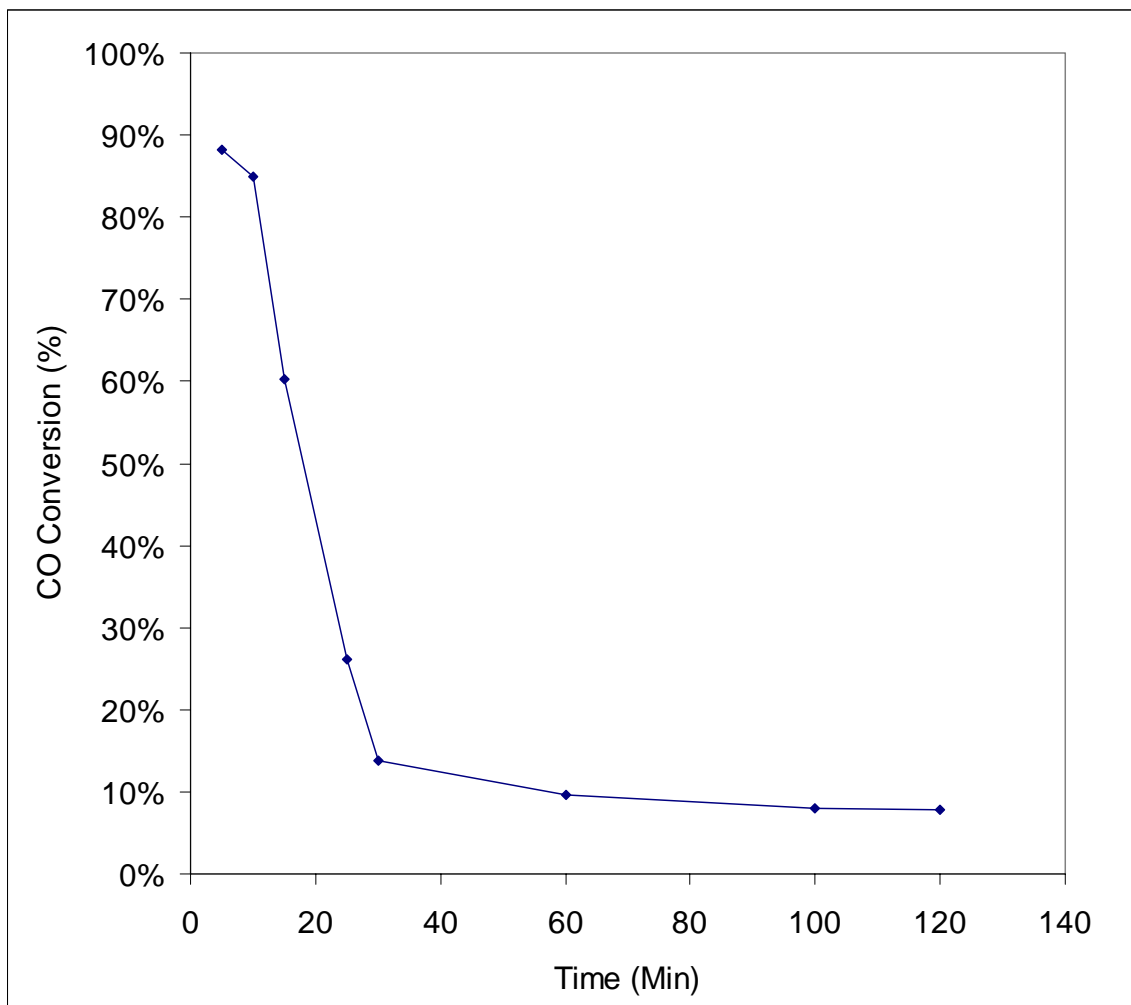III.1.2.2   Platinum Supported on TiO_2:
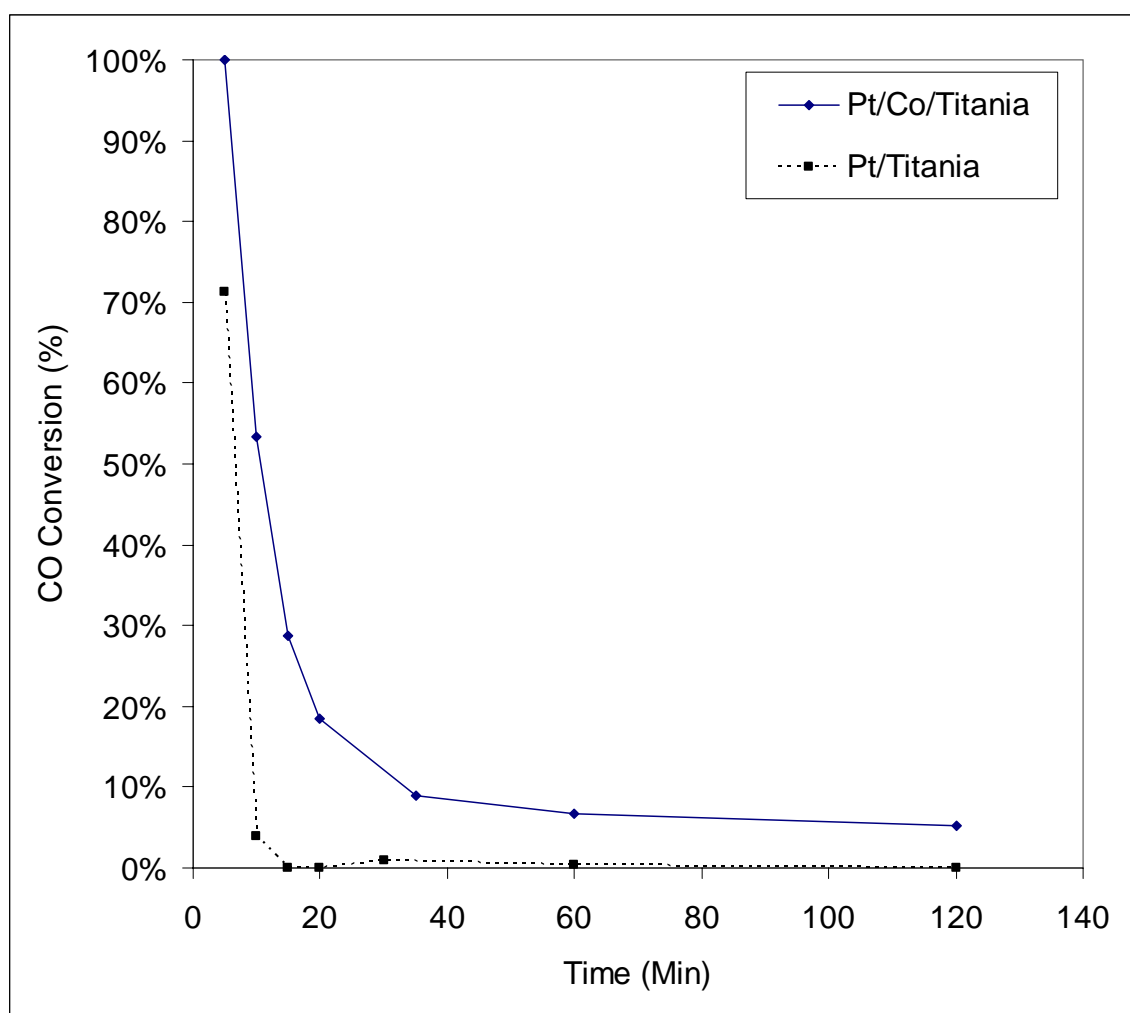
Figure 3.5: Activity Test of Platinum Based Titania Supported Catalysts

Testing Conditions:

Inlet CO Concentration = 2%

Relative humidity= 90%

Catalyst Loading= 0.1 gm

Reactor Configuration= packed bed

Figure 3.5 shows the activity test for titania based Platinum catalysts. The unpromoted Pt/TiO_2 catalyst shows high activity in the beginning but drops rapidly. The cobalt promoted catalyst shows better activity. The conversion is 100% for first 5 minutes and then drops rapidly.

III.1.3 Miscellaneous catalysts

Few more catalysts were tested for CO oxidation are listed in table 3.3

Table 3.3: Tests of miscellaneous catalysts

Sr. No.	Catalyst	IC (%)	t_{drop} (min)	Notes
1.	$Pd – CeO_2 - TiO_2$	22%		1 wt% Pd
2.	CuO/CeO_2	10		
3.	Hopcalite 1	14%		Cu, Mn mixed oxide
4.	Co/TiO_2	2		
5.	Mn/TiO_2	8		
6.	CuCl	61		Adsorbant
7.	Hopcalite $_3$	25%		Ru added ,without moisture
8.	Mn/SiO_2	8%		

None of these catalysts showed appreciable conversion for CO oxidation.
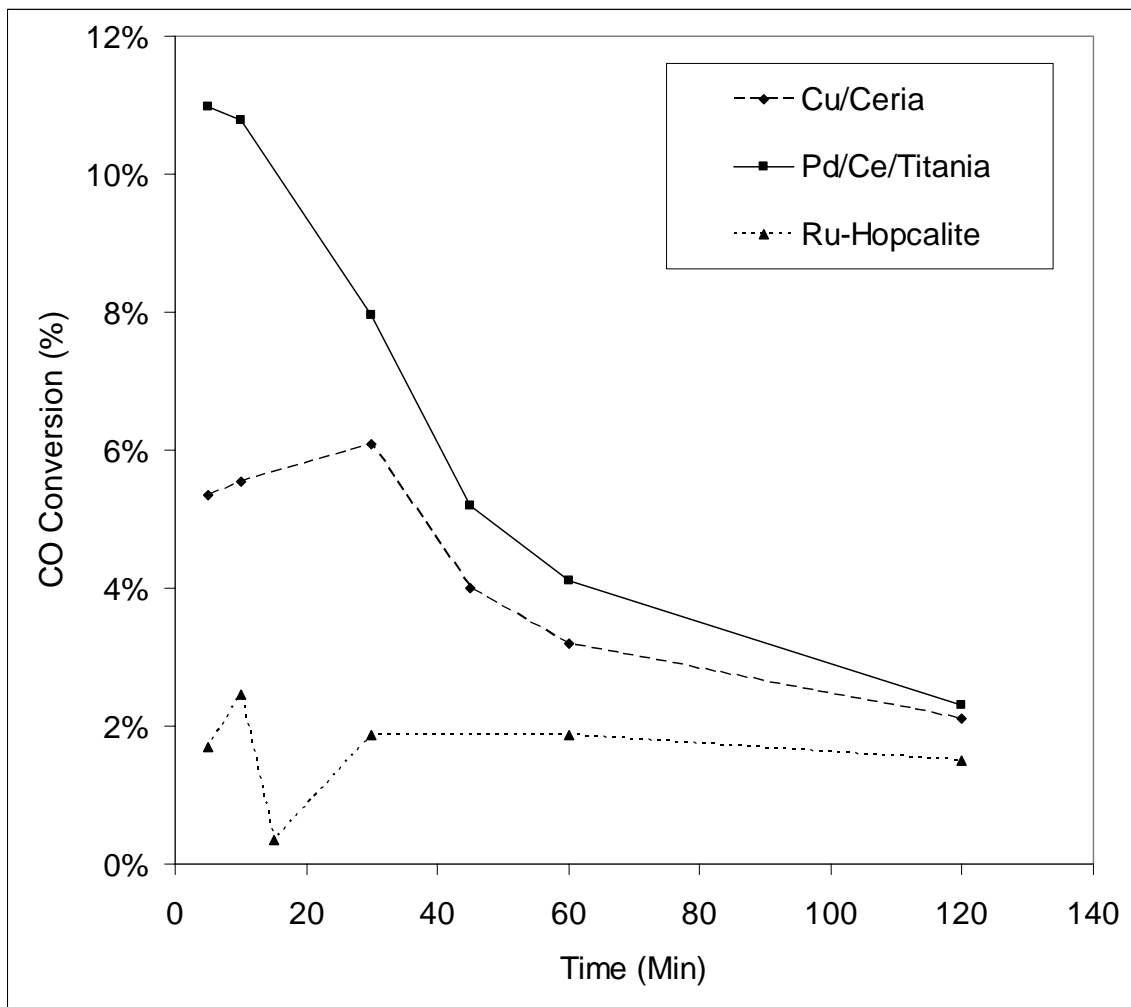
Figure 3.6: Activity Tests of Pd/Ce/Titania, Cu/Ceria and Ru-hopcalite

Testing Conditions:

Inlet CO Concentration = 2%

Relative humidity= 90%

Catalyst Loading= 0.1 gm

Reactor Configuration= packed bed

Figure 3.6 shows the activity test of Pd/Ce/TiO$_2$, Cu/CeO$_2$ and Ru-Hopcalite catalysts for low temperature oxidation. As seen here, none of these catalysts shows appreciable conversion of carbon monoxide.

III.1.4 Commercial Catalysts and Sorbents
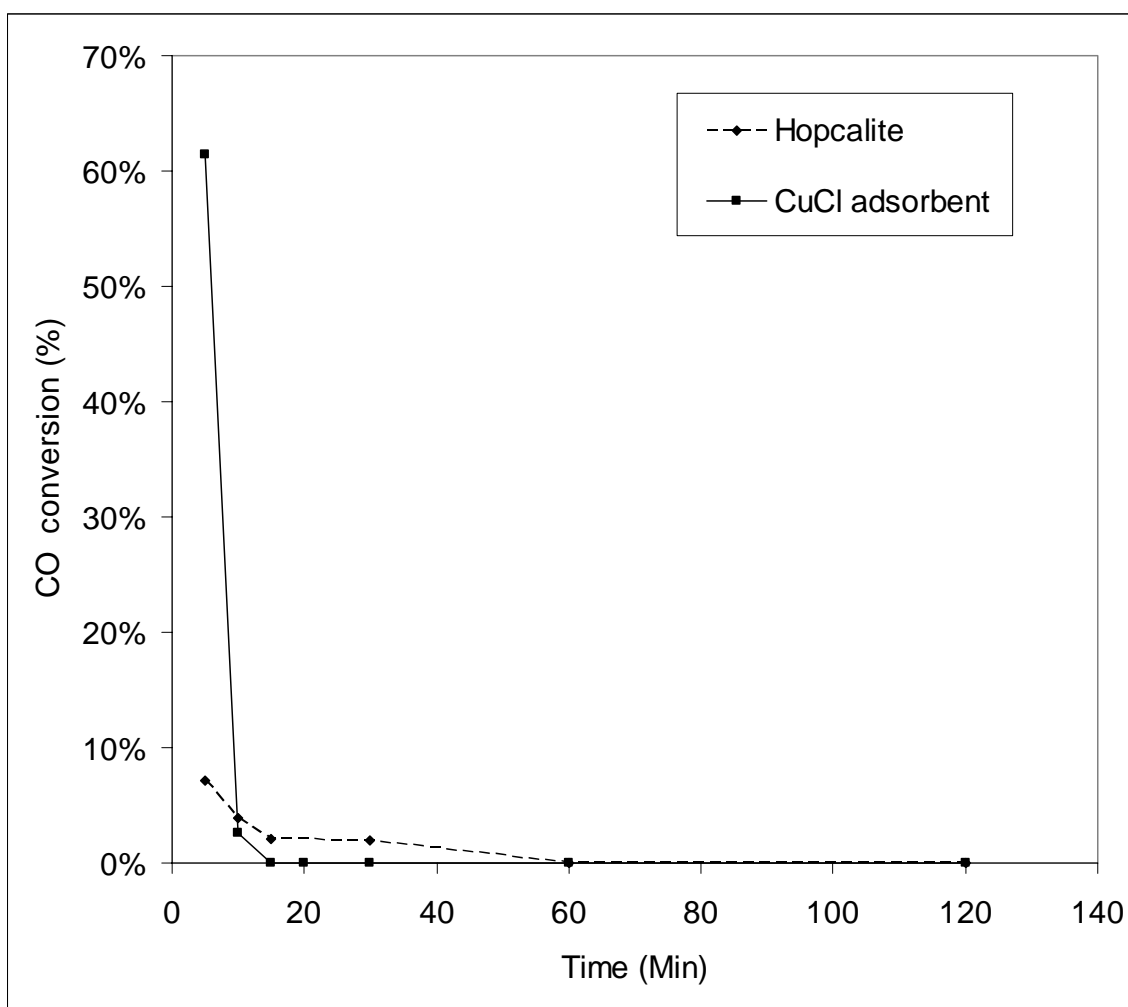
Figure 3.7: Activity Test of Commercially Available CuCl Adsorbent and Hopcalite Catalyst

Figure 3.7 shows the activity tests of commercially available CO removal products i.e. cuprous chloride adsorbent and hopcalites (Cu - Mn mixed oxide) catalyst.

CuCl was very active for first few minutes and the activity dropped suddenly. This means the adsorbent has very short breakthrough time. The CO removal action happens to be by formation of Cu(CO)Cl complex as it is well known in literature. Hopcalites do not show appreciable activity under the given conditions. Hopcalites are known to deactivate very fast in presence of moisture as mentioned in chapter 1.

III.2   Catalyst Selection

Amongst the various catalysts tested $Pt/Mn/SiO_2$ after calcinations and $Pt/Co/Al_2O_3$ with reduction as pre-treatment under flowing hydrogen at 250 ^0C were chosen to be suitable candidates for low temperature oxidation of carbon monoxide. Between these two catalysts, $Pt/Mn/SiO_2$ was chosen to be the first candidate as it does not need any pre-treatment before using.

III.3 Effect of Catalyst Making Process and Composition on the Performance of Pt/SiO₂

III.3.1 Effect of Promoter:

Figure 3.8 shows the comparison between activities of promoted and un-promoted Pt/SiO₂ catalysts. It also shows the activity of Mn/SiO₂ catalyst.
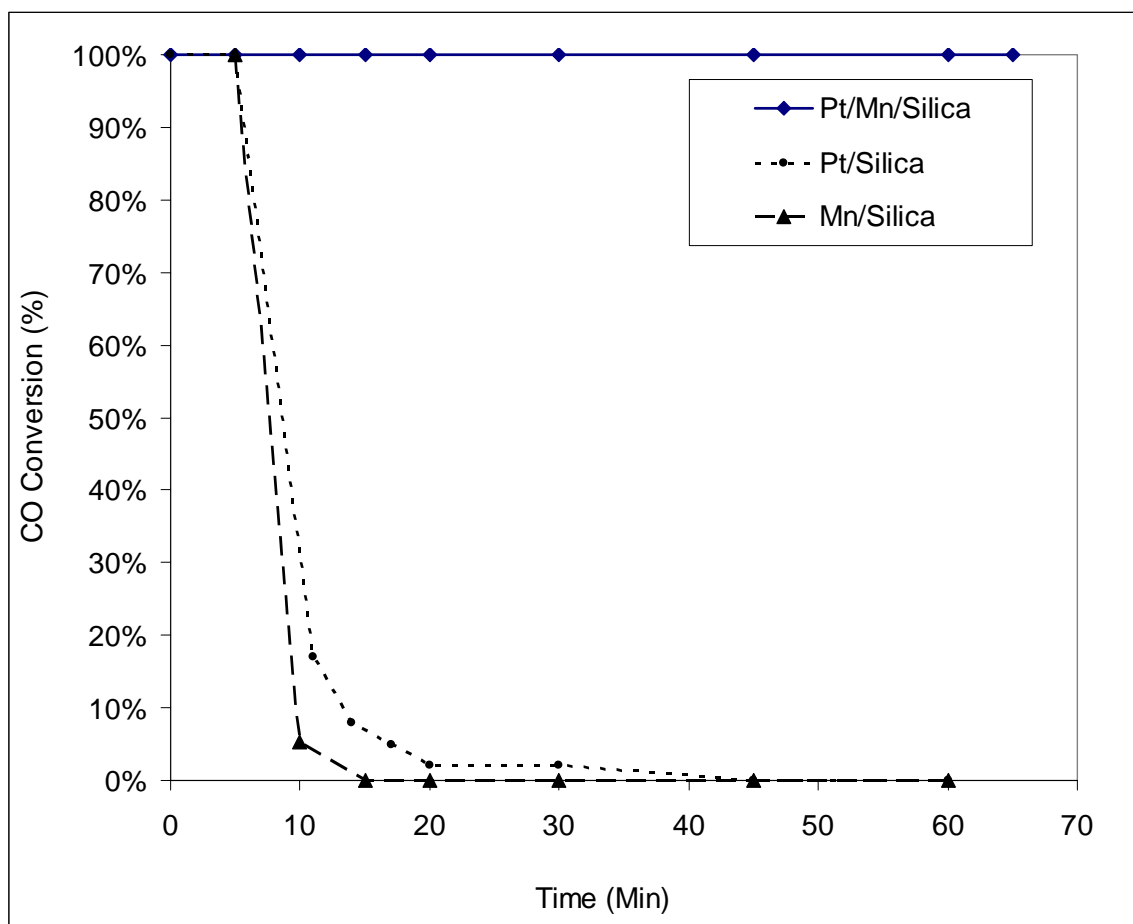
Figure 3.8: Comparison of promoted and un-promoted Pt/silica catalysts

Conditions:

Inlet CO concentration = 2500 ppm

Relative Humidity= 90%

Reactor configuration= microfibrous bed

Promoter= cobalt (Co:Al = 0.4)

As shown in the figure, unpromoted Pt/SiO_2 loses activity quite rapidly. In the first 10 minutes CO conversion drops from 100% to 10%. On the other hand manganese promoted Pt/SiO_2 catalyst shows much sustained activity.

III.3.2 Effect of Promoter on the Activity of Pt/Al_2O_3:

Figure 3.9 shows the enhancement in activity due to addition of promoter to Pt/Al_2O_3.
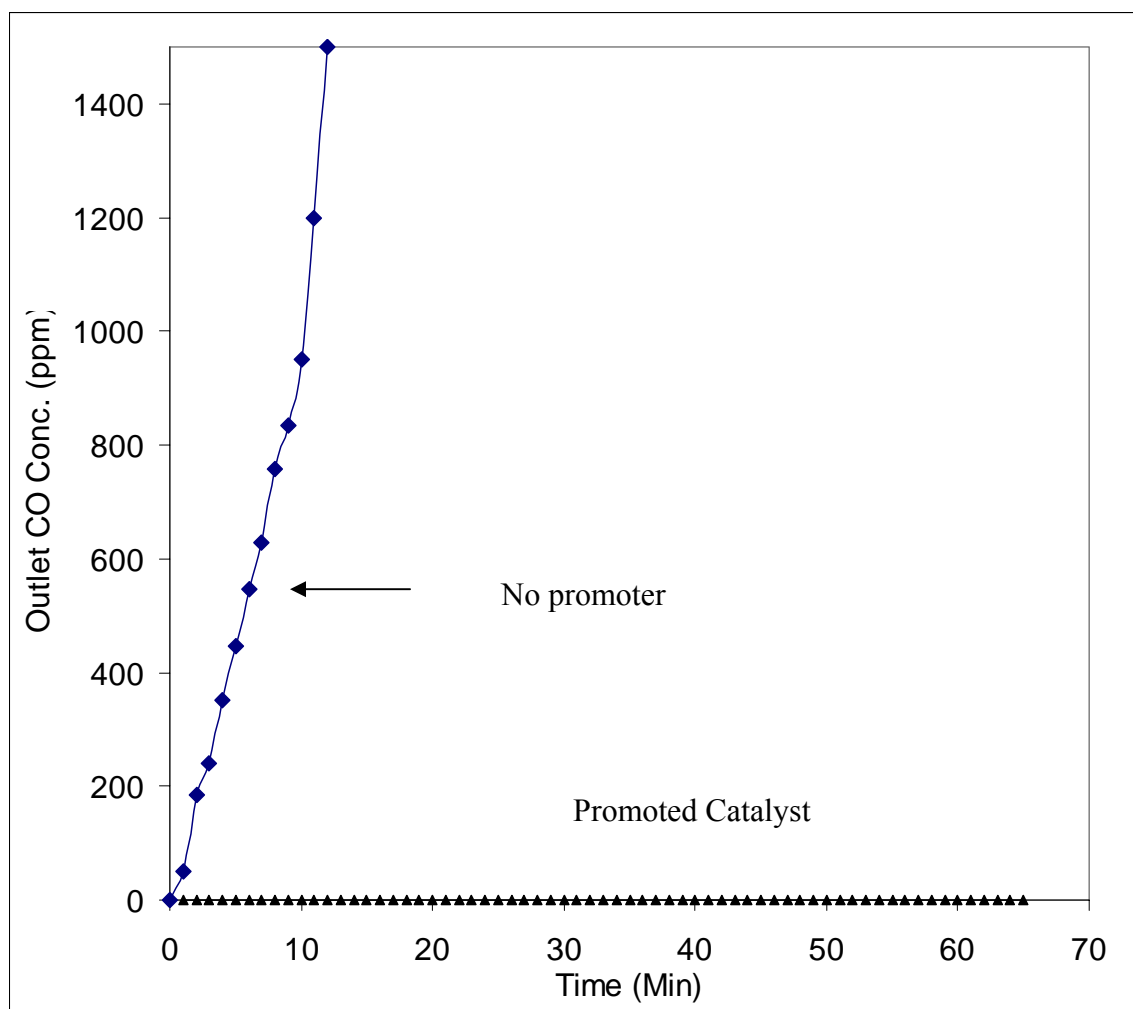
Figure 3.9: Comparison between promoted and un-promoted Pt/Al_2O_3 catalysts,

Conditions:

Inlet CO concentration = 2500 ppm

Relative Humidity= 90%

Reactor configuration= microfibrous bed

Promoter= cobalt (Co:Al = 0.4)

III.3.3 Comparison between Different Promoters:

Figure 3.10 shows the comparison between Pt/SiO$_2$ catalysts promoted by different transition metal promoters. As seen in the figure, among Mn, Co, Fe and Ce, Mn was found to be the best promoter. Co promoted catalyst also shows some activity in the beginning. Fe and Ce promoters do not enhance the activity appreciably.
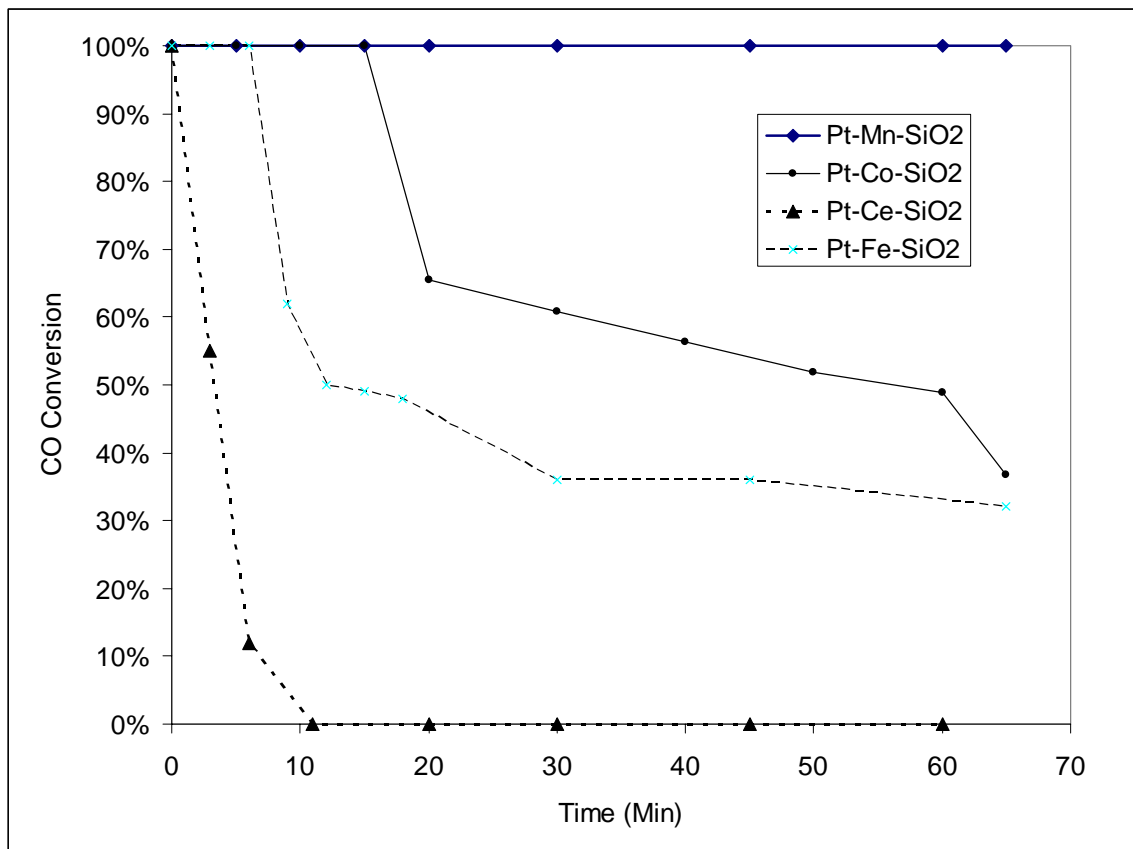
Figure 3.10: Comparison of Various Transition Metal Promoters for Pt/SiO$_2$ Catalyst

Conditions:

Inlet CO Concentration = 2%

Relative humidity= 90%

Catalyst Loading= 0.1 gm

Reactor Configuration= packed bed

III.4 Effect of Operating Conditions on the Performance of Pt/Mn/SiO$_2$

This section discusses the effect by various operating conditions as well as catalyst making parameters and catalyst composition on the performance of Pt/Mn/SiO$_2$ catalyst.

III.4.1 Effect of Temperature

Figure 3.11 shows the effect of operating temperature on the performance of Pt/Mn/SiO$_2$ catalyst. The temperatures studied are 20^0C, 50^0C and 100^0C.

Figure 3.11: Effect of Operating Temperature on the Performance of Pt/Mn/SiO$_2$ catalyst

Conditions:

Inlet CO Concentration = 2%

Relative humidity= 90%

Catalyst Loading= 0.1 gm

Reactor Configuration= packed bed

As shown in figure 3.11, the rate of deactivation of Pt/Mn/SiO$_2$ catalyst decreases

as temperature increases. This can be explained by enhancement in desorption of CO

from the surface due to increase in temperature. Thus temperature helps in slowing down the deactivation process of the catalyst. As temperature is increased to 100^0C, there is no deactivation shown by the catalyst.

III.4.2 Effect of Inlet CO Concentration

Figure 3.12 and 3.13 show the effect of inlet CO concentration on the activity of Pt/Mn/SiO$_2$ catalyst. Figure 3.12, shows the effect of inlet CO concentration when the inlet concentration rages between 1% and 2%. The catalyst loading was 0.1 g. The reactor was operated in integral mode here. The reactor was operated close to a differential mode with much lower catalyst quantities and higher flow rates with lower concentrations of CO. The CO concentrations studies were 2500, 5000 and 7500 ppm shown in figure 3.13.

Figure 3.12: Effect of Inlet CO Concentration on the Performance of Pt/Mn/SiO$_2$ Catalyst

Conditions:

Inlet CO concentration = 2%

Relative humidity= 90%

Catalyst Loading= 0.1 gm

Reactor configuration= packed bed

Figure 3.13: Effect of Inlet CO Concentration on the Performance of Pt/Mn/SiO$_2$ Catalyst

Conditions:

Inlet CO concentration = 2%

Relative humidity= 90%

Catalyst loading= 0.016 gm

Reactor configuration= packed bed

As seen in figure 3.12 and 3.13, at higher inlet concentration of CO, the deactivation of catalyst is much faster. This observation similar to the effect of temperature effect also shows the deactivation by irreversible adsorption of CO on the

72

surface of the catalyst. All the catalysts here were used under dry condition. Hence moisture is not responsible for deactivation.

III.4.3 Effect of Promoter Loading

Figure 3.14 shows the effect of promoter loading on the activity of manganese promoted Pt/SiO$_2$ catalyst.
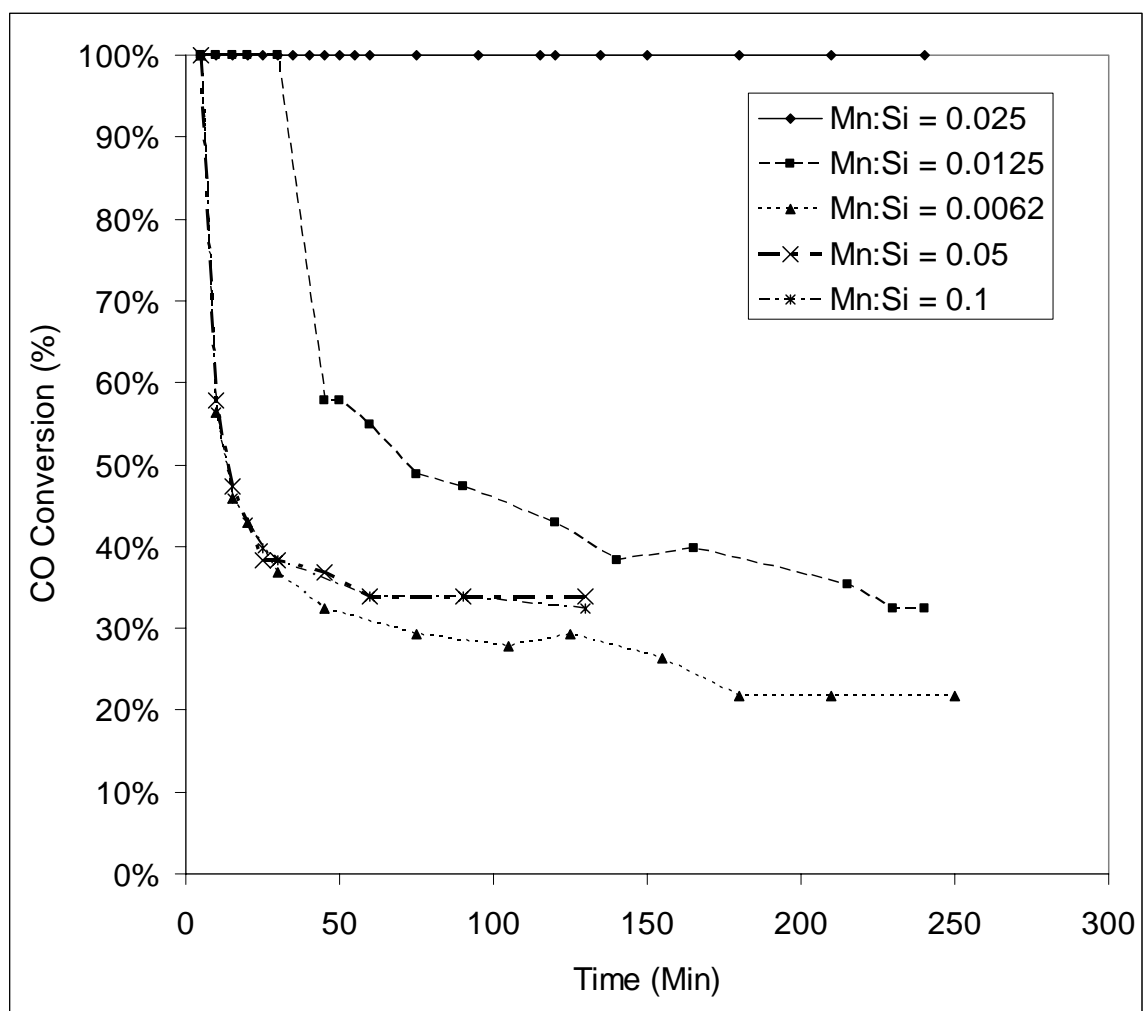
Figure 3.14: Effect of Manganese Concentration on Pt/Mn/SiO$_2$ Performance

Conditions:

Inlet CO concentration = 2%

Relative humidity= 90%

Catalyst loading= 0.1 gm

Reactor configuration= packed bed

As seen in the figure, manganese loading of Mn:Si =0.025 shows the highest catalytic activity. Concentrations above or below 0.25 molar solution of manganese salt do not yield good results. Thus these exists an optimum ratio of manganese to platinum.

III.4.4 Effect of Support on the Activity of Promoted Pt/SiO$_2$

Figure 3.15 shows the effect of various supports on the activity of manganese promoted Pt/SiO$_2$ catalyst. The supports were chosen due to different properties. Alumina being acidic, silica and carbon being neutral to Na-Y-zeolite being basic in nature.
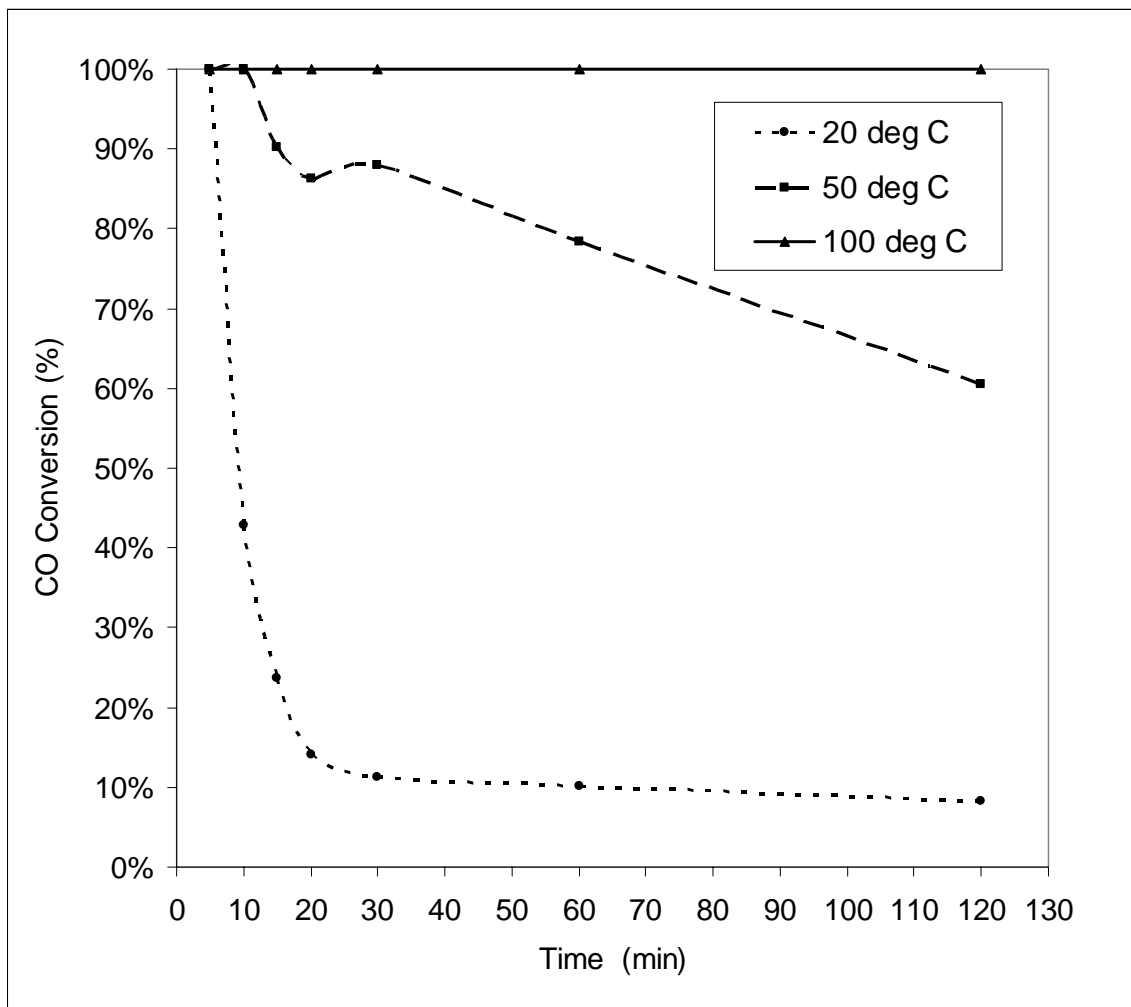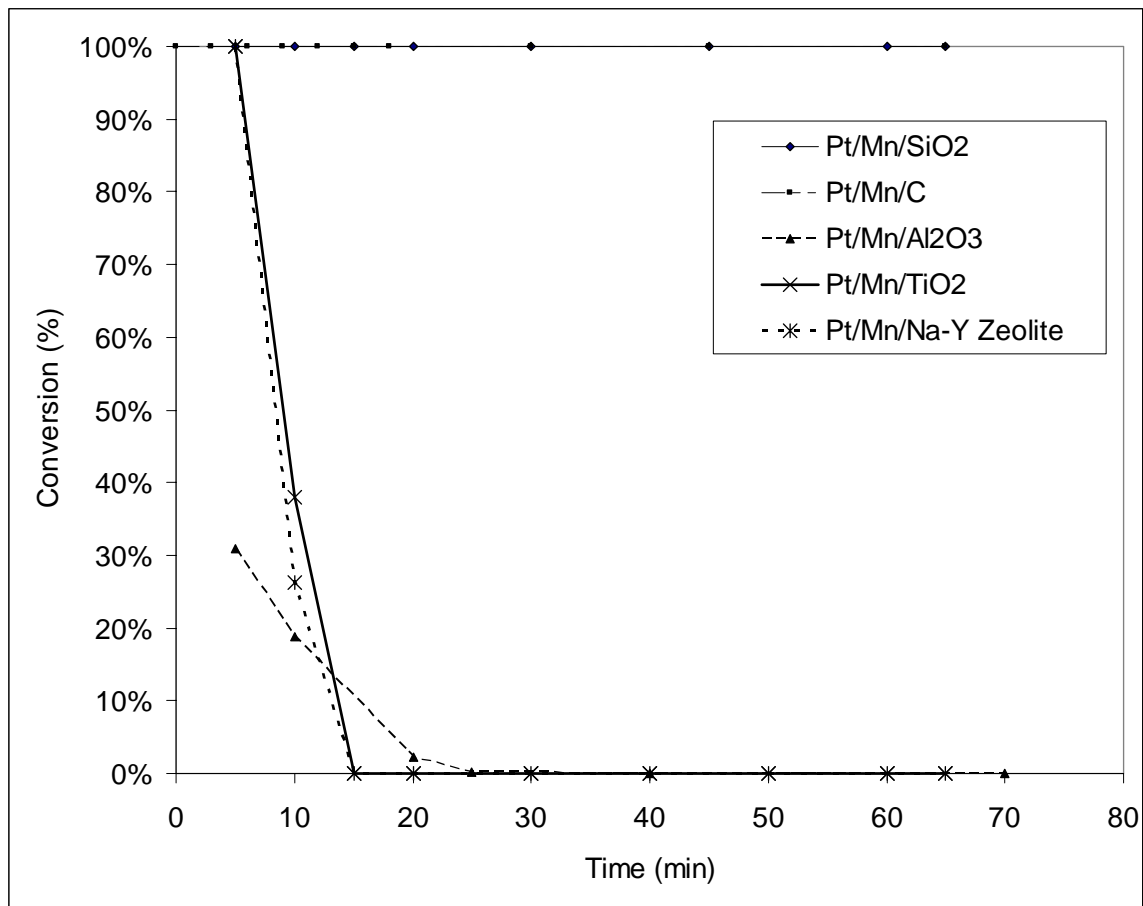
Figure 3.15: Effect of Support on Performance of Promoted Pt Catalysts

Conditions:

Inlet CO Concentration = 2%

Relative humidity= 90%

Catalyst loading= 0.1 gm

Reactor configuration= packed bed

As observed in figure 3.15, silica supported catalyst has highest activity among all the

supports tested.

III.5 Catalyst Activity Details of Pt/Mn/SiO$_2$ to Comply with EN 403

This section shows the effect of various operating conditions to comply with accepted and proposed standards for CO removal.

III.5.1 Effect of GHSV:

Figure 3.18 shows the effect of GHSV on CO conversion. The face velocity was equivalent to 30 LPM flow rate through 500 cm^2 area. The flow rate number comes from EN 403 standards as mentioned before. The area is maximum area that a person can have for fire escape hood.
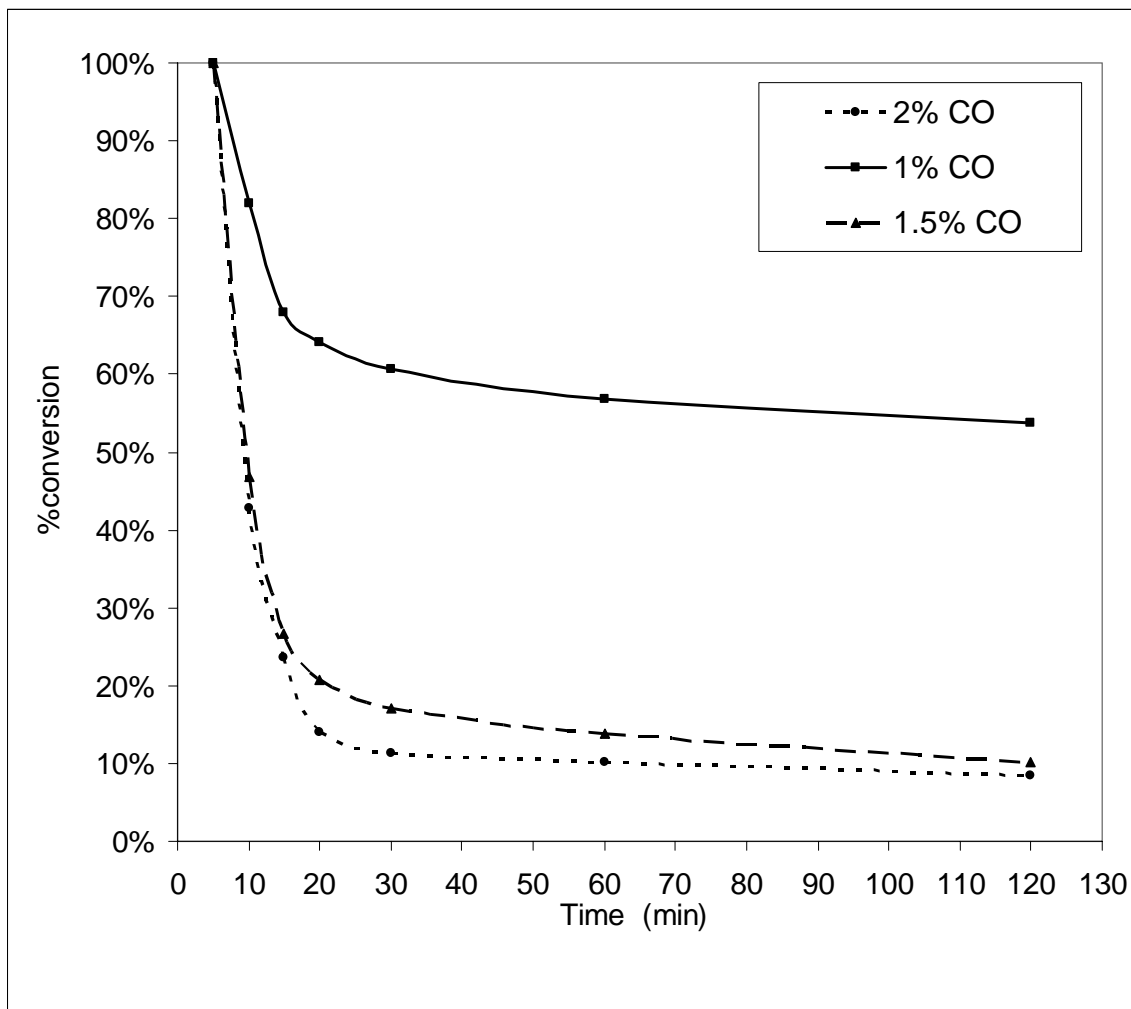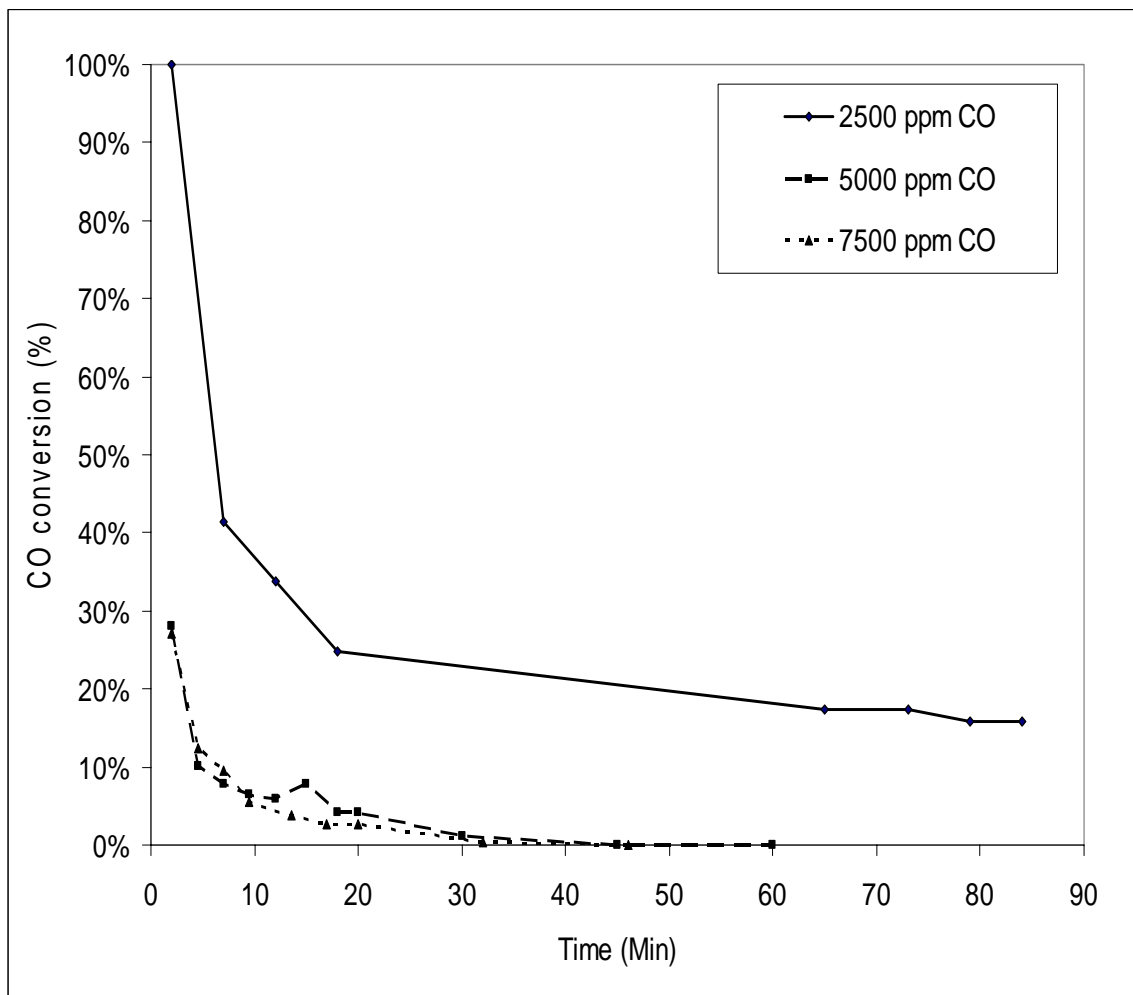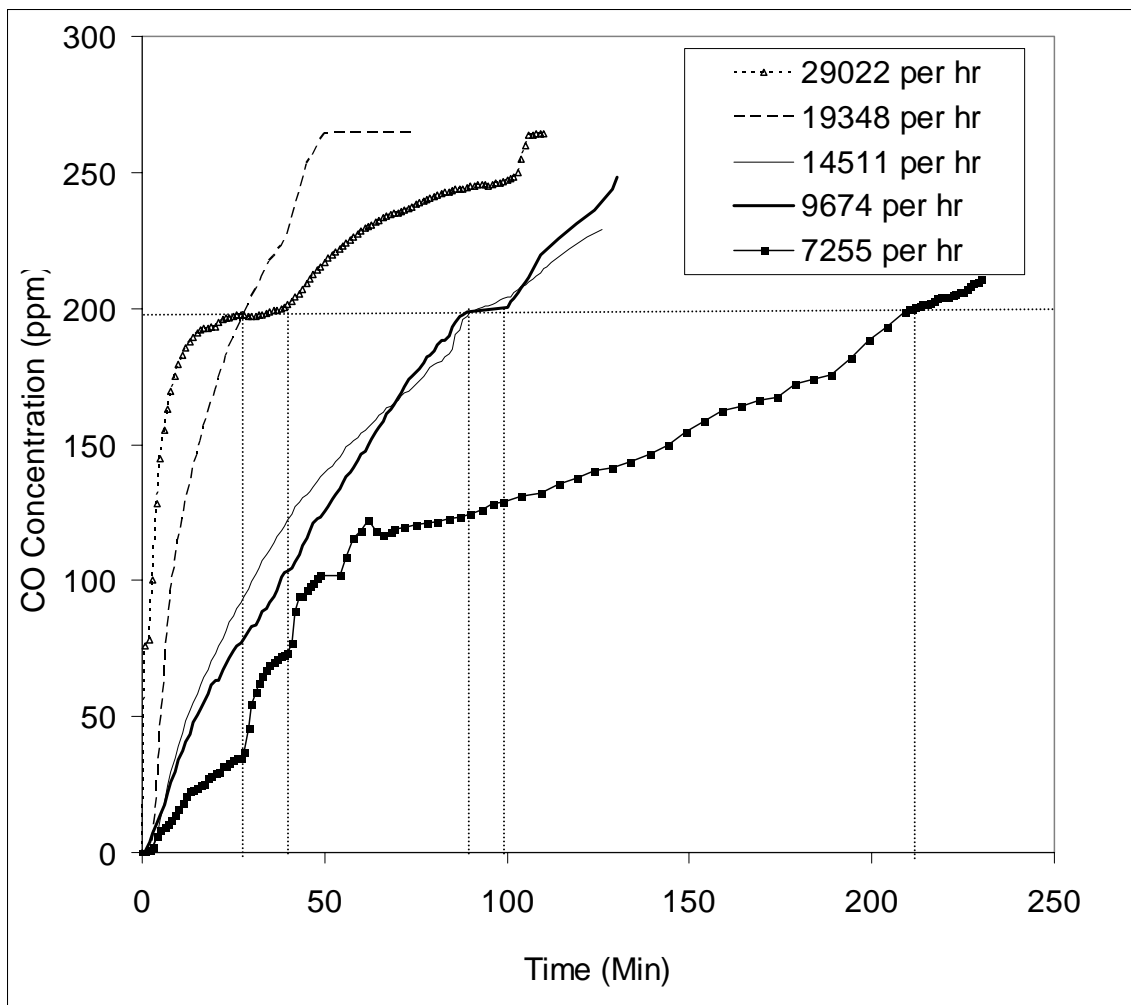
Figure 3.16: Effect of GHSV on the Performance of Pt/Mn/SiO$_2$ Catalyst

Conditions:

Inlet CO Concentration = 2500 ppm

Relative humidity= 90%

Reactor Configuration= microfibrous bed

As shown in figure 3.16, the conversion of CO drops rapidly as GHSV is increased. Time corresponding to 200 ppm of CO concentration is an important

parameter according to EN 403 standards. This is the maximum time upto which the gas mask consisting of CO removal catalyst can be used without any health problems.

Table 3.4 shows the permissible time for which the mask incorporating this catalyst can be used corresponding to each GHSV.

Table 3.4: Gas Life Corresponding to GHSV

Sr. No.	GHSV Hr-1	Permissible Time (min)
1	7255	210
2	9674	98
3	14511	90
4	19348	39
5	29022	29

The maximum GHSV value of 29022 Hr-1 corresponds to a bed depth of 2 mm. Thus a layer of 2 mm think, when incorporated in a fire escape mask of 500 cm^2 area, can provide protection from 2500 ppm carbon monoxide for 29 minutes. Thus this configuration passes the EN 403 standards.

III.6   Intermediate Goal Setting

While this research was progressing towards escape masks meeting EN 403 standards, a survey of commercial products was undertaken. One of the startling observations was that most of the escape masks had canisters and hoods instead of regular masking around the face. At the same time, more stringent CBRN and ANSI/ISEA 110-2003 standards were being proposed. Based on these two major happenings; following various goals of this research work were formulated. These goals are listed in Table 3.5.

Table 3.5: Research Goals Based on Intermediate Findings and Survey

Attribute	Goal
Catalyst activity time	60 minutes minimum
Pressure drop	four fold lower than commercial products (commercial products have a pressure drop of about 45 mm of water through the catalyst bed alone)
Catalyst mass	Order of magnitude reduction (current commercial products have catalyst mass of approximately 170 gm)
Bed depth	Order of magnitude reduction (Current commercial products have a bed depth of about 45 mm)
Standards	Ability to meet more stringent CO reduction standards which were in the proposal stages.
Canister cross section area	85 cm^2 maximum

Based on these formulated goals and information available from these standards, various combinations of following operating variables and parameters became the sample space under consideration. The range of parameters and operating variables has been given in Table 3.6.

Table 3.6: List of Operating Variables and Parameters with Range

Operating variable/ parameter	Range
Catalyst activity time	15, 30 45 and/or 60 minutes
Pressure drop	70 mm of water (maximum permissible)
Inlet CO concentration	1200 – 10000 ppm
Face velocity	6.88 – 21.5 cm/sec
Relative humidity	> 90%
Bed depth	4 mm
Reaction mixture	Carbon monoxide, air, moisture
Temperature	25 ^{0}C
Pressure	1 atm

III.7   Effect of Face Velocity on Activity of Pt/Mn/SiO$_2$

Figure 3.17 and 3.18 show that the approximate bed depth should be minimum 1 cm to meet EN 403 standard at higher face velocities.
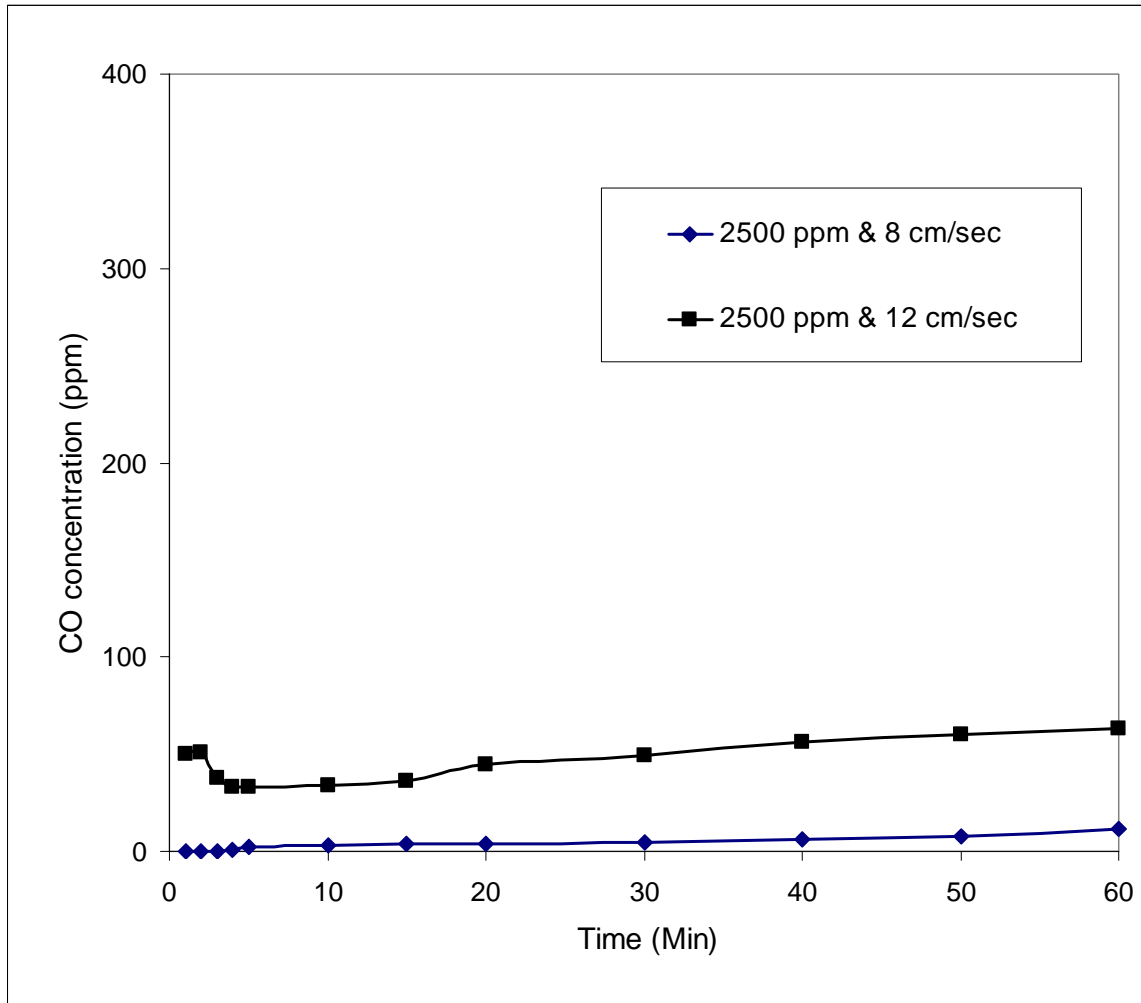
Fig 3.17: Effect of Face Velocity on Catalyst Activity (Pt/Mn/SiO$_2$)

Conditions:

Catalyst: Pt/Mn/SiO$_2$

Relative Humidity = 90%

Inlet CO Concentration = 2500 ppm
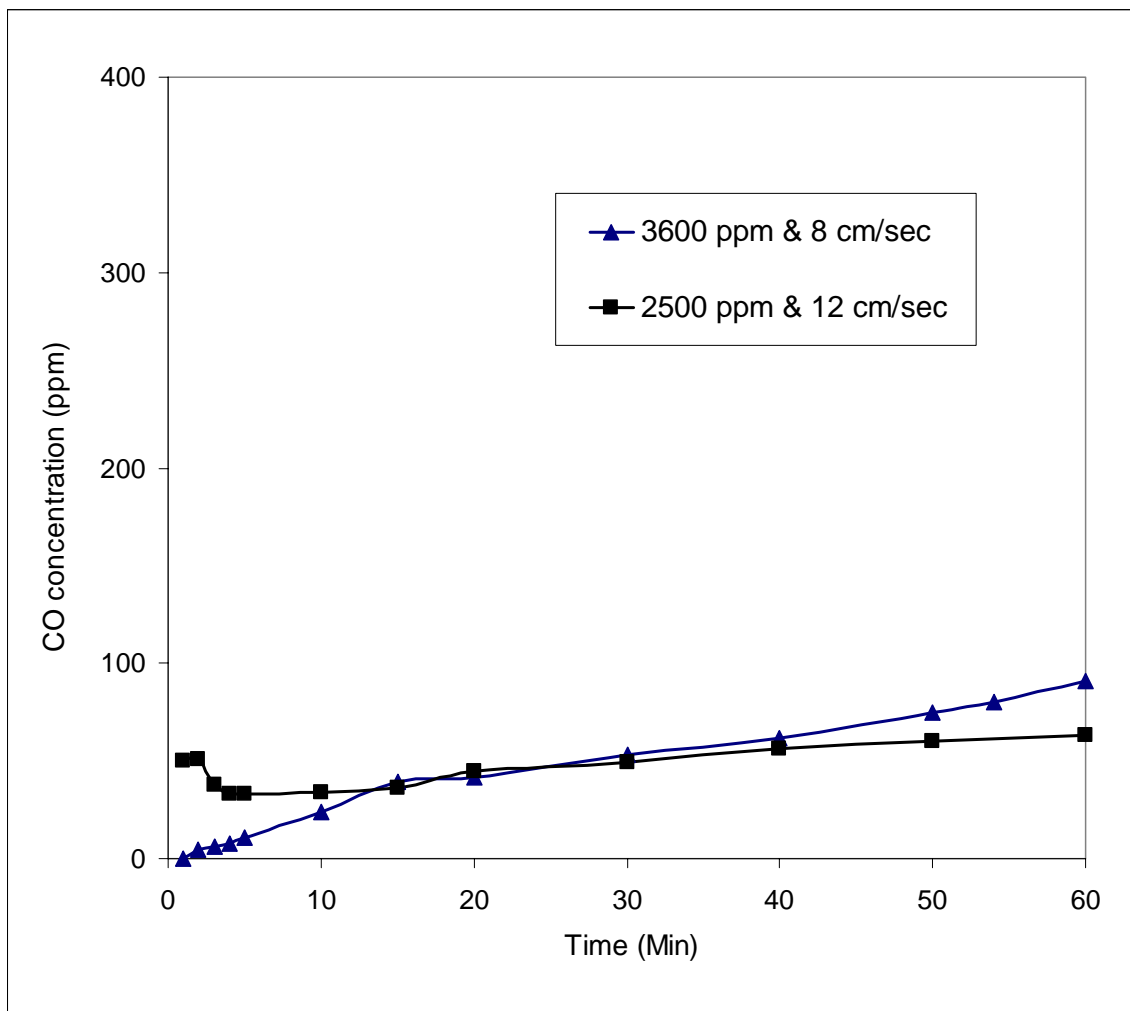
Bed Depth = 1 cm

Figure 3.18: Activity Tests of Pt/Mn/SiO$_2$

Conditions:

Catalyst: Pt/Mn/SiO$_2$

Relative humidity = 90%

Bed Depth = 1 cm
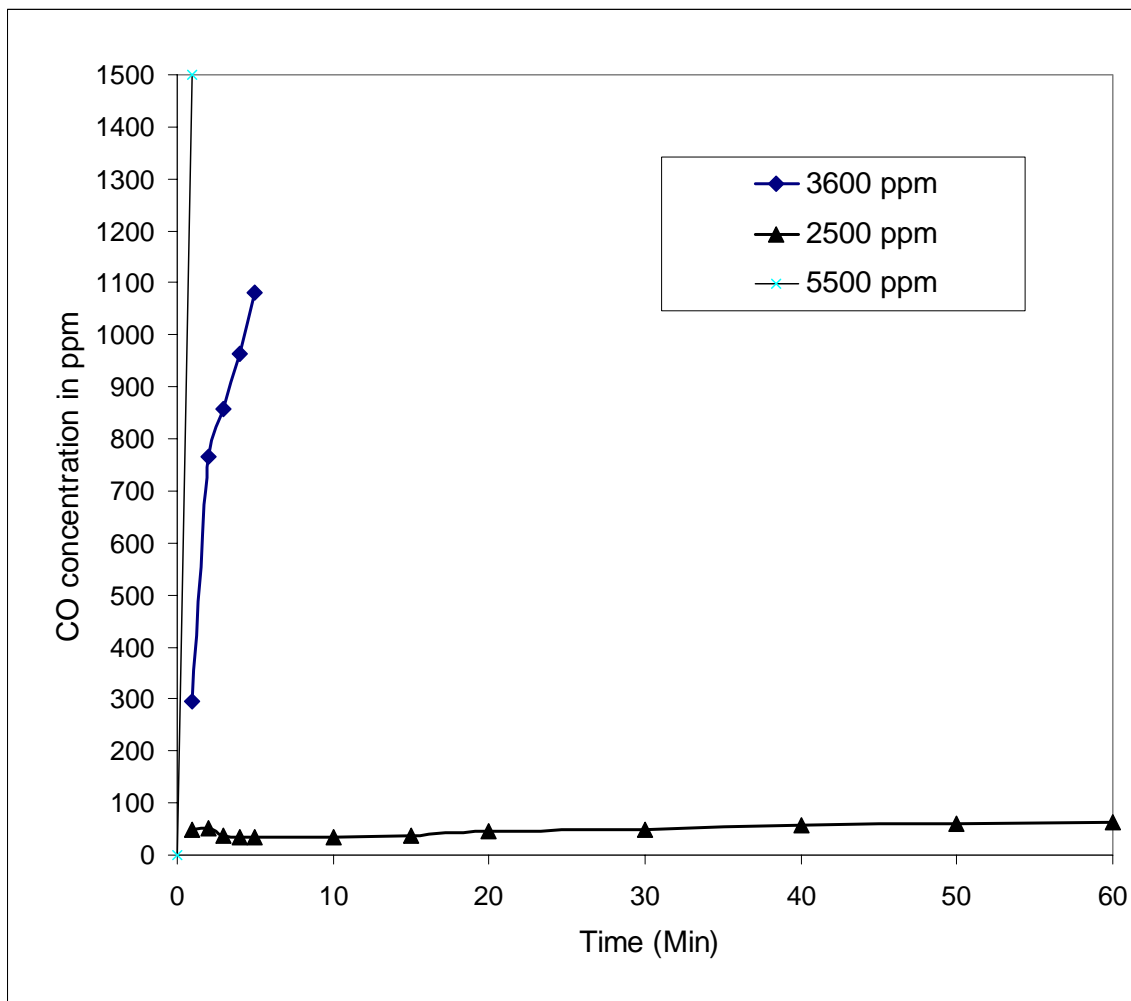
Figure 3.19: Effect of Inlet CO Concentration on Activity of Pt/Mn/SiO$_2$

Conditions:

Face velocity = 12 cm/sec

Bed depth = 1 cm

Relative humidity = 90%

Figure 3.19 shows that the catalyst fails to meet CBRN general standard at a bed depth of 1 cm.
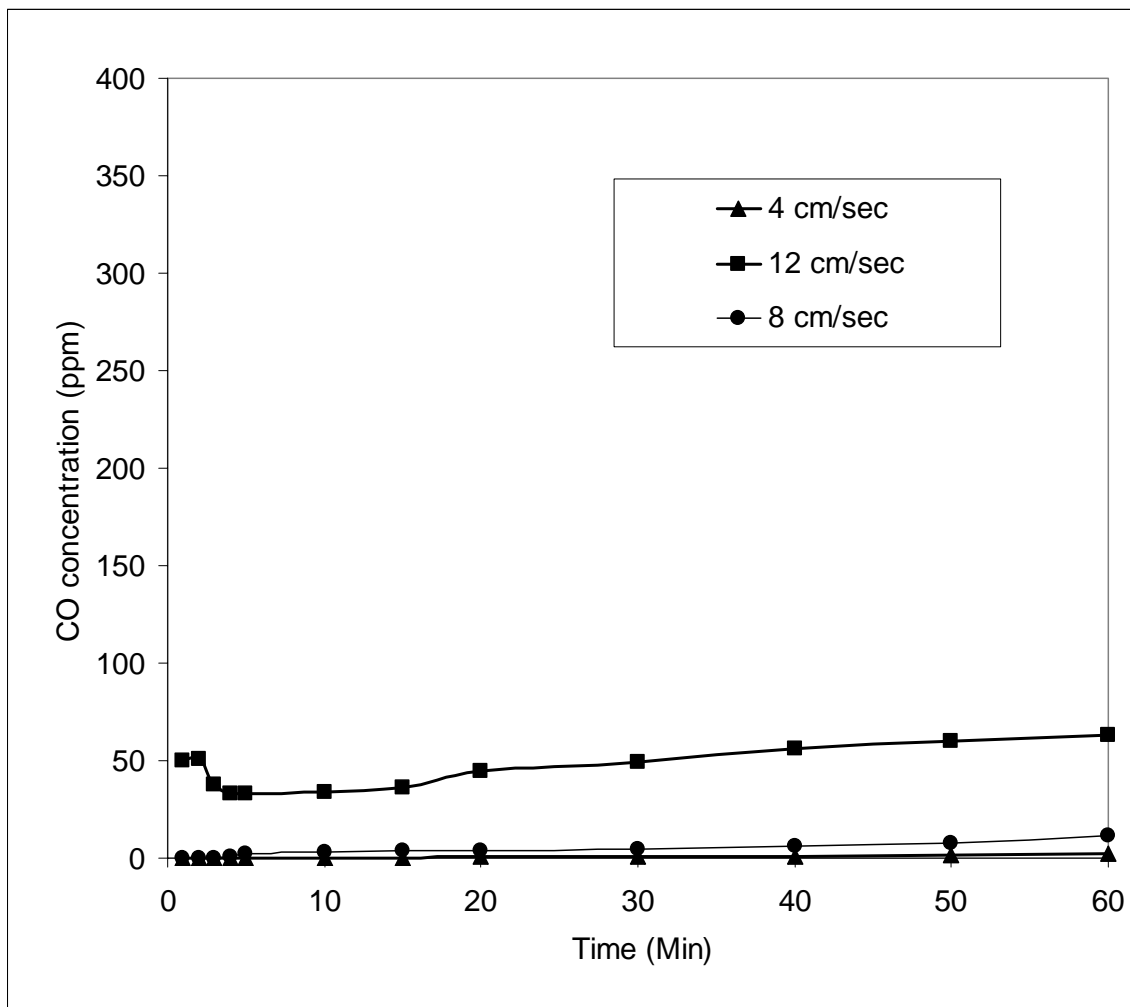
Figure 3.20: Effect of Face Velocity on Activity of Pt/Mn/SiO$_2$

Conditions:

Inlet CO concentration= 2500 ppm

Bed depth = 1 cm

Relative Humidity = 90%

Figure 3.21 shows the effect of bed depth to meet conditions corresponding to CBRN general standards. As seen form the figure, a bed depth of 1.5 cm is necessary to meet this standard. Some more stringent standards such as CBRN specific category

would even need deeper bed. This would substantially increase the cost of these materials as well as pressure drop which directly corresponds to breathing resistance. Primarily due to these considerations, testing and development of the second catalyst (Pt/Co/Al$_2$O$_3$) was undertaken.
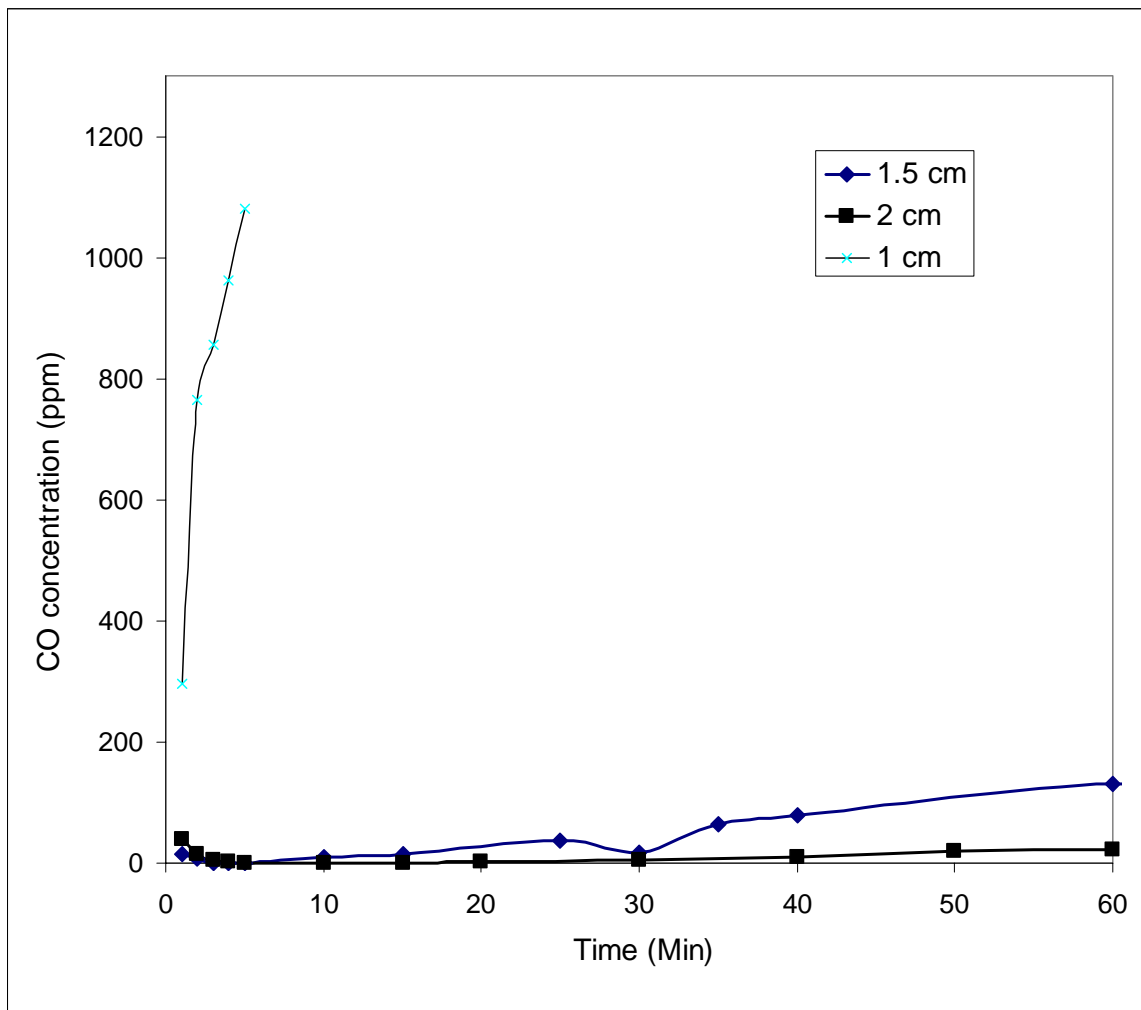
Figure 3.21: Effect of Bed Depth on Activity of Pt/Mn/SiO$_2$

Conditions:

Inlet CO concentration = 3600 ppm

Face velocity = 12 cm/sec

Relative humidity = 90%

III.8 Testing of Pt/Co/Al$_2$O$_3$ for Meeting Different Test-protocols:

As mentioned in chapter 1, as of now there are following different test protocols in consideration:

- EN 403 (European Standards)

- CBRN: (NIOSH standards)

- ANSI/ISEA 110-2003 (ANSI/ISEA standards)

Out of these, EN 403 standards are the only ones in practice. Rest of the standards are in various stages of proposal. This section deals with testing CO oxidation catalysts under conditions pertinent to each test protocol. The figures shown in this section are corresponding to EN403 tests only. All the results pertaining to meeting NIOSH- CBRN and ANSI/ISEA 110-2003 #6, #7 are documented in appendix B.

III.8.1 EN403

Following are the different test conditions for EN403 standards.

Inlet CO Concentration   = 2500, 5000, 7500, 10000 ppm

Face Velocity   = Min 5.88 cm/sec (30 LPM into 85 cm^2)

Temperature   = 22 ^{0}C

Bed Thickness   = 4 mm

Relative Humidity   = 90%

Figure 3.22 shows performance of CO oxidation catalyst at 2500 ppm inlet and 12.5 cm/sec face velocity.
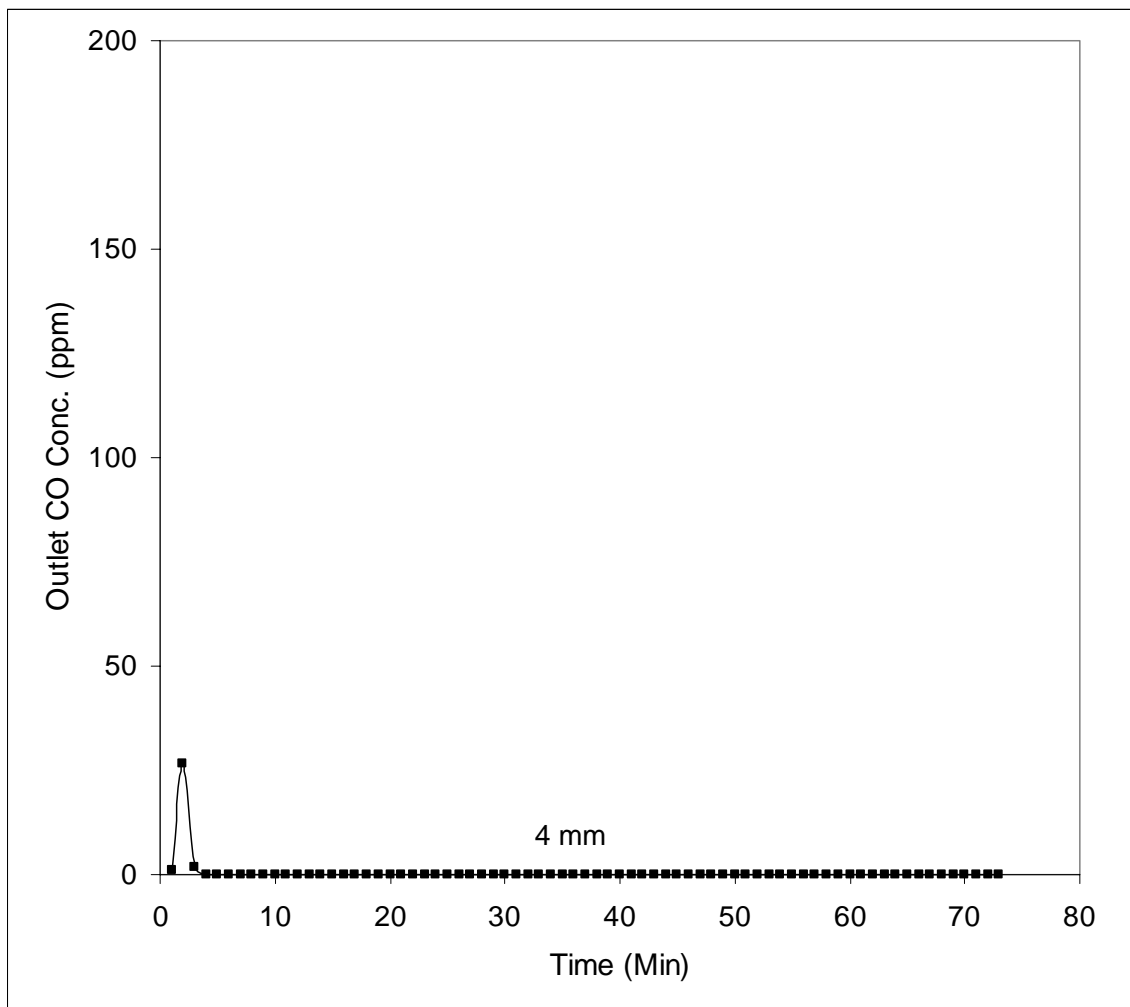
Figure 3.22: Catalyst Test for EN 403 (2500)

Conditions:

Face velocity = 12.5 cm/sec

Temperature = 22 ^{0}C

Bed cross section = 20.26 cm^2

Bed Depth = 4 mm

Note: The detector logs data at the rate of 20 per minute, for clarity of graphs, all the data

points are not shown in figures 3.22 through 3.25.

Figures 3.23, 3.24, and 3.25 show catalyst testing for meeting 5000, 7500 and 10000 ppm inlet CO condition at 5.88 cm/sec face velocity as stated in the EN 403 document respectively.
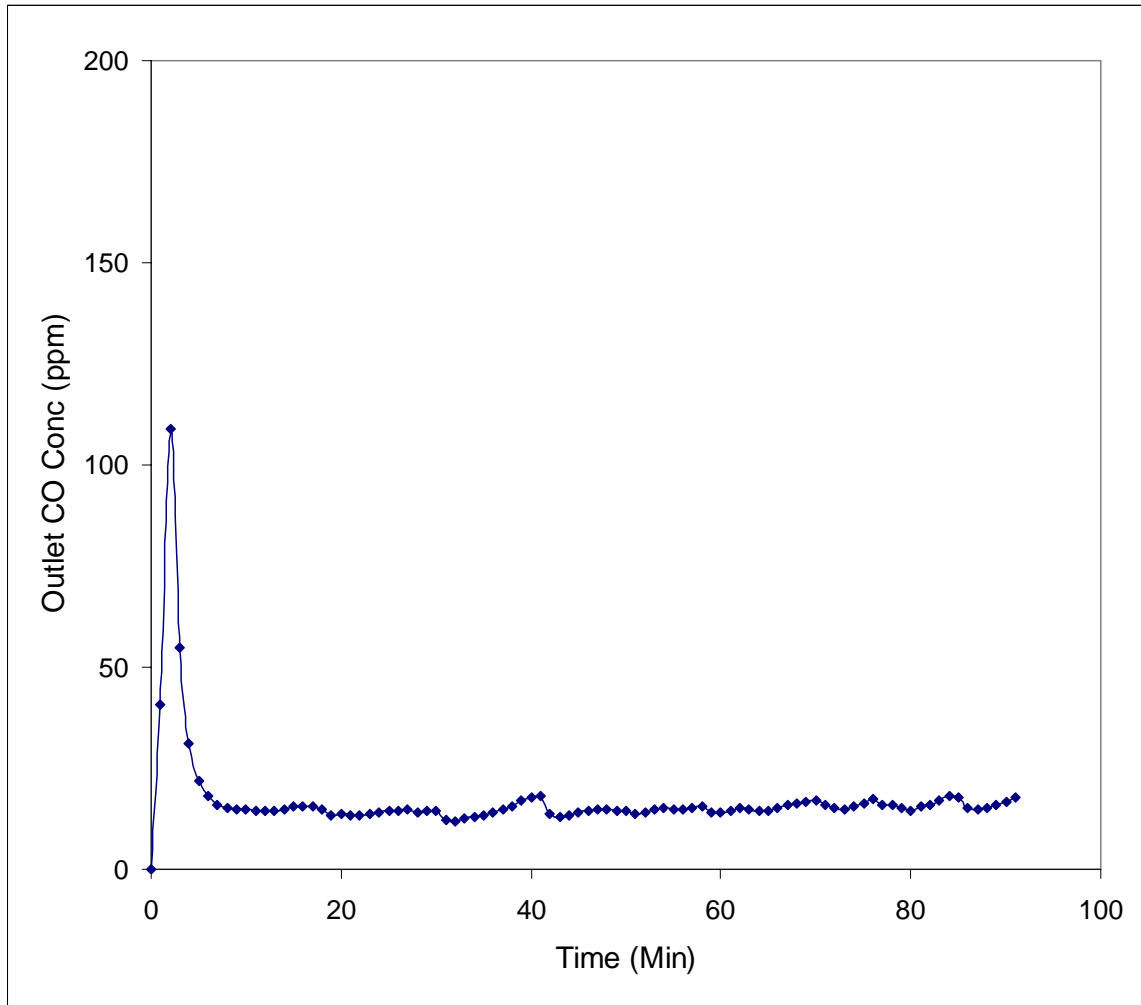
Figure 3.23: Catalyst Test for EN 403 (5000)

Conditions:

Face velocity = 5.88 cm/sec

Temperature = 22 ^{0}C

Bed cross section = 20.26 cm^2
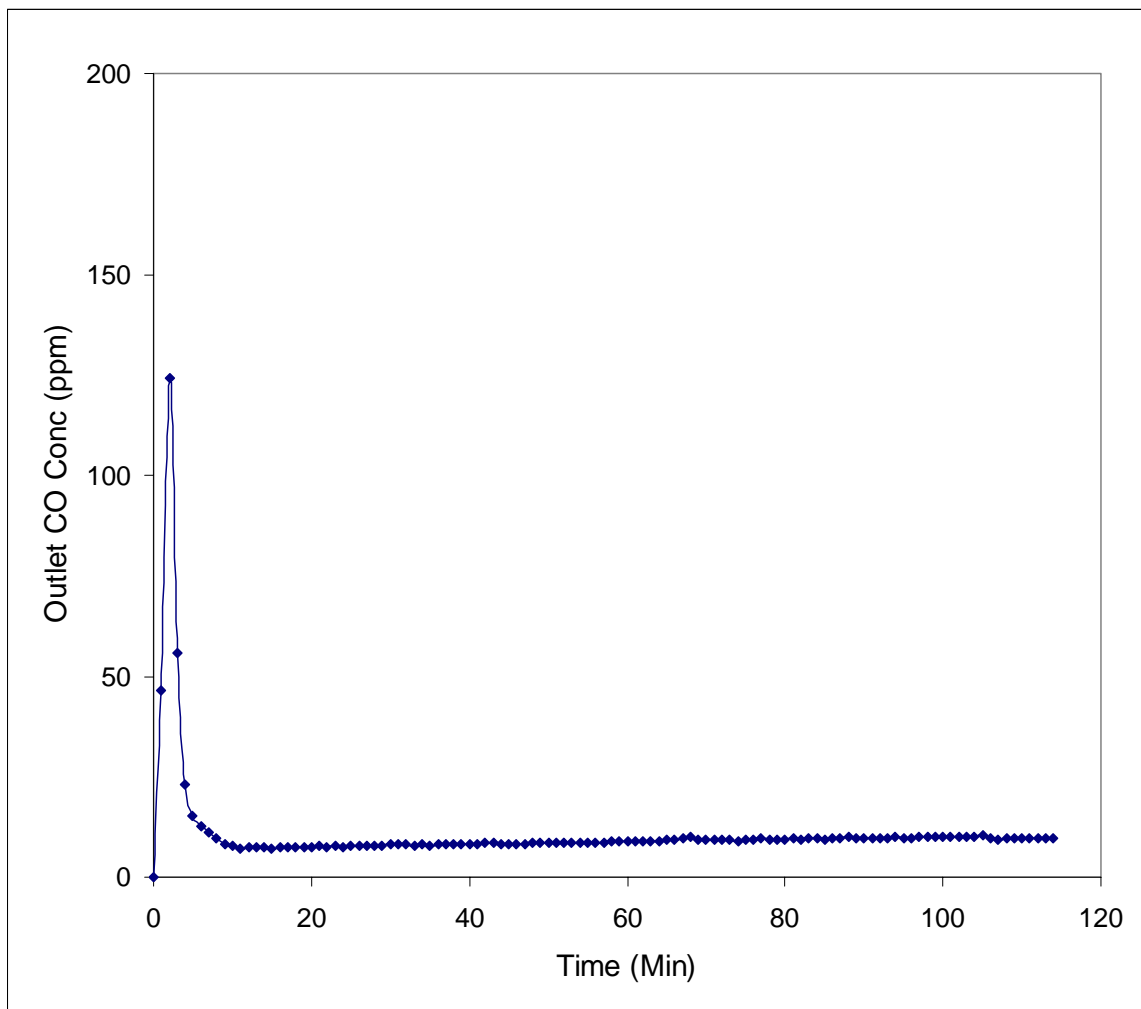
Figure 3.24: Catalyst Test for EN 403 (7500)

Conditions:

Face velocity = 5.88 cm/sec

Inlet CO conc. = 7500 ppm

Temperature = 22 ^{0}C

Bed cross section = 20.26 cm^2
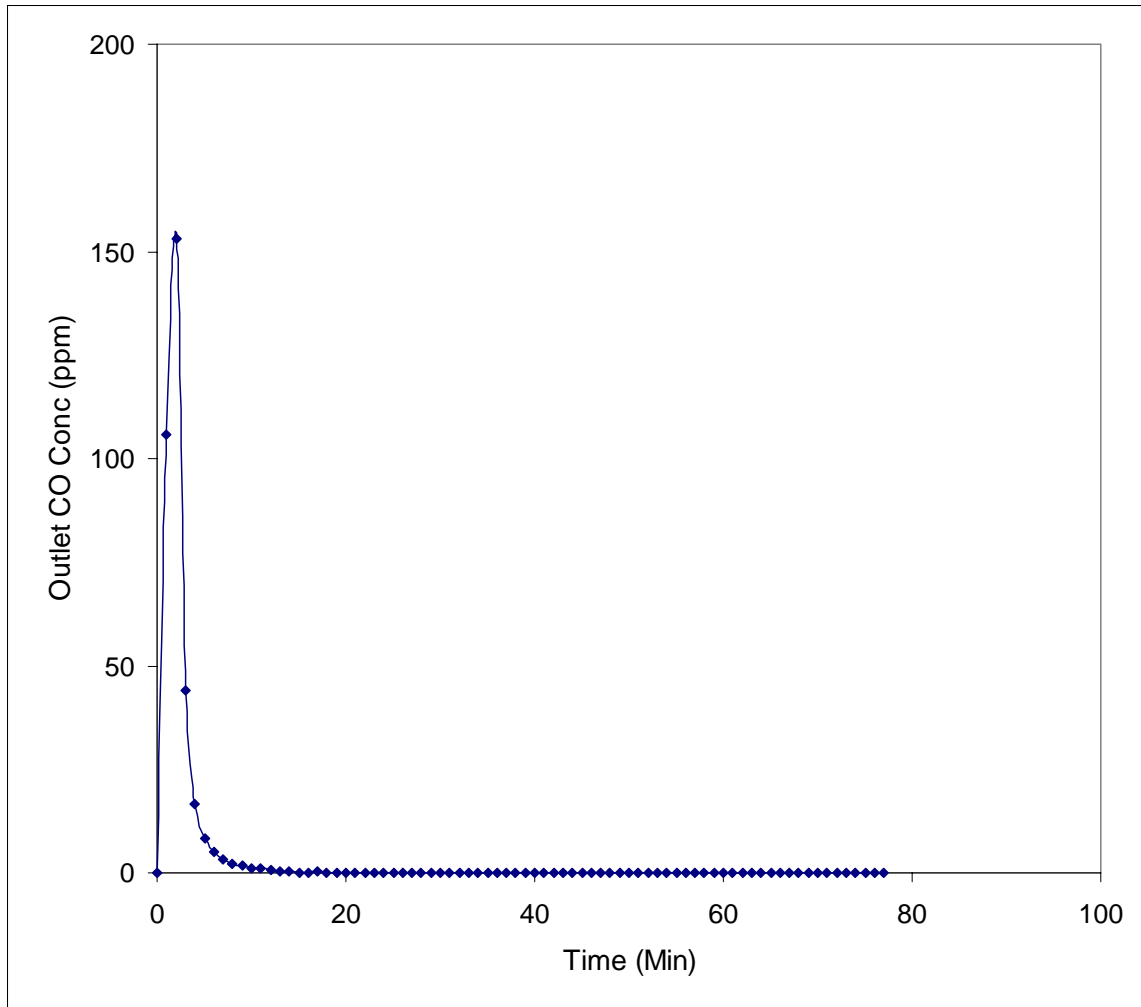
Figure 3.25: Catalyst Test for EN 403 (10000)

Conditions:

Face velocity = 5.88 cm/sec

Inlet CO conc. = 10000 ppm

Temperature = 22 ^{0}C

Bed cross section = 20.26 cm^2

As observed from figures 3.22, 3.23, 3.24 and 3.25 the outlet CO concentration follows a peculiar trend of rising immediately and falling off. This trend can be attributed

to adiabatic rise in temperature since CO oxidation is an exothermic reaction. Due to this increased temperature, the self-inhibition of CO reduces thereby increasing the conversion. CO oxidation on Pt catalyst has been known as self-inhibition type of reaction in literature.

This observation has been supported by temperature profile in figure 3.26. As seen from the figure, the temperature of the reaction mixture increases rapidly to close to adiabatic flame temperature in first three minutes.
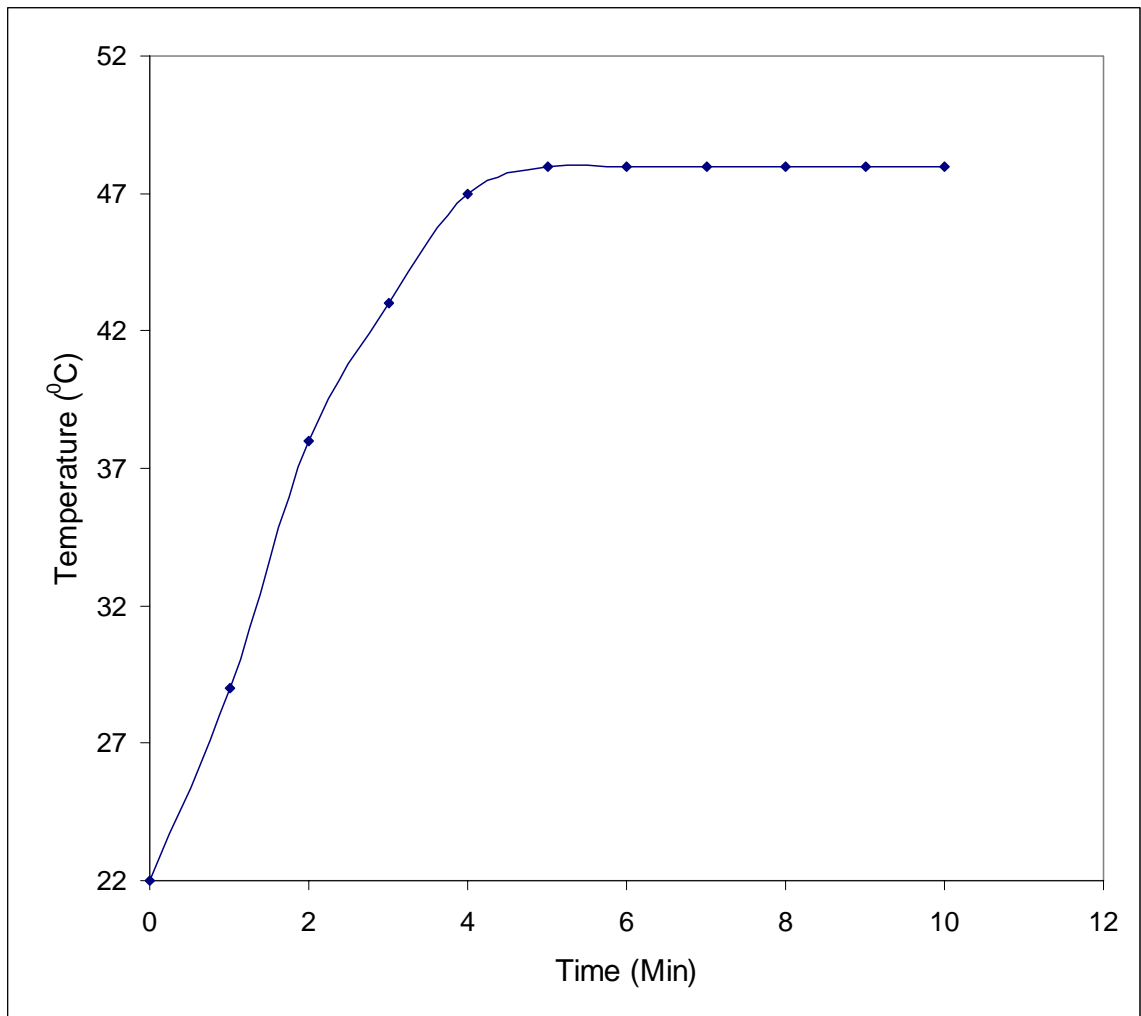
Figure 3.26: Adiabatic Temperature Rise for CO Oxidation Reaction

Conditions:

Inlet CO conc = 3600 ppm

Face velocity = 6.8 cm/sec

Catalyst bed depth = 4 mm

Relative humidity = 90%

The calculation of adiabatic flame temperature has been separately attached as appendix C. As the temperature increases, the conversion increases and outlet concentration of carbon monoxide falls. The gap in measured temperature and adiabatic flame temperature is due to heat loss as effect of improper insulation. The reactor had not been insulated to closely imitate the conditions as faced by the catalyst bed in actual escape mask. One hypothesis that supports this observation could be centered on formation of multiple steady states.

III.9 Multiple Steady States in CO Oxidation:

There can be different reasons for formation of multiple steady states such as (i) thermokinetic interaction [3.1], (ii) isothermal coupling between a self-inhibition reaction and either intra-paticle diffusion limitations [3.2] or intraparticle transport limitations [3.3], (iii) coupling among two or more steps in the overall reaction scheme [3.4].

It has long been known that, exothermic catalytic reactions follow non-linear dynamics. This primarily happen because of two different driving forces working in opposite of each other.

For a simple reaction;

A → B
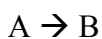
Rate of a reaction can be written as;

$r_A = k * C_A$

where

$k = A * \exp(-E_a/RT)$

where

A = Arrhenius constant

Ea = Activation energy

R = Universal gas constant

T = temperature

k = Reaction rate constant

r_A = Rate of reaction

C_A = Concentration of reactant A.

As temperature goes-up due to exothermic nature of the reaction, rate of reaction increases due to increasing k. At the same time, concentration of A starts decreasing thereby forcing the rate to slow down. As a result of these two opposite acting forces, multiplicity results in the reaction. Multiplicity is a result of formation of multiple steady states in a reaction.

This can be represented by following schematic of heat, generation and removal curves.
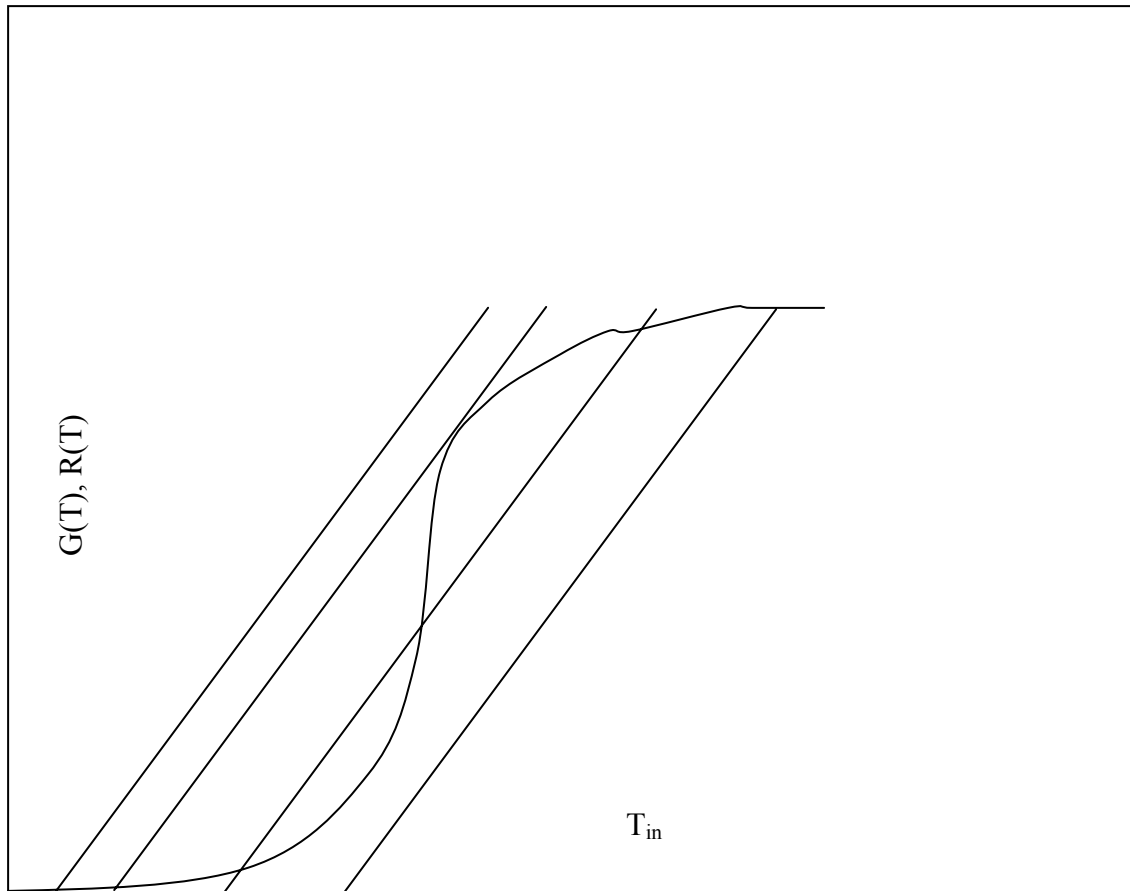
Figure 3.27: Schematic Representation of Heat Generation and Heat Removal Curves as Functions of Inlet Temperature

As observed from figure 3.27, the S shaped curve is a typical representation of a heat generation curve. The lines on the graph correspond to heat removal curves for that particular inlet temperature. At steady state heat removal rate and heat generation rate should be same. The intersection of these two plots would be steady states corresponding to that inlet temperature.

Moreover carbon monoxide reaction has also been known to follow the Langmuir-Hinshelwood Kinetics. The rate expression can be written as;

$$r_A = \frac{k_A * C_A}{(1 + K_A C_A)^2}$$

Where

K_A = Equilibrium adsorption constant

Thus this reaction can be classified as one that is self-inhibition type. At high CO concentrations, the denominator is large compared to numerator and hence the reaction rate goes down. One more reason for CO oxidation being self-inhibition type is irreversible adsorption of CO on the surface of platinum. This phenomenon has been investigated by several researchers in the past.

These reasons and observations led to following experimental as well as theoretical investigations.

III.9.1 Investigations of Multiplicity in Low Temperature CO Oxidation
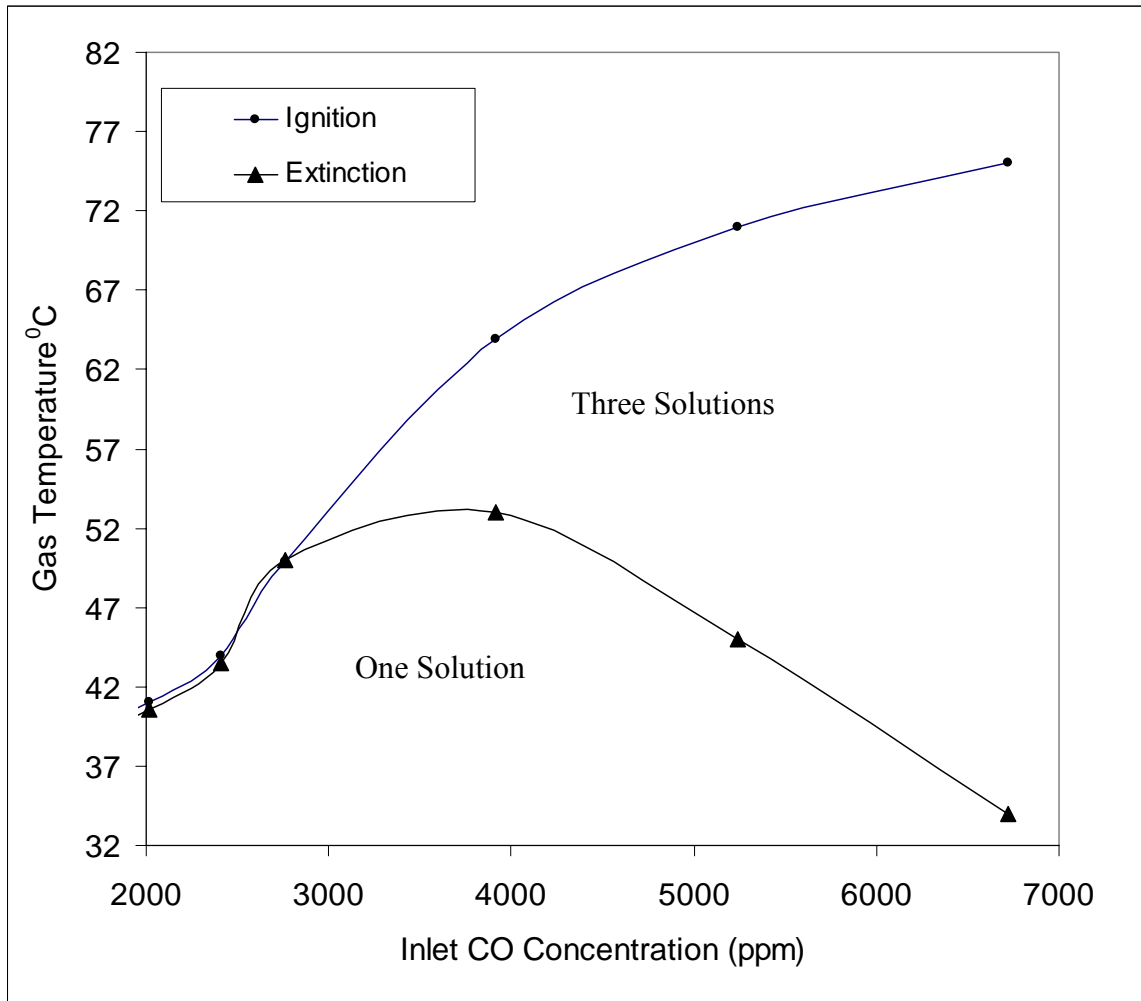
Figure 3.28: Cross Section of the Bifurcation Set in the Plane of Gas Temperature and

CO Feed Volume Fraction

Conditions:

Inlet CO conc = 3600 ppm

Face velocity = 6.8 cm/sec

Catalyst bed depth = 4 mm

Relative humidity = 90%

As seen in figure 3.28, the ignition temperature increases monotonically with inlet CO concentration. The graph of extinction temperature vs. CO fraction has a local maximum. The region with two stable states is bounded between the two graphs. Under the extinction branch, only one solution exists which means only one stationary state exists.

Similar results were observed by Harold and Luss [3.5] who performed oxidation of carbon monoxide on the surface of single pellet of Pt/Al_2O_3. Multiple steady states were observed for all CO concentration in the range of $0.6 - 8\%$ and gas temperatures in the range of 20 -250 ^0C. The multiplicity was observed by measuring temperature of the center of pellet as a function of gas temperature and CO mole fraction. At most only two stable stationary states were found for any given set of operating conditions. It could be deduced from studying the bifurcation map that thermokinetic coupling and intraparticle transport limitations were affecting the system.

Numerous researchers attempted in different capacities to model the multiple steady states behavior of CO oxidation reaction.

Harold and Luss [3.5] attempted to fit the multiplicity behavior of CO oxidation using a bimolecular Langmuir-Hinshelwood rate expression, interparticle and intraparticle transport resistances, and an estimate for the intraparticle activity profile. The kinetic model was found adequate to describe the trends but could not predict quantitative behavior.

Herz and Marin [3.6] attempted to fit the rate data of CO oxidation on platinum surface. The findings indicate that reaction models with no CO adsorption equilibrium

assumption fit the rate data more correctly compared to Langmuir-Hinshelwood rate expression that assumes adsorption equilibrium.

Harold and Garske [3.7] proposed various models that can fit experimental rate date at various conditions. It has been demonstrated that the common three step model consisting of reversible CO adsorption, dissociative oxygen adsorption and a Langmuir reaction step can predict qualitatively the reaction behavior under ultra high vacuum conditions. It could predict the shape of the multiplicity region in the catalyst temperature – CO pressure plane. A new method has been proposed in which parameter space has been divided into regions in which different shapes of temperature-CO pressure bifurcation maps would be observed. Five different models have been proposed.

Zhdanov and Kasemo [3.8] proposed that effect of oxide formation on the surface of platinum should be taken into account to accurately describe the shape of bifurcation map in CO oxidation. According to authors, at ultra high vacuum and high CO pressure conditions it may be sufficient to use Langmuir-Hinshelwood model to predict bistability but it would be necessary to take into account oxide formation under oxygen rich environment at atmospheric pressure. Monte Carlo simulations performed could predict the shape of bifurcation map qualitatively under oxygen rich environment. These predictions were found to be in agreement with STM studies of CO oxidation on platinum.

III.9.2 Hysteresis Effects:

This section deals with observations and explanation of hysteresis phenomenon in low temperature CO oxidation reaction.
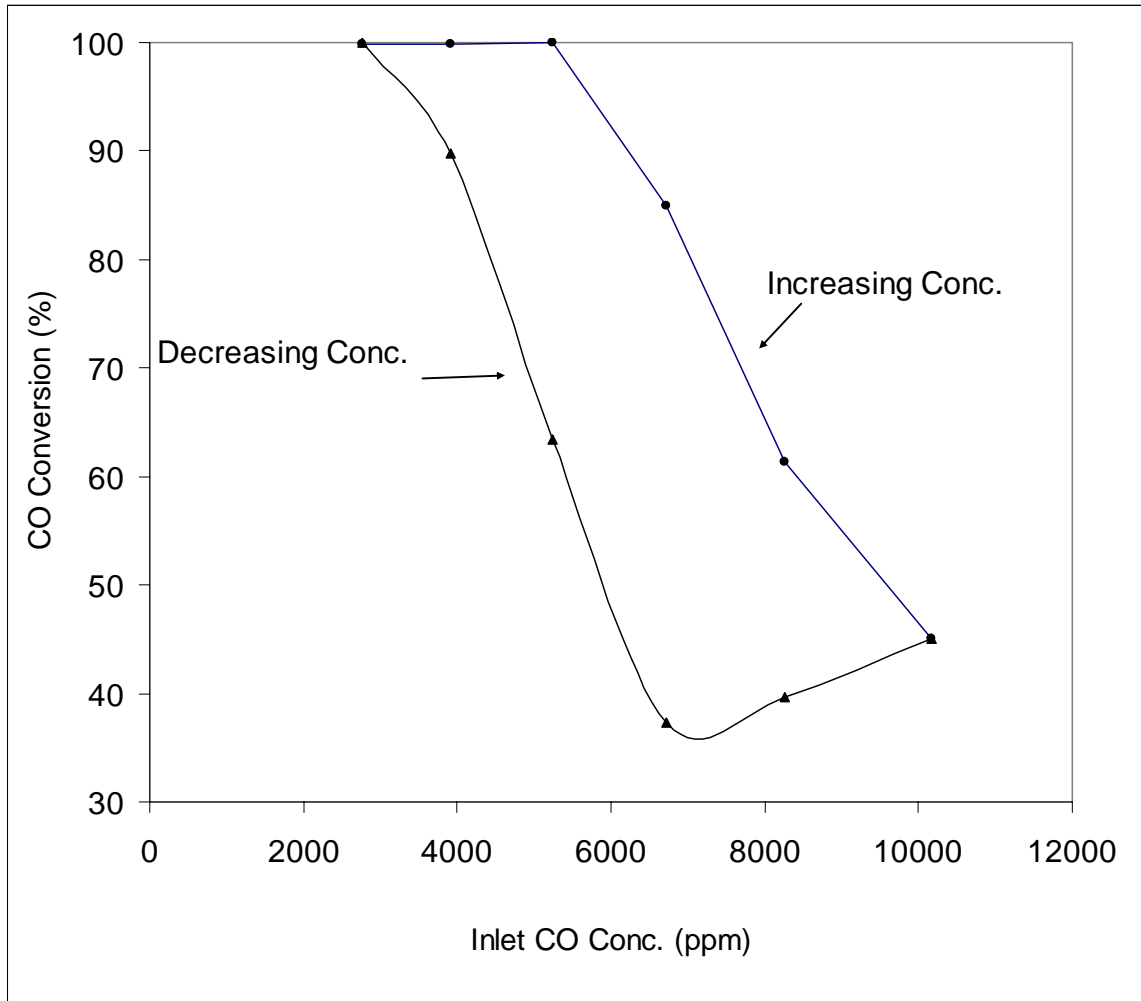
Figure 3.29: Hysteresis Phenomenon in Low Temperature Oxidation of Carbon Monoxide

Conditions:

Face Velocity = 12.5 cm/sec

Catalyst bed depth = 4 mm

Relative Humidity = 90%

As seen in figure 3.29, the inlet CO concentration has been changed from 2500 to 11000 ppm. As inlet CO concentration increase from 2500 to 5500 ppm, the conversion remains constant 100 %. As the inlet concentration increases beyond 6000 ppm, the conversion falls down to 85% and keeps on decreasing with increasing CO concentration. When the CO concentration is decreased from 11000 ppm to 2500 ppm, the conversion-inlet CO concentration follows a different route. The conversion for concentrations between 2500 and 11000 is much lower compared to corresponding conversion on the increasing concentration plot. On the decreasing concentration arm of the graph, CO conversion keeps on decreasing even after decreasing inlet CO concentration down to 6000 ppm. As the concentration falls below 6000 ppm, conversion starts to increase, and attains a 100% level at 2500 ppm, thereby resuming its original position.

This particular phenomenon is a clear indication of occurrence of multiple steady states in low temperature CO oxidation for a promoted precious metal catalyst. Similar results have been observed by many researchers in the past for platinum as catalyst.

R Jaree et al [3.9] report formation of hysteresis and extinction waves in catalytic CO oxidation caused by reactant concentration change. The reaction was studied in packed bed configuration of Pt/Al_2O_3. A model had been proposed to explain this phenomenon.

Bykov et al [3.10] suggest that Langmuir-Hinshelwood mechanism can be used to predict multiplicity of steady states in CO oxidation.

Abramova et al [3.11] take into account the surface non-uniformities of the catalyst to propose a model to explain low temperature CO oxidation at low CO

concentrations. This work has been proposed as an extension of ZBG (Ziff, Gulari, Barshad) model.

Haaland et al [3.12] relate the formation of hysteresis loops in CO oxidation to CO island formation. FTIR studies performed to observe the ratio of intensities of the absorption bands due to linear and bridge bonded CO. This ratio was found to be constant thereby suggesting CO island formation. The hysteresis phenomena in both CO reaction probability and CO surface coverage were found to be inversely related. This also suggests blocking of active sites by carbon monoxide on the Pt surface.

Salanov et al [3.13] explained the nature of hysteresis in oxidation of carbon monoxide on platinum. With excess oxygen in the reaction mixture formation of surface oxide of platinum takes place thereby that in turn leads to changing surface properties of platinum and hence the nature of the Hysteresis loop.

III.9.2.1   Steady State Temperature Hysteresis:
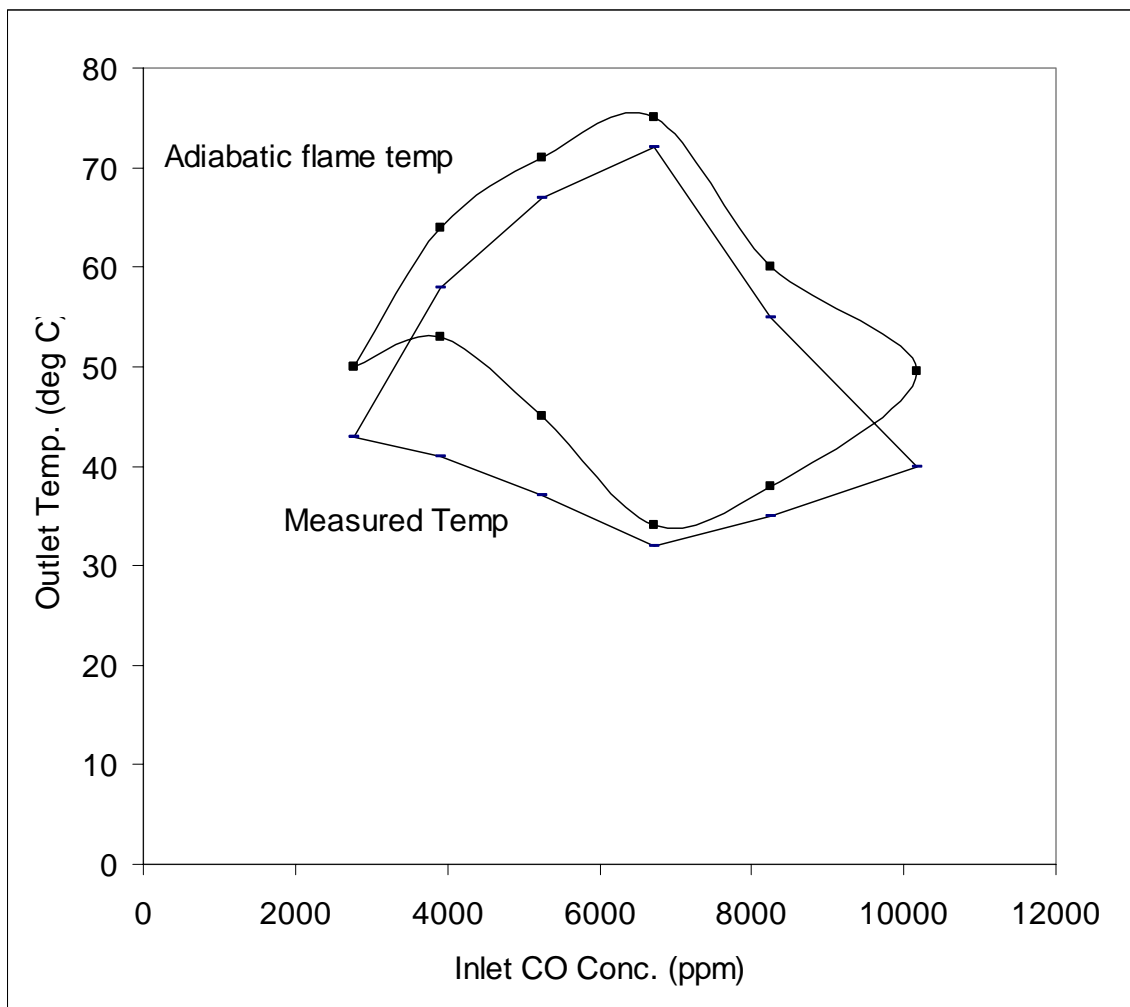
Fig 3.30: Steady State Temperature Hysteresis

Conditions:

Temperature = 22^0C

Face velocity = 12 cm/sec

Catalyst: $Pt/Co/Al_2O_3$

Relative humidity = 90%

Figure 3.30 shows thermal hysteresis in CO oxidation. As seen from the figure, the steady state temperature rises as a function of inlet CO concentration up-to 6500 ppm value. As the concentration increased beyond 6500 ppm, the temperature starts dropping rapidly and keeps on reducing even if the concentration has been decreased to about 6500 ppm. When concentration has been decreased further to about 5000 ppm, the temperature starts rising and resumes its original value at 2500 ppm inlet concentration. Thus the reaction follows an altogether different path while the concentration decreases.

III.10 Effect of Moisture:

One of the very interesting observations in this research work was 'enhancement in catalyst activity in presence of moisture'.

This section explains the effect of moisture content in the feed on activity of the catalyst. As observed in various experiments during the progress of this research, moisture has been found to be enhancing the activity of the catalyst. Figure 3.31 shows the study of hysteresis phenomenon in the absence of moisture. Comparison of this figure with figure 3.29 shows that on the decreasing branch of concentration, catalyst behavior is radically different. Same can be mentioned for increasing concentration branch of the hysteresis map. In presence of moisture, conversion remains at 100% for the concentration range of 2500 – 5500 ppm. Under dry conditions, conversion drops well below 90% when inlet concentration increases beyond 3000 ppm. For the decreasing concentration branch, in presence of moisture, conversion resumes at 100% once the concentration is decreased to 2500 ppm whereas under dry conditions the conversion remains at a much lower value of 68%.

III.10.1   Hysteresis under Dry Conditions
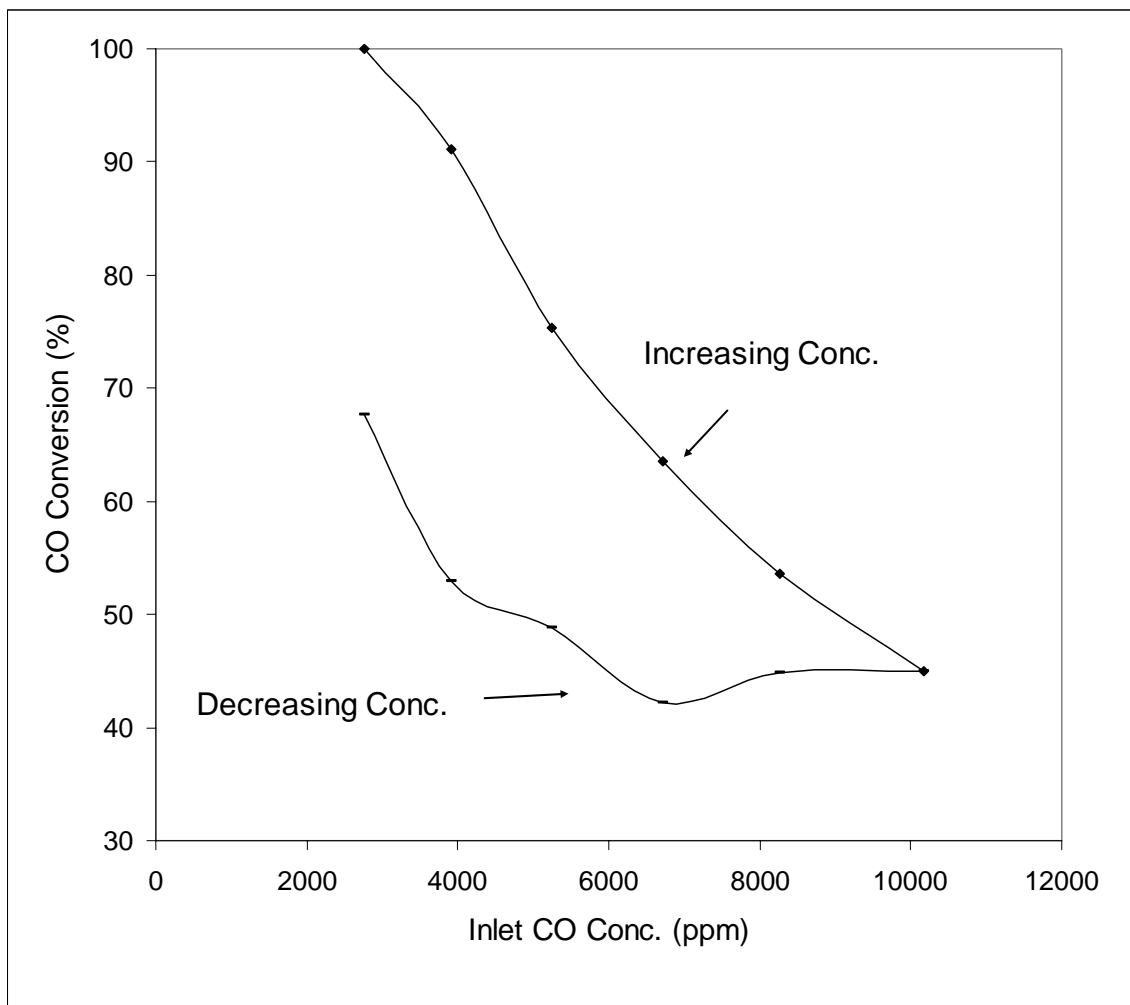
Fig 3.31: Hysteresis Phenomenon in Absence of Moisture

Conditions:

Temperature = 22^0C

Face Velocity = 12 cm/sec

Catalyst: Pt/Co/Al$_2$O$_3$

Relative Humidity = 0%

III.10.2   Effect of Moisture on Hysteresis
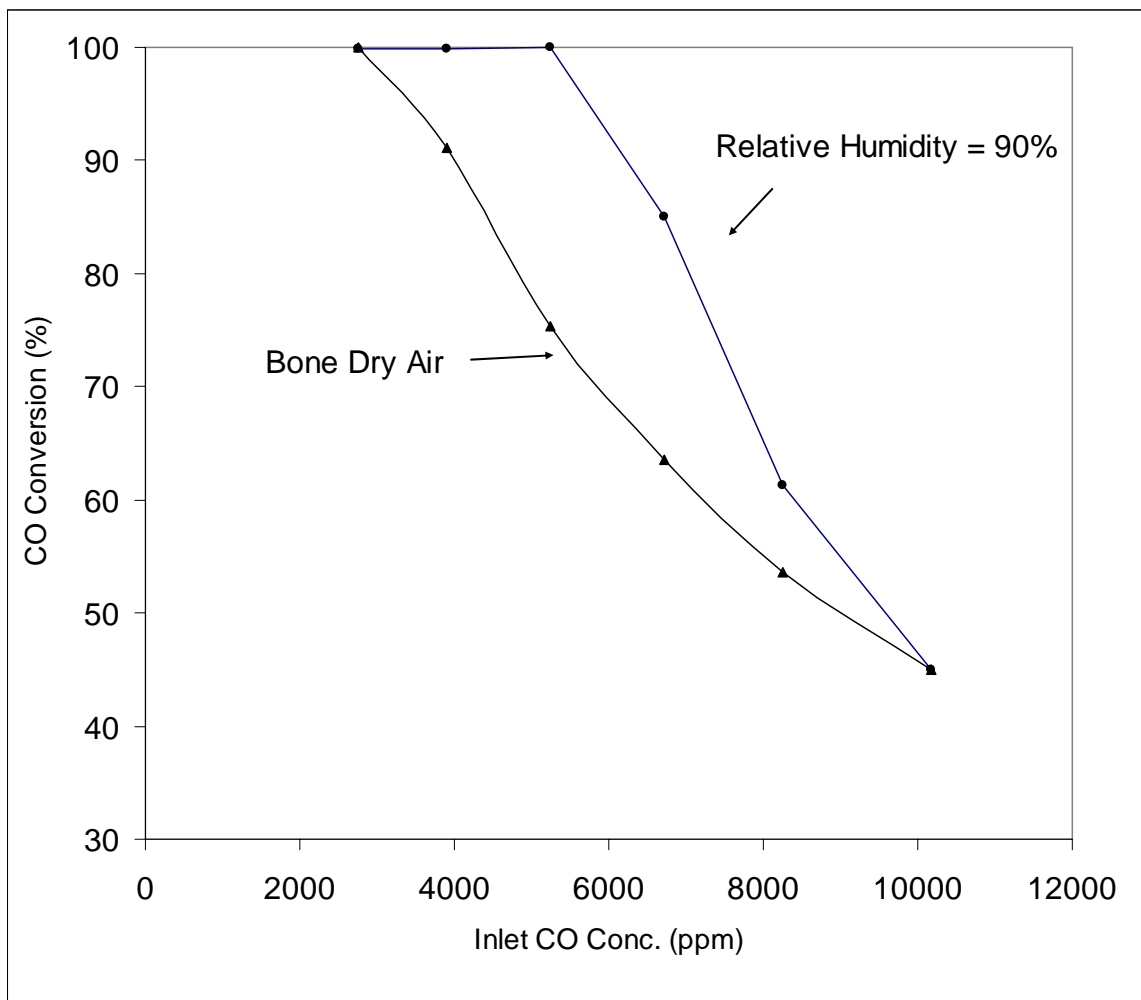
Figure 3.32: Effect of Moisture on Hysteresis

Conditions:

Temperature = 22^0C

Face velocity = 12 cm/sec

Catalyst: Pt/Co/Al$_2$O$_3$

Relative humidity = 90%

Figure 3.32 shows the comparison of catalyst activity under dry and wet feed conditions. The conversion is much higher for a given CO concentration. It has also been confirmed that the activity difference between two feed conditions is reversible.

III.10.3 Effect of Moisture on Pt/Mn/SiO$_2$
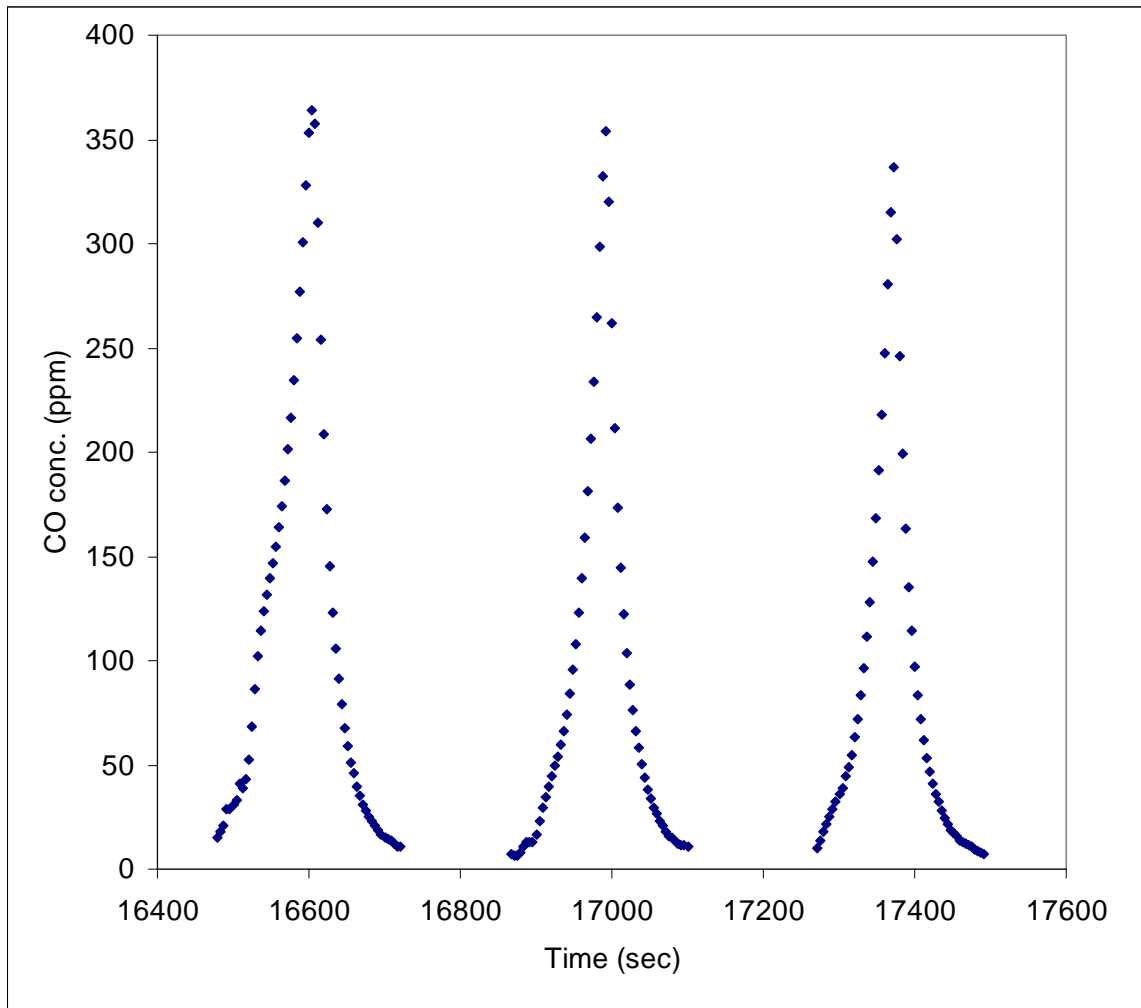
Figure 3.33: Effect of Moisture on CO Oxidation Process - Reversible Nature of Activity

Conditions:

 Inlet CO concentration = 2500 ppm

Relative humidity at the beginning = 90%

Face velocity = 8 cm/sec

Catalyst = Microfibrous entrapped $Pt/Mn/SiO_2$

As shown in figure 3.33, the original feed introduced while testing the activity of this catalyst had relative humidity of about 90%. During the course of the reaction, when the feed nature changed from wet to dry, conversion of carbon monoxide keeps on dropping. As soon as the feed nature resumed back to original, the conversion started increasing and reached its original value. Same experiment was repeated several times to confirm the behavior. From this behavior it can be observed that, moisture helps the catalyst to regain its activity by reducing the surface coverage of carbon monoxide which tends to poison the catalyst. Figure 3.34 shows a comparison of activity under dry conditions and with feed having about 90 % relative humidity.
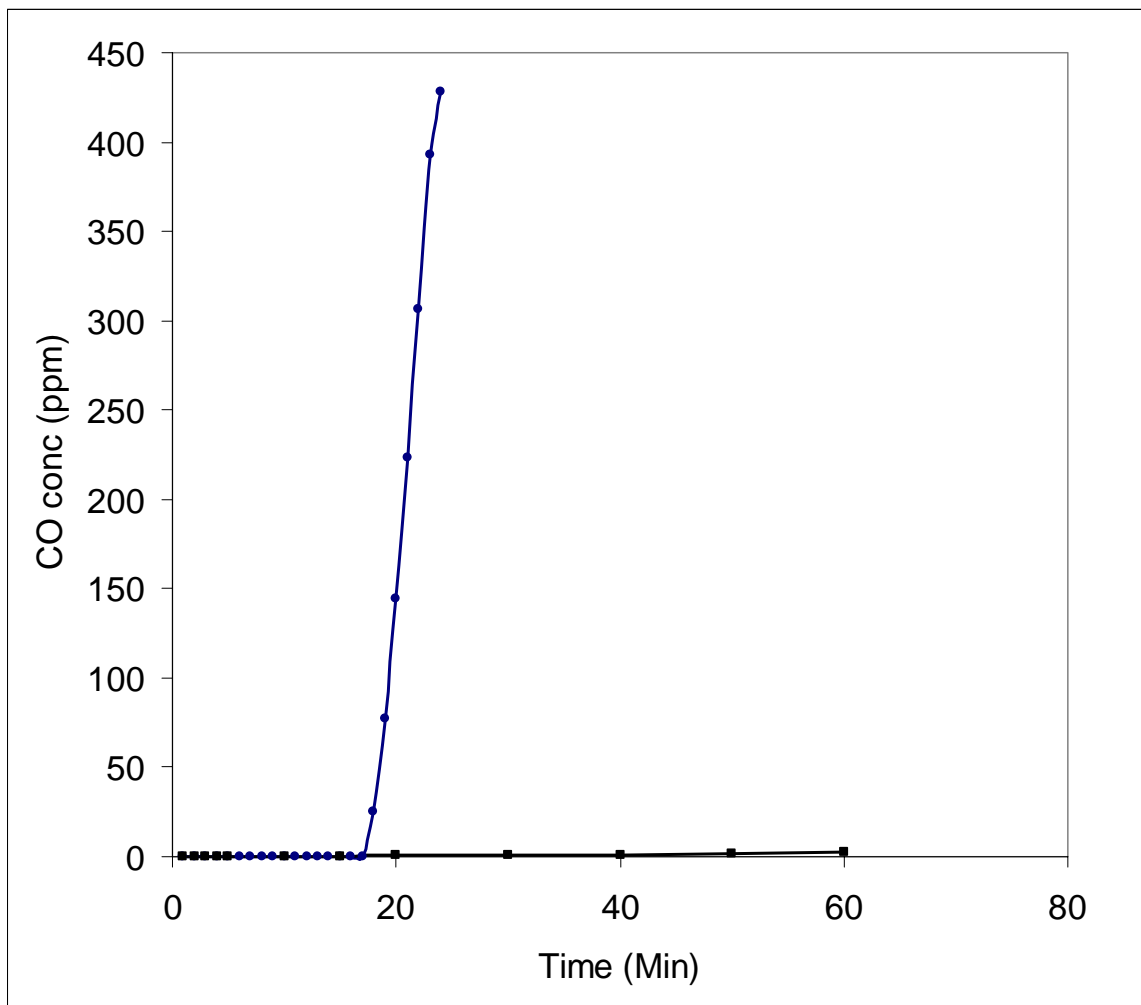
Figure 3.34: Effect of Moisture on Catalyst Activity

Conditions:

Inlet CO Concentration = 2500 ppm

Face Velocity = 4 cm/sec

Catalyst = Pt/Mn/SiO$_2$

As seen from figures 3.32, 3.33 and 3.34, it is clear that presence of moisture is very beneficial for low temperature oxidation of carbon monoxide. This can happen due to various different reasons. A vast body of literature suggests different mechanisms by means of which water can participate in the reaction and help enhance the catalyst activity for oxidation.

Lavin and Jackson [3.14] investigated the effect of moisture on carbon monoxide oxidation. The conclusion reached was hydroxyl ion coming out of water dissociation reacts with carbon monoxide to produce carbon dioxide and sets a proton free.

$OH + CO = CO_2 + H$
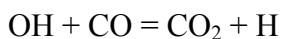
This reaction is exothermic to the tune of 24 Kcal which helps the temperature rise hence the reaction. The yield of CO_2 increased as the moisture content of the feed was increased everything else remaining same.

Same effect has been observed by Allers et.al. [3.15]. While measuring angular and velocity distribution of carbon dioxide desorbing as reaction product of carbon monoxide oxidation on Pt (1, 1, 1), four different peaks corresponding to CO_2 desorption were observed (α β_3, β_2, β_1). These four different peaks could be related to different mechanisms of CO_2 production. α was ascribed to Where α –CO_2 coincides with the O_2 desorption from and the dissociation of pure chemisorbed molecular oxygen, and thus indicates a reaction channel coupled with desorption and dissociation of O2, β_1-CO, corresponds to the reaction path investigated before by many researchers and is most likely due to the reaction at the boundaries of ordered CO and oxygen islands. The formation of β_2, β_3 peaks was less clear at this point of time. Bergeld et al [3.16] performed experimental investigation of low temperature CO oxidation on Pt(1, 1, 1) in

presence of water and studied TPR. From observation of TPR spectrum an autocatalytic route has been explained. The mechanism proposed consists of following stages:

$2O_{ad} + CO_{ad} + 2H_2O_{ad} \rightarrow O_{ad} + CO_{ad} + 3OH_{ad}$

$\rightarrow CO_{2g} + O_{ad} + 2H_{ad} + 2OH_{ad}$

$H_{ad} + OH_{ad} \rightarrow H_2O_{ad} \rightarrow H_2O_g$

$OH_{ad} + OH_{ad} \rightarrow H_2O_g + O_{ad}$

$H_{ad} + O_{ad} \rightarrow OH_{ad}$
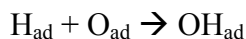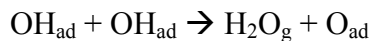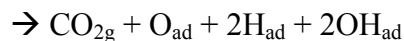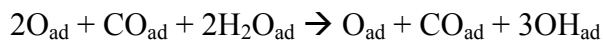
The overall autocatalytic mechanism suggested was;

$CO_{ad} + OH_{ad} \rightarrow CO_{2ad} + H_{ad}$
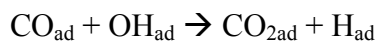
This reaction leads to the formation of one more OH_{ad} and hence the reaction becomes autocatalytic. This mechanism also explained the origin of β_2 and β_3 peaks of earlier observed CO_2 desorption.

Xue-Qing Gong and P. Hu [3.17] studied the catalytic role of water using density function theory (DFT). The CO oxidation barrier under dry condition is 0.8 eV. In the presence of water this barrier reduces to 0.33 eV. The reduction in barrier happens primarily because of H-bonding between H in water and the O at the transition state (TS) that stabilizes the TS. Secondly, CO can readily react with OH with a barrier of 0.44 eV. Thirdly in the H_2O + OH mixed phase, CO can be easily converted to CO_2 through two steps; CO reacts with OH to form COOH that in turn loses one H to a nearby H_2O molecule and at the same time an H in water transfers to a OH leading to CO_2 formation. The conclusions of this research include;

i. The reaction $CO + O + H_2O \rightarrow CO_2 + H_2O$ is not responsible for low temperature CO oxidation, even though the barrier of 0.33 eV seems to be in accordance with CO_2 desorption temperature

ii. The possibility that CO oxidation at boundaries of CO domains and $H_2O + OH$ mixed phases being a major source of CO_2 desorption is negligible

iii. It is likely that CO oxidation occurring in the $H_2O + OH$ mixed phase is the major source for CO_2 formation at low temperature. The various elementary steps involved are;

$$2H_2O + O \rightarrow 2OH + H_2O - (1)$$

$$CO + OH \rightarrow COOH - (2)$$

$$COOH + H_2O + OH \rightarrow CO_2 + H_2O + H_2O - (3)$$
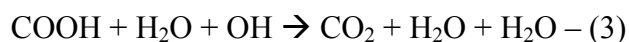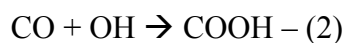
In reaction (3), H_2O plays a bridge role thereby passing a H from COOH to a OH. Thus water promotion could be divided into two classes; class I, H-bonding between the H of H_2O and an electronegative species such as O in the reaction of $CO + O + H_2O \rightarrow CO_2 + H_2O$, water can stabilize the transition state of the of the reaction and hence reduce the barrier. Class II, Water first dissociates and then H and OH participate in the reaction. As a result the reaction mechanism changes and a favored route is formed via OH formation.

III.10.4   **Water Promotion Effect on CO oxidation over Promoted Pt/Al$_2$O$_3$**

For the promoted catalyst, transition metal oxide acts as a carrier for oxygen and platinum surface adsorbs carbon monoxide as well as water, and may produce OH ions. The OH ions formed may help CO$_2$ desorption as described above. Also only water and CO are competing for active sits on platinum as against the well known competitive inhibition of the active sites by carbon monoxide over oxygen.

In addition, carbon monoxide has tendency to form islands on Pt surface. Haaland and Williams [3.12] studied CO island formation effect on the surface of platinum using Fourier transform infrared spectroscopy. The ratio of intensities of the absorption bands due to both linear and bridge bonded CO was constant during oxidation. These observations were interpreted as resulting from CO island formation.

Our hypothesis here is that, water helps break the CO islands on the Pt surface, thereby reducing active site loss. Hence moisture can be helpful for low temperature CO oxidation reaction as observed.

III.11 Self-sustained Oscillations
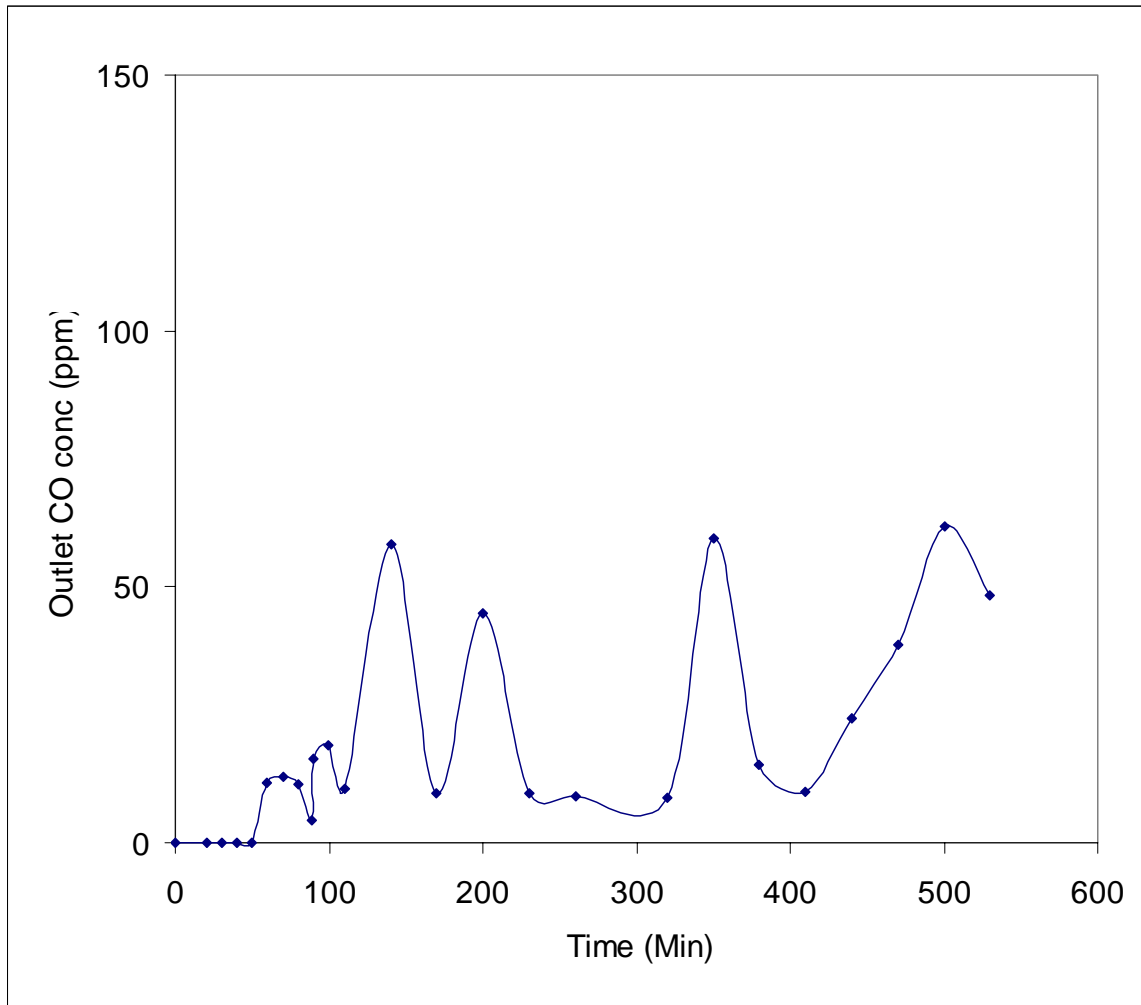
Figure 3.35: Self-sustained Oscillations in CO oxidation

Conditions:

Inlet CO concentration = 2500 ppm

Face velocity = 8 cm/sec

Bed depth = 1 cm

Catalyst: microfibrous entrapped Pt/Mn/SiO$_2$

Moisture: 3% (Relative humidity ~ 90-100%)

Approximate temperature rise = 7-8 ^0C

As seen in figure 3.35, self-sustained oscillations have been observed in the low temperature oxidation of carbon monoxide. There could be various reasons why self-sustained oscillations can be present in this reaction.

Lagos et al [3.18] modeled the behavior of heterogeneously catalyzed CO oxidation on Pt surface. Experimental data indicate presence of three different regimes, steady state, oscillatory and a quasi-chaotic regime. The explanation of various regimes has been provided by means of phase diagram analysis.

McCarthy et al [3.19] explain various reasons why oscillations could be present in CO oxidation. The reasons could be classified in two broad categories (i) thermal behavior and (ii) intrinsic kinetics that characterizes this reaction. Thermal oscillations happen due to inter-phase temperature gradients. Within intrinsic kinetics; either two different reactions could be rate limiting or autocatalytic reaction step exists. During isothermally performed it was concluded that the intrinsic kinetics contain two different rate determining steps as possibility of autocatalytic reaction did not exist. The two different rate determining steps take over the process dynamically as surface concentration of CO changes from low to high and vice-versa. Rate equation of the following form could be taken into account to explain such an observation.

$$R_o = \frac{1}{\left(\left(\frac{1}{k_1 * C_{co}}\right) + \left(\frac{1}{Cco / K_2}\right)\right)}$$

Thus at low CO partial pressures linearity is exhibited while at high CO partial pressures, negative order is evident. Maxima can be observed.

Turner et al [3.20] studied oscillations in carbon monoxide oxidation over polycrystalline Pt wire at atmospheric pressure. The oscillations were observed in both temperature of Pt wire and concentration of carbon dioxide formed over a wide range of CO concentration ($0.001 < P_{co}/PO_2 < 0.045$), temperature range of 150^0C to 350^0C. These oscillations were believed to occur between two branches of Langmuir-Hinshelwood reaction mechanism. Slow formation of sub-surface oxide and further reductions was believed to be the reason of oscillations. When chemisorbed oxygen reacts with Pt surface, some of it gets incorporated under the surface and starts formation of oxide layer thereby deactivating the surface. When this surface gets exposed to carbon monoxide, it reduces back to Pt metal active site. Thus the activation-deactivation triggered by surface oxide formation led to oscillations. A model proposed called the 'oxide model' described qualitatively the oscillatory behavior.

Collins et al [3.21] proposed 'carbon model' to explain temporal oscillations observed in carbon monoxide oxidation. Combinations of Langmuir-Hinshelwood reaction steps with activation-deactivation due to carbon formation was assumed to be the cause of oscillations. Coupling between carbon removal by reaction with gaseous oxygen and carbon removal by reaction with chemisorbed oxygen happening at comparable rates led to oscillations. This model could qualitatively represent experimental data.

Ladas et al [3.22] linked oscillations formation to surface faceting by in-situ LEED studies. They proposed a mechanism in which facet formation on a CO covered 1X1 surface and the removal of facets by a thermal reordering process get coupled to

cause kinetic oscillations. An increase in the period of oscillations was observed as extent of   faceting   increased.

Tsai et al [3.23] observed oscillations in Pt catalyzed CO oxidation between low, intermediate and high activity. The oscillations were direct effect of coupling between two different catalytic loops called as coupled catalytic oscillators.

Imbihl et al [3.24] explained formation of autonomous kinetic oscillations in CO oxidation over Pt. The main hypothesis was, surface defects induce oscillations. The reaction was studies over a single crystal of Pt under isothermal conditions at very low pressure.

Note: Figure 3.35 does not show all the readings on the curves for clarity purposes.

III.12 Comparison of Same Particle Size Catalyst in Packed and Microfibrous Entrapped Configuration

This section details the observations of anomalous activity behavior of the catalyst when in microfibrous configuration. It was observed that the activity for same catalyst loading and operating condition was higher in microfibrous beds compared to equivalent packed bed and operating conditions. Following four different bed configurations were selected:

    i.   Packed bed

    ii.   Diluted packed bed with alpha-alumina as diluent

    iii.   Layered packed bed with layers of microfibrous materials between packed beds

    iv.   Microfibrous bed

Configuration number ii and iii were added to test for following effects if observed;

    a. Thermal behavior of reaction differs vastly in packed bed and diluted packed bed mode

    b. Due to addition of layers of microfibrous bed the gas flow channeling was taken care of, which otherwise can happen in packed beds.

Figure 3.36 shows schematic of different configurations for activity comparison.
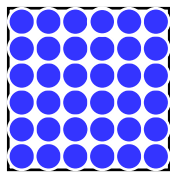
Packed Bed
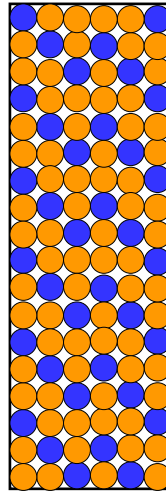
Diluted
Packed Bed
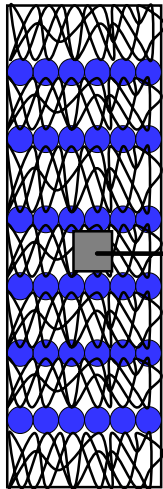
Layered Packed
Bed
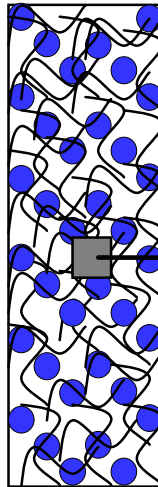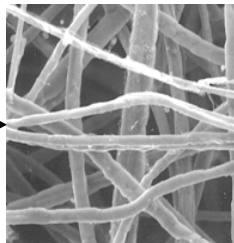
Microfibrous Bed

Figure 3.36: Schematic of Different Bed Configurations
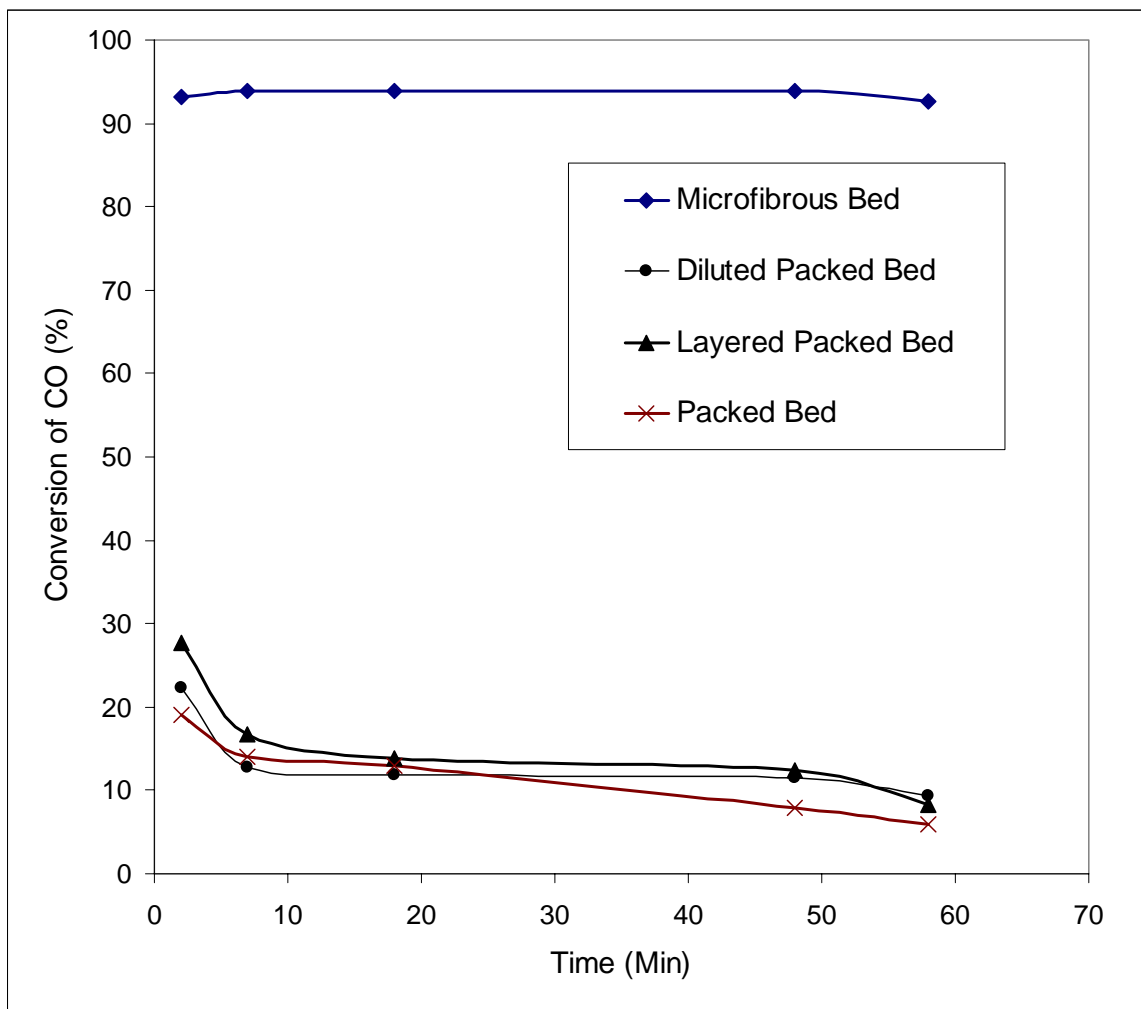
Fig 3.37: Comparison of Catalyst Activity for Different Bed Configurations

Conditions:

Inlet CO Concentration = 2500 ppm

Relative Humidity = 90%

Reactor Diameter = 0.5 cm

Experimental conditions for the demonstrations were; temperature of 25ºC at atmospheric pressure and particle size of 150-250 μm. The microfibrous media for both of the CO oxidation tests used nickel fibers of 4 and 8 μm in a weight ratio of 1:3. The nickel fibers, particulates and cellulose are cast into a preform by wetlay papermaking technique. The resulting preform is sintered at 950ºC in H_2 atmosphere for 30 minutes. The sintered media contains approximately 18 vol. % particulates, 1.6 vol. % fibers and ca. 80 % bed voidage. Both of the CO oxidations of sintered media were done in an 8 mm I.D. tube with bed depth of 1 cm. The packed beds of catalyst powder were tested in a 4 mm ID tube. Each test employed the same amount of catalyst powder. Other conditions for low temperature oxidation of CO were as follows: Transition metal promoted platinum on silica gel catalyst ($Pt-M_n-SiO_2$), inlet CO concentration of 2500 ppm, GC detection limit is 40 ppm CO, oxygen concentration of 20% with balance nitrogen, face velocity of 8 cm/sec, relative humidity of 86%. The CO oxidation catalyst deactivates due to reactant inhibition, so conversion as a function of time data is shown as Figure 3.37.

Conversion of CO by manganese promoted platinum on silica at low temperature is shown In Figure 3.37. Conversion is plotted against time since the reaction is deactivated by reactant poisoning. The results for the three different packed beds of catalyst particles are all about the same. At ten minutes after the reaction was started the conversion for the three packed beds are about fifteen percent and for the microfibrous mesh it is about ninety-five percent. If a rate constant is calculated from these data it indicates that the reaction rate for the catalyst in the microfibrous mesh is about 1.8 times

higher than for the packed beds. The microfibrous mesh catalyst also shows less deactivation during the experiment than the packed beds.

Studying computational fluid dynamics of flow and reactions over microfibrous beds has been proposed to be one way to explain the anomalous increase in activity of the catalyst. It has been hypothesized that, observing residence time distribution within microfibrous bed should throw some light on this phenomenon. Another hypothesis is that of enhancement in external mass transfer due to presence of wires. A comprehensive experimental analysis followed by theoretical explanation would explain this effect.

CHAPTER IV

ANALYSIS OF COMMERCIAL PRODUCTS

This chapter deals with testing and analysis of commercially available products for fire escape applications. All these products meet existing EN403 standards. These products served as intermediate bench marks while the research was progressing. The products selected for analysis are:

1. Drager parat C ®

2. Essex plus 10®

3. Sundstrom SR 77®

Products 1 and 2 are Hopcalite based, while third mask is precious metal monolith based. All these products carry a price-tag in the neighborhood of USD 170.

IV.1 Commercial Product I: Drager® Fire Escape Mask Details

Components:

1. Hood

2. Canister

    a. Particulate filter (HEPA)

    b. Hopcalite

    c. Particulate filter

3. Half Mask

4. Visor

5. Exhalation valve

Table 4.1 lists all the technical, performance and product details of Parat c®.

Table 4.1: Details of Parat C®

Sr. No.	Attribute	Value
1	Canister Weight	262.2 gm
2	Canister Cross-sectional Area	71 cm^2
3	Catalyst	Hopcalite
4	Catalyst Weight	173 gm
5	Canister depth	45 mm
6.	Breakthrough time	15 minutes

Figure 4.1 shows the drager® mask done by a researcher. As seen here the orange color hood goes around the face and head. The mask also has a half face visor. Air breathed in

passes through the canister into the half face mask. While breathing out, the air flows

through the exhalation valve on the left side of the face.

Figure 4.1: Drager Escape Mask Done

Figure 4.2: Drager Canister
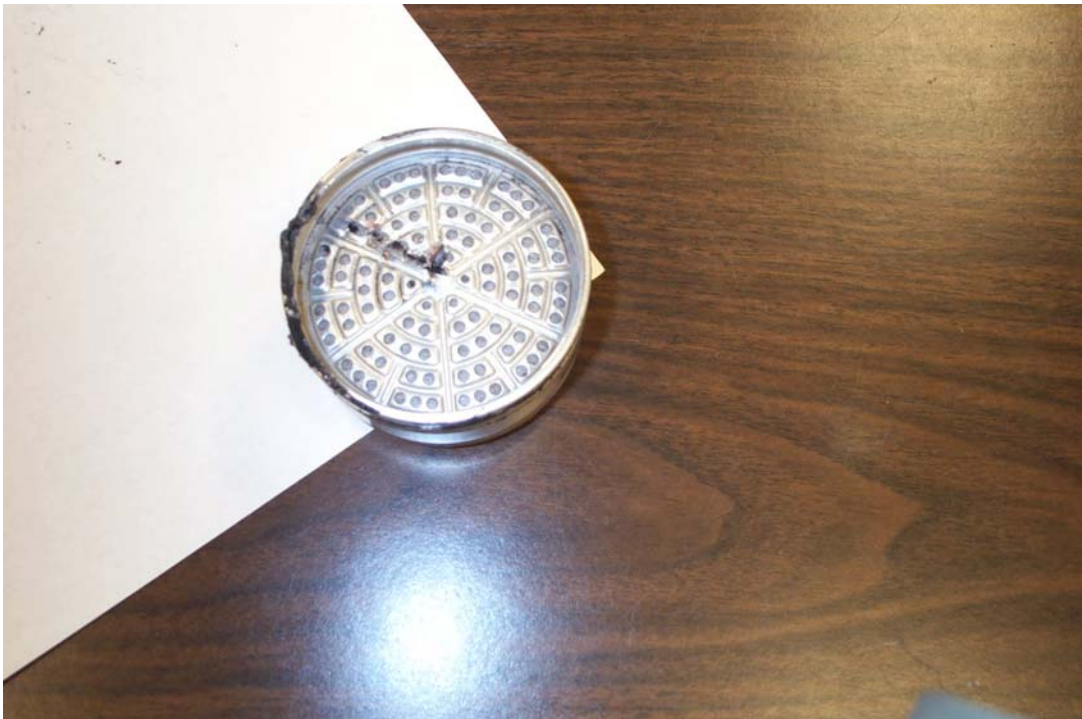
Figure 4.3: Drager Canister Opened

Figures 4.2 and 4.3 show pictures of canister as it is and when opened respectively. The canister is a metallic housing that incorporates Hopcalite, HEPA and another particulate filter inside. The catalyst bed configuration is packed bed.

IV.2   Commercial Product II : Essex® plus 10® Details

Figure 4.4: Essex plus 10® Mask Done

Figure 4.4 shows the Essex plus 10 mask done by a researcher. The design of this product is markedly different from other commercial hoods. The whole hood is made up of transparent material hence the mask does not need a visor. The front side of the canister shown in figure 4.5 is a rectangular housing. The back side of the canister is a cylindrical housing that holds the monolith for CO removal and copper heat sink in place is shown in figure 4.6. The front side of the canister houses charcoal cloths for removal of other gases. Figure 4.7 shows the monolith for CO removal.
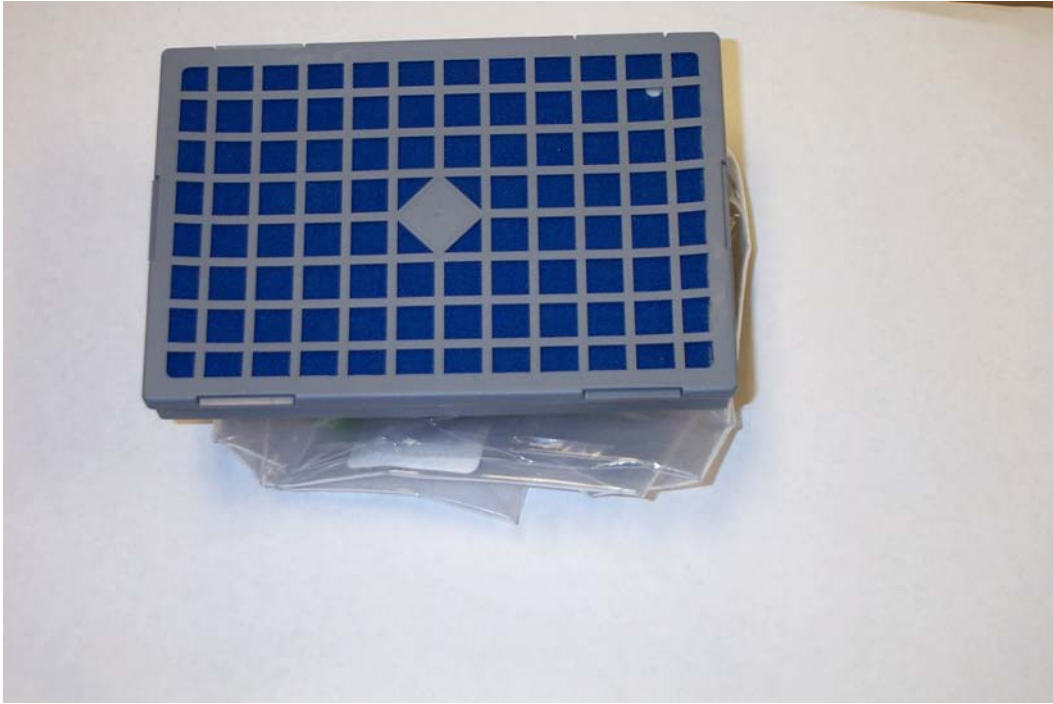
Picture 4.5: Essex Canister Front View

Figure 4.6: Essex Canister Back Side
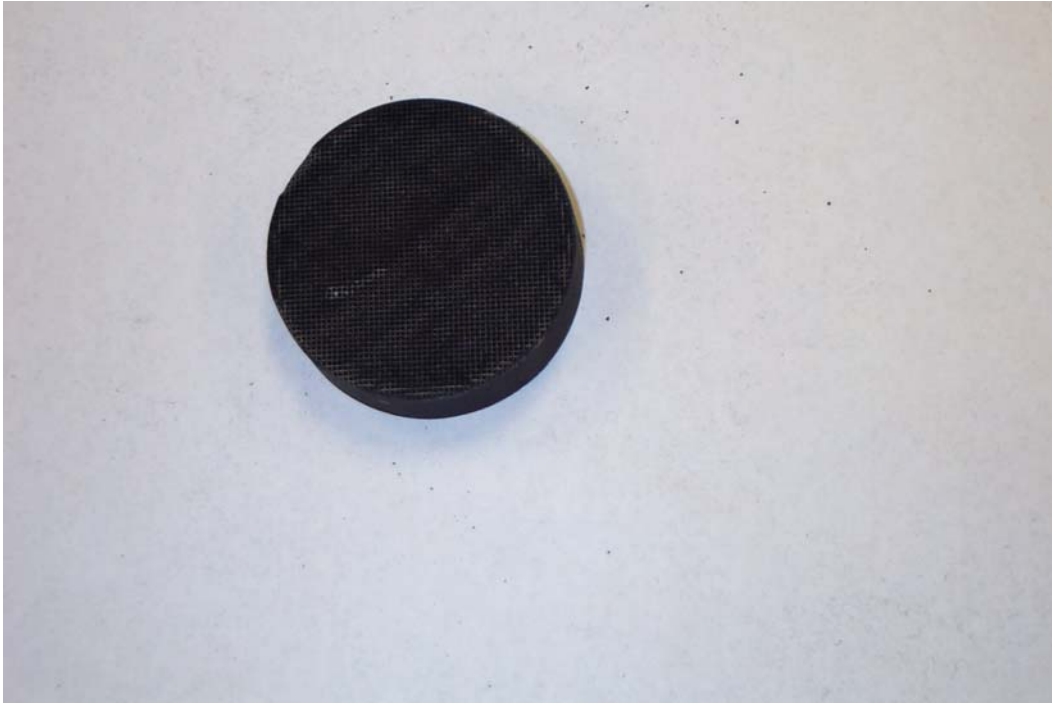
Figure 4.7: Essex plus10® Carbon Monoxide Oxidation Monolith

Components:

1. Hood

2. Fire retardant Nomex® layer

3. Canister

    a. Activated carbon coated cloth: 21 layers

    b. Precious Metal monolith

    c. Copper monolith: heat sink (7 layers of perforated copper discs riveted

        together

4. Exhalation valve

Table 4.2 lists all the technical, performance and product details for Essex plus 10®.

Table 4.2: Technical Details of Plus 10®

Sr. No.	Attribute	Value
1	Canister weight	244.6 gm
2	Weight of precious metal monolith	56.03 gm
3	Catalyst	Precious metal monolith
4	Diameter of monolith	76 mm
5	Channel diameter	1 mm
6	Height of monolith	20 mm
7	Weight of heat sink	168 gm
8	Diameter of heat sink	65 mm
9	Heat sink height	8 mm
10	Breakthrough time	15 minutes

IV.3   Commercial Product III: Sundstrom® SR 77® Product Details

The product details for this product had been obtained through personal communications with a research scientist from Sundstrom of Sweden [4.1]

The SR77® consists of following:

1. Hood

2. Visor

3. Canister

4. Half mask

5. exhalation valve

Table 4.3 lists all the technical, performance and product details for SR 77®

Table 4.3: Product details of SR 77®

Sr. No.	Attribute	Value
1	Total weight	590 gm
2	Canister diameter	96 mm
3	Canister height	45 mm
4	Total height	48.5 mm
5	Activated carbon type BR1 NC " from Suthcliff"	78 cc
6	Activated carbon type ER2 "from Suthcliff"	18 cc
7	"Drier"Molekyl Sil"	66 CC
8	CO converter Moleculite	140 CC
9	Total weight including canister/top	2946 gm
10	Breakthrough time	>35 minutes

IV.4 Commercial Product Testing

This section shows the details of commercial products tested for catalyst activity for carbon monoxide removal. The products tested are Drager Parat C and Essex plus 10.

IV.4.1 Testing of Drager® Canister

Figure 4.8: Drager Parat C® test for EN 403

Test Conditions:

Testing standards: EN 403

CO concentration: 2500 ppm

Inlet flow rate: 30 LPM

Temperature: 22^0C

Pressure: 1 atm

Relative humidity: 90%

As seen in figure 4.8, the canister gives nineteen minutes of gas life before it deactivates.

It is rated for 15 minutes of gas life.
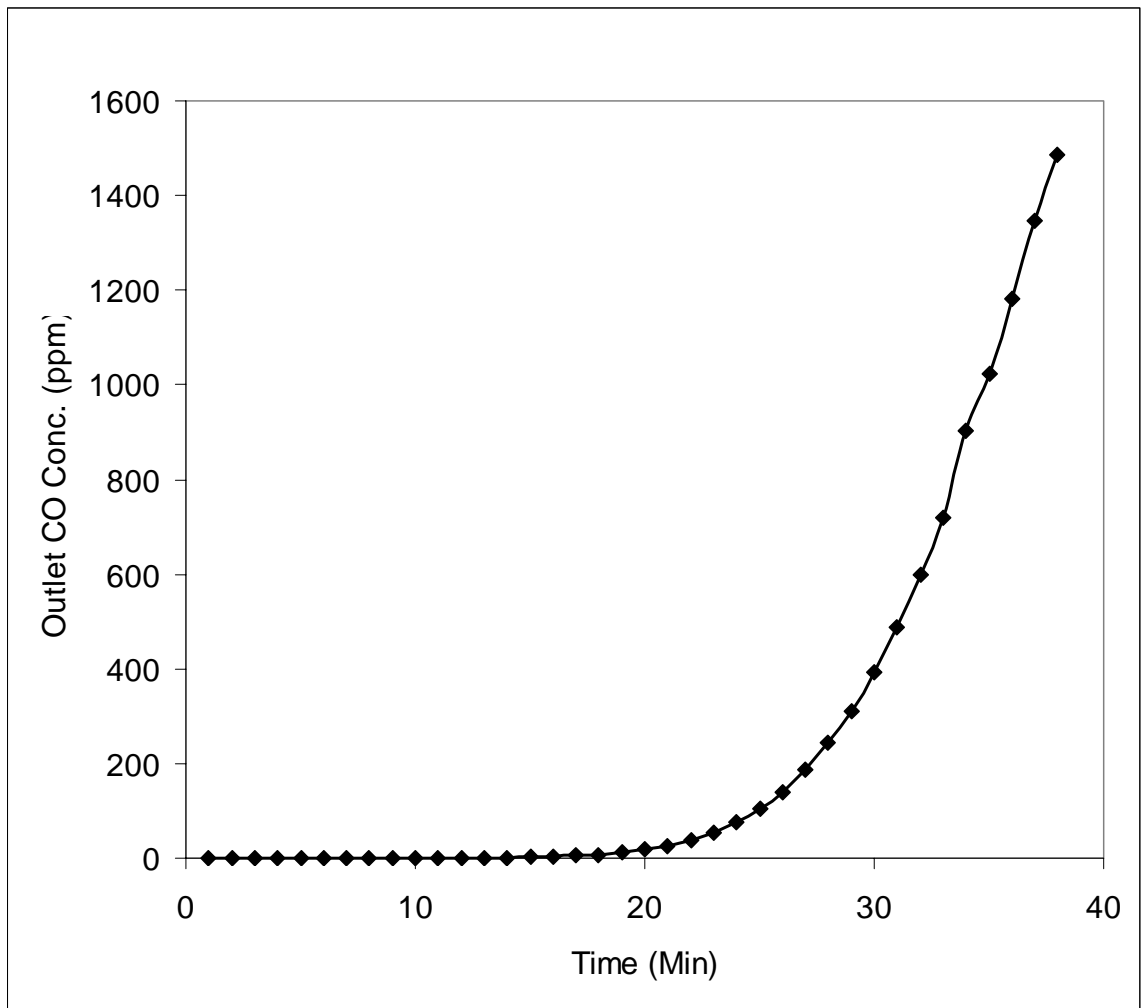
Figure 4.9: Drager Parat C® Test for EN 403

Test Conditions:

Testing standards: EN 403

CO concentration: 5000 ppm

Inlet flow rate: 30 LPM

Temperature: 22^0C

Pressure: 1 atm

Relative humidity: 90%

As seen in figure 4.9, the canister gives about 26 minutes of gas life before it deactivates. Higher concentration of CO for the same flow rate further increases the temperature adiabatically thereby increasing the activity of the catalyst.
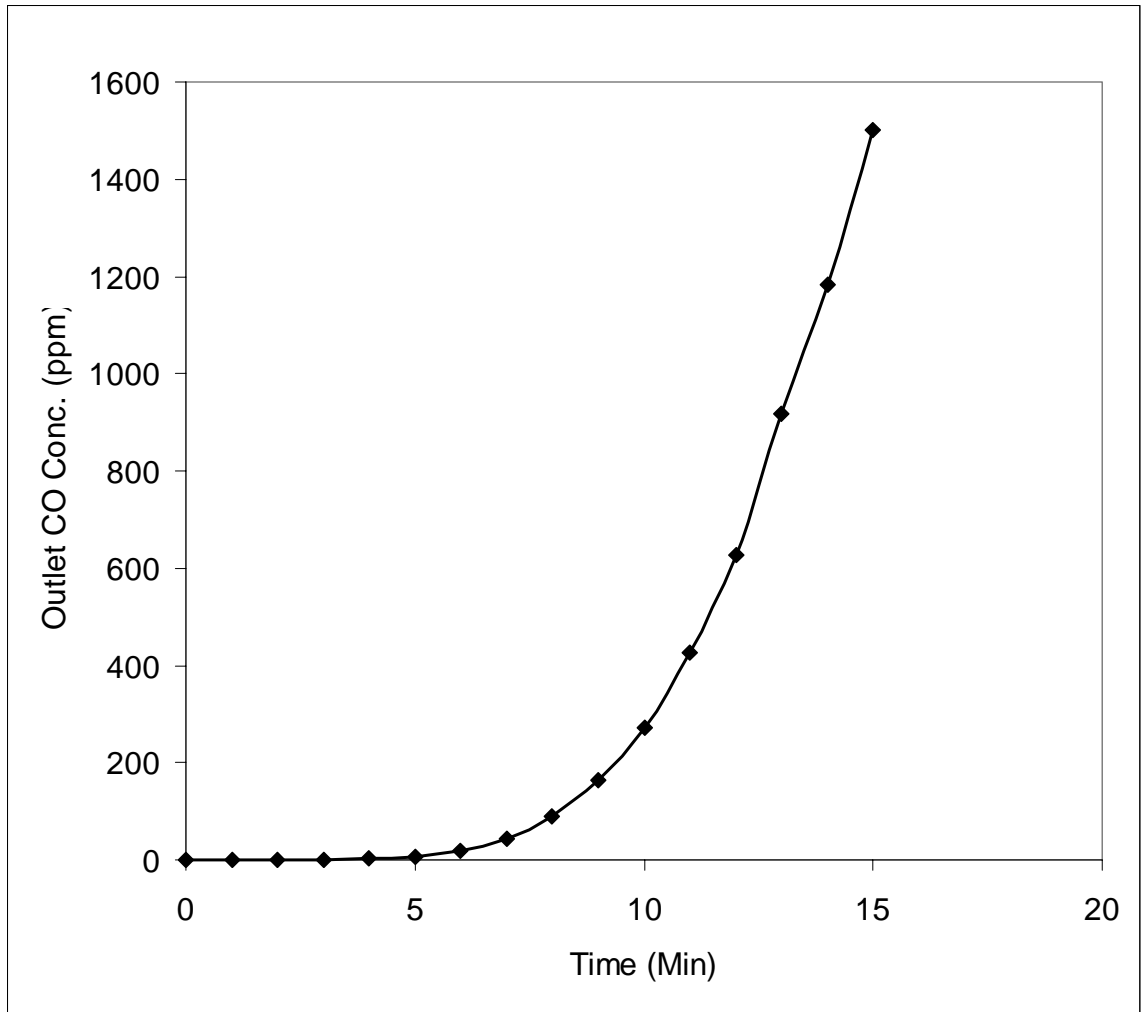
Figure 4.10: Drager Parat C® Test for CBRN General

Test Conditions:

Testing standards: CBRN (general category)

CO concentration: 3600 ppm

Inlet flow rate: 64 LPM

Temperature: 22^0C

Pressure: 1 atm

Relative humidity: 90%

135

As shown in figure 4.10, this canister fails to meet the 15 minute test as specified in

CBRN general document.
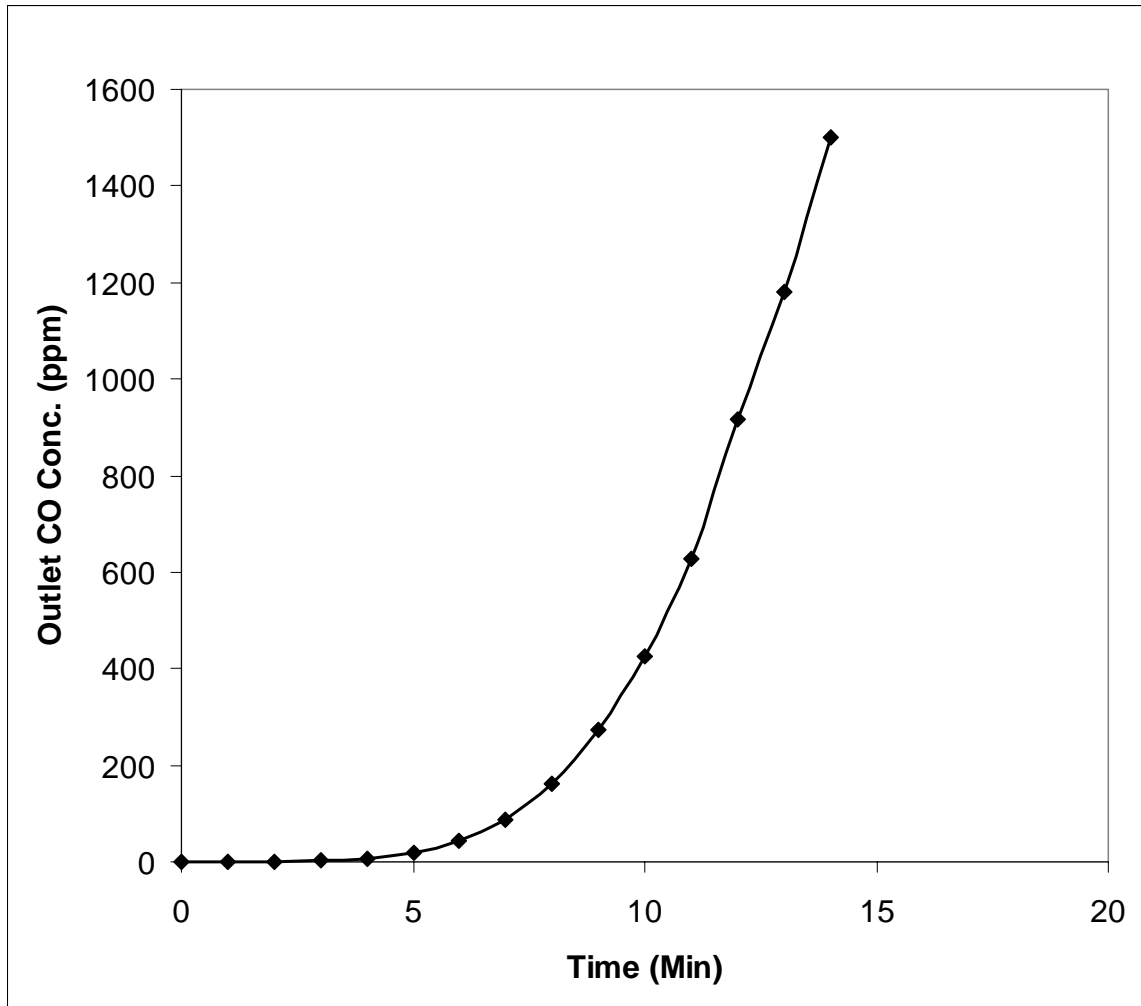
Figure 4.11: Drager Parat C® Test for ANSI 110-2003 #6

Test Conditions:

Testing standards: ANSI #6

CO concentration: 3000 ppm

Inlet flow rate: 93 LPM

Temperature: 22^0C

Pressure:			1 atm

Relative humidity:	90%

As seen in figure 4.11, drager canister fails to meet the 15 minutes test conditions as specified in ANSI/ISEA 110-2003.

IV.4.2   **Testing of Essex Plus10® Monolith**

This section shows the test results of Essex plus10® monoliths. Figure 4.12 shows the results of testing of monolith for EN 403 standards. As seen in the figure, monolith shows a behavior similar to microfibrous materials. In the beginning the outlet CO concentration increases and then falls down to almost zero. The monolith was stable running for about 1 hour. This product has been rated for 15 minutes gas life.
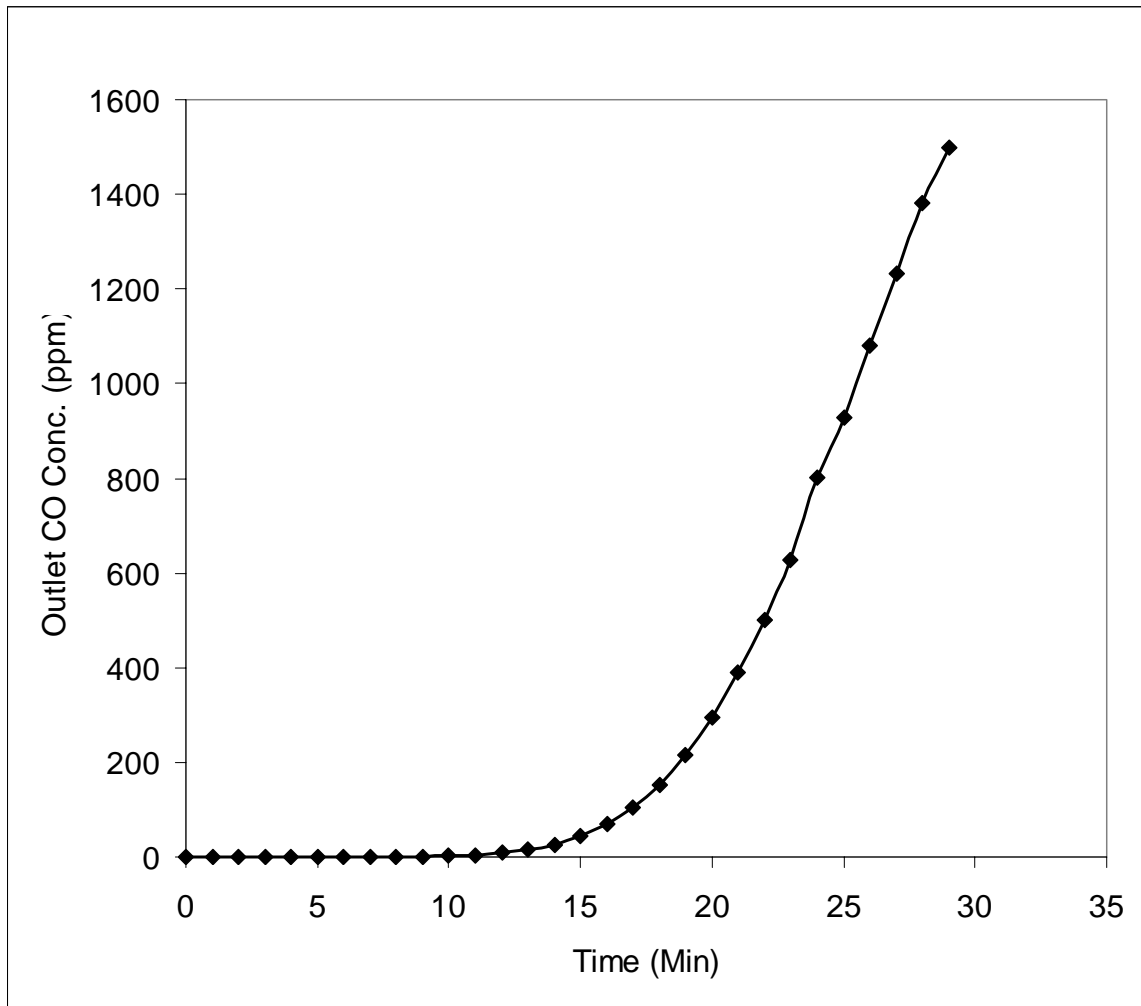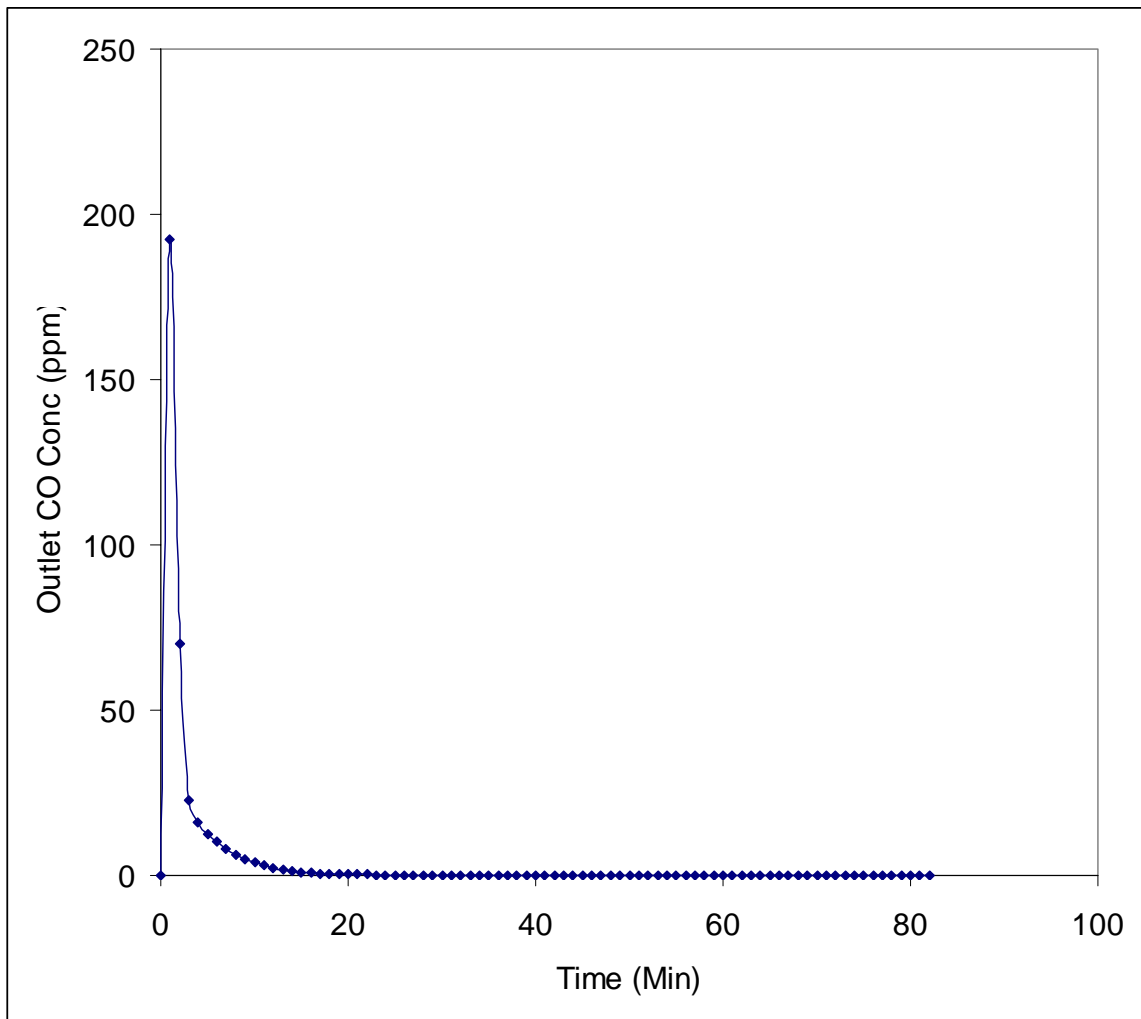

Figure 4.12: Essex® Monolith Test for EN 403

Conditions:

Testing standards: EN 403

CO concentration: 2500 ppm

Inlet flow rate: 30 LPM

Temperature: 22^0C

Pressure: 1 atm

Relative humidity: 90%

Test for ANSI #6 Standards
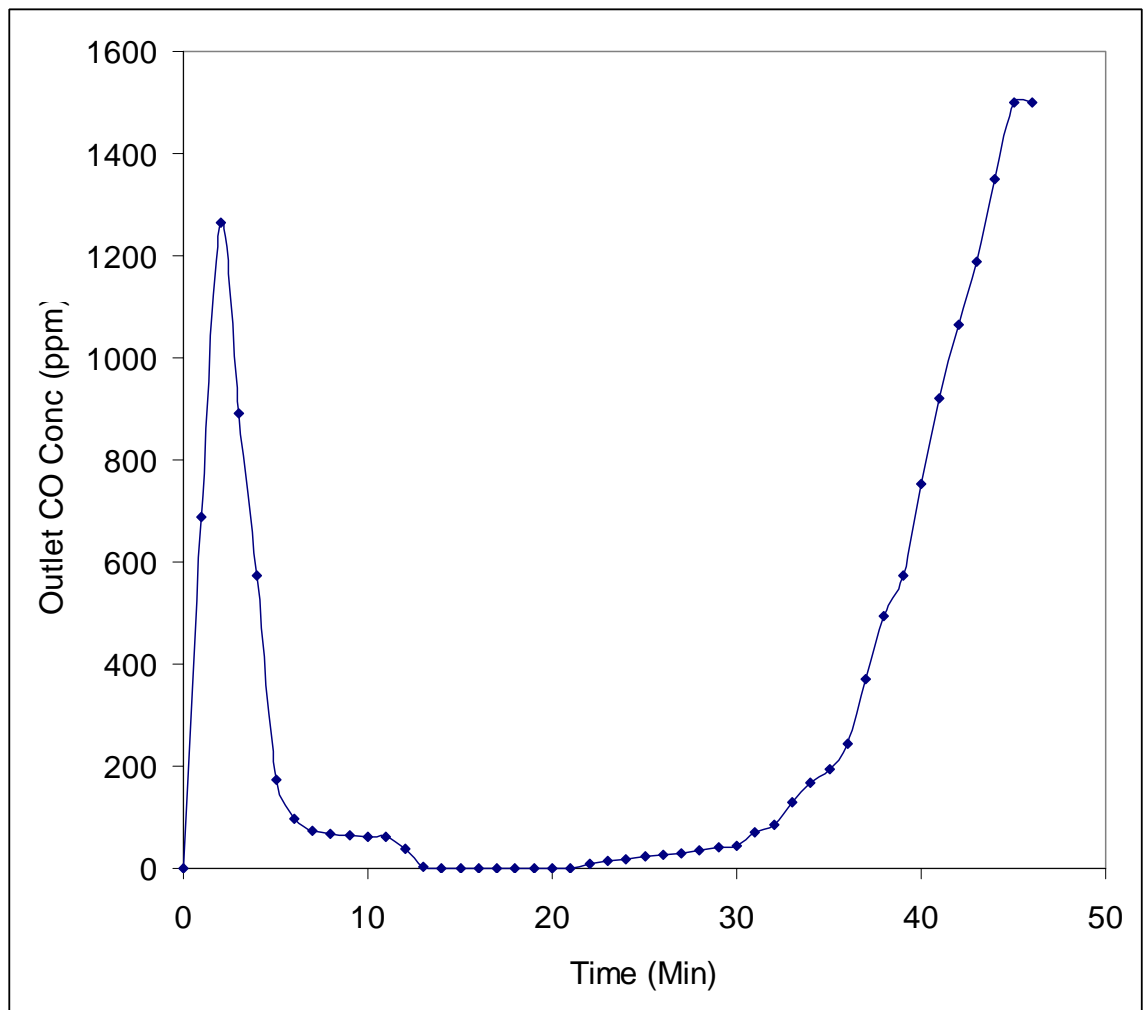
Figure 4.13: Testing of Essex® Monolith for ANSI #6

Conditions:

Testing standards: ANSI #6

CO concentration: 3000 ppm

Inlet flow rate: 93 LPM

Temperature: 22^0C

Pressure: 1 atm

Relative humidity: 90%

Figure 4.13 shows the test results for ANSI #6 standards. The concentration rises in the beginning upto approximately 1200 ppm. The monolith fails to meet the instantaneous requirement of 200 ppm outlet CO.

Figure 4.14 and 4.15 show results of CBRN general category test and inspired air temperature tests respectively. As seen from these figures the monolith fails to meet both these standards.
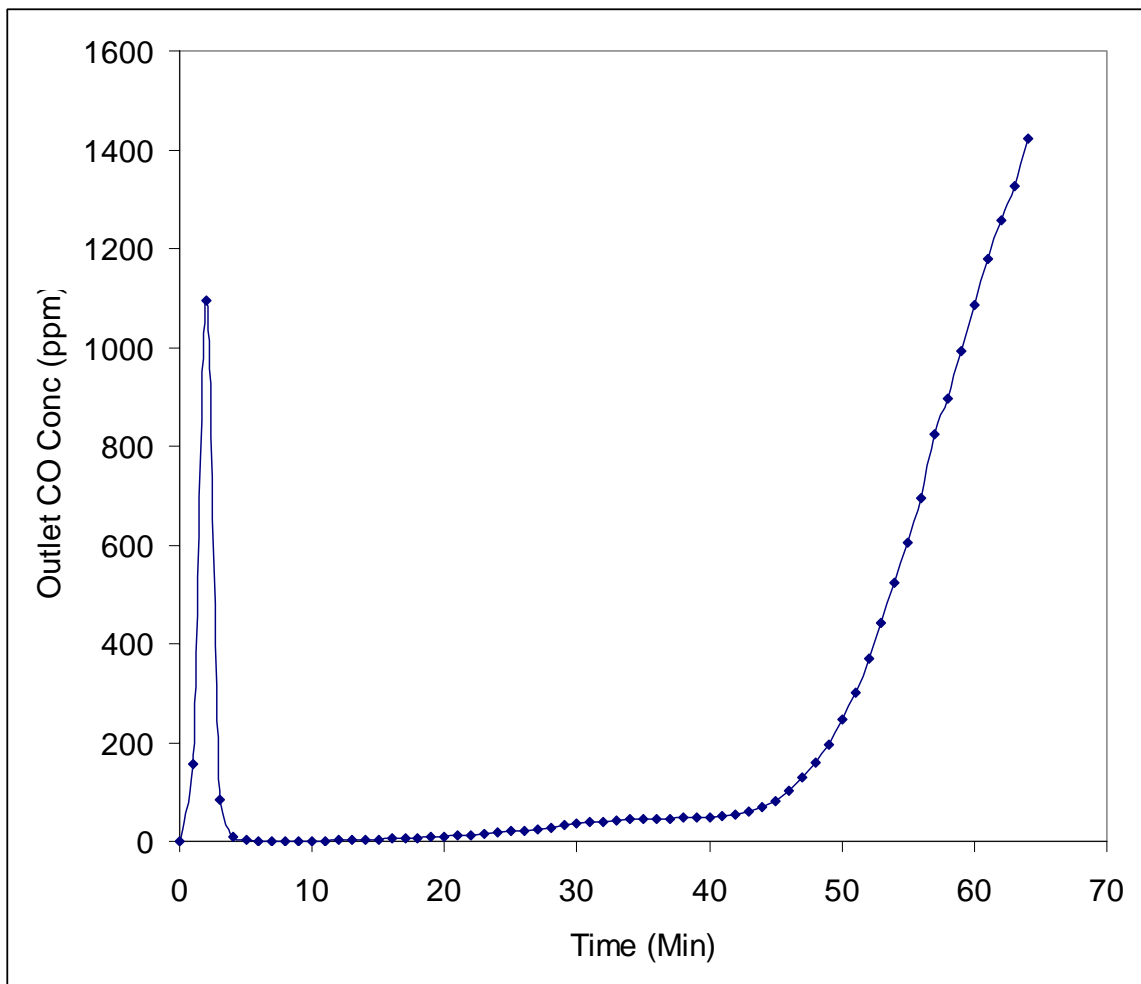
Figure 4.14: Testing of Essex® Monolith for CBRN General Category

Conditions:

CO concentration: 3600 ppm

Inlet flow rate: 64 LPM

Temperature: 22^0C

Pressure: 1 atm

Relative humidity: 90%
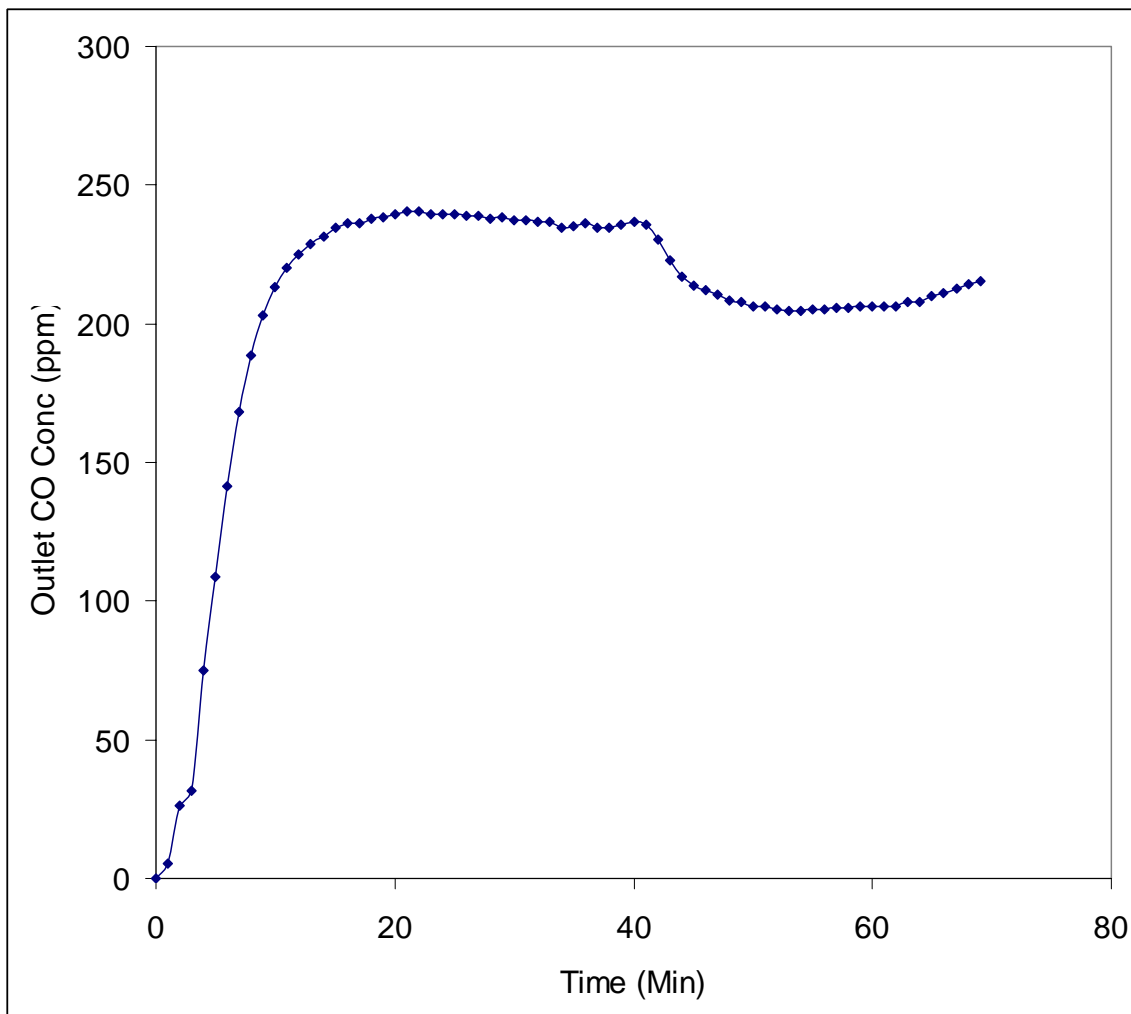
Figure 4.15: Testing of Essex® Monolith for Inspired Air Temperature Test

Conditions:

CO concentration: 1200 ppm

Inlet flow rate: 40 LPM

Temperature: 22^0C

Pressure: 1 atm

Relative humidity: 90%

IV.5 Comparison of CM^3 (MiniCOT) Catalyst with Commercial Catalysts

Table 4.4 shows the comparison of performance attributes of MiniCOT with parat C® and SR 77®.

Table 4.4: Comparison of MiniCOT attribute with commercial products

Attribute	Parat C®	SR 77®	MiniCOT
Standards Passed	EN 403	EN 403	**EN 403**
Area	71 cm^2	73 cm^2	**85 cm^2**
Total Catalyst Loading	173 gm (Hopcalite)	182 gm (Carbon = 58 gm) (Mol Sieve = 40 gm) (Hopcalite = 84 gm)	**16 gm**
Total Bed Depth	4.5 cm	4.5 cm	**4 mm**
Pressure Drop thro' the bed	> 40 mm of H$_2$O	> 40 mm of H$_2$O	**8 mm H$_2$O***
Time	19 min	35 min	**> 60 min**

As seen in the tables, with regards to the original goals, following achievement were made possible:

1. Order of magnitude reduction in catalyst loading

2. Four fold reduction in pressure drop

3. Gas life of canisters > 1 hr

4. Order of magnitude reduction in bed depth

*The pressure drop tests are discussed in details in chapter 5 (Technology Transfer).

CHAPTER V

TECHNOLOGY TRANSFER

After catalyst development and activity testing on laboratory scale it was found that catalyst met all the imposed standards for gas mask canister testing. As previously discussed the only standards that are actually in practice are EN 403.

The next logical step in the development process was to transfer the technology from bench to actual scale. The preparation of microfibrous wet-lay preform part had already been commercialized for a similar application before under the supervision of Intramicron Inc. This wet lay process corresponds to block I in figure 5.6. Sintering has also been scaled-up for a previous application which is represented by block III in figure 5.6. All the previous applications corresponded to development of adsorbents. MiniCOT technology transfer would be the first technology for catalytic applications. Some of the unique things pertaining to catalyst preparation were the primary challenges in the technology transfer activity. Reductions in cost of manufacturing and batch times are parts of the technology transfer process.

Other challenges present were catalyst aging studies and breathing resistance offered by the bed at higher flow rates. This chapter has been divided into following major sections:

1. Catalyst aging studies

2. Pressure drop tests (breathing resistance)

3. Process analysis to reduce costs and time

4. Identification and elimination of possible redundancies in process

V.1   Accelerated Aging Tests:

This section shows the results of accelerated aging tests of this catalyst.

Accelerated aging tests needed to be performed for following two reasons:

1. Final use of the catalyst would be in a fire escape mask that also contains other sorbents to remove acid gases, organic vapors etc.

2. Shelf life is a very important parameter since this face mask would be used at one time only, being anytime after manufacturing.

Figure 5.1: Comparison of Catalyst Activity with Aged Catalyst in Presence of TEDA/C, at 70^0C for 48 hrs

Conditions:

Inlet CO concentration = 3600 ppm

Relative humidity =   90%

Bed cross section =   20.26 cm^2

Figure 5.1 shows the comparison of activity of fresh catalyst to a catalyst that was aged for 48 hours in presence of TEDA/C (Tri-ethylene Diamine/carbon) which is a common sorbent for removal of organic vapors, acid gases etc. As seen from the figure, the activity of the catalyst aged in presence of TEDA/C drops drastically in first few minutes. The observation can be supported by deactivation of catalyst due to TEDA vapors.
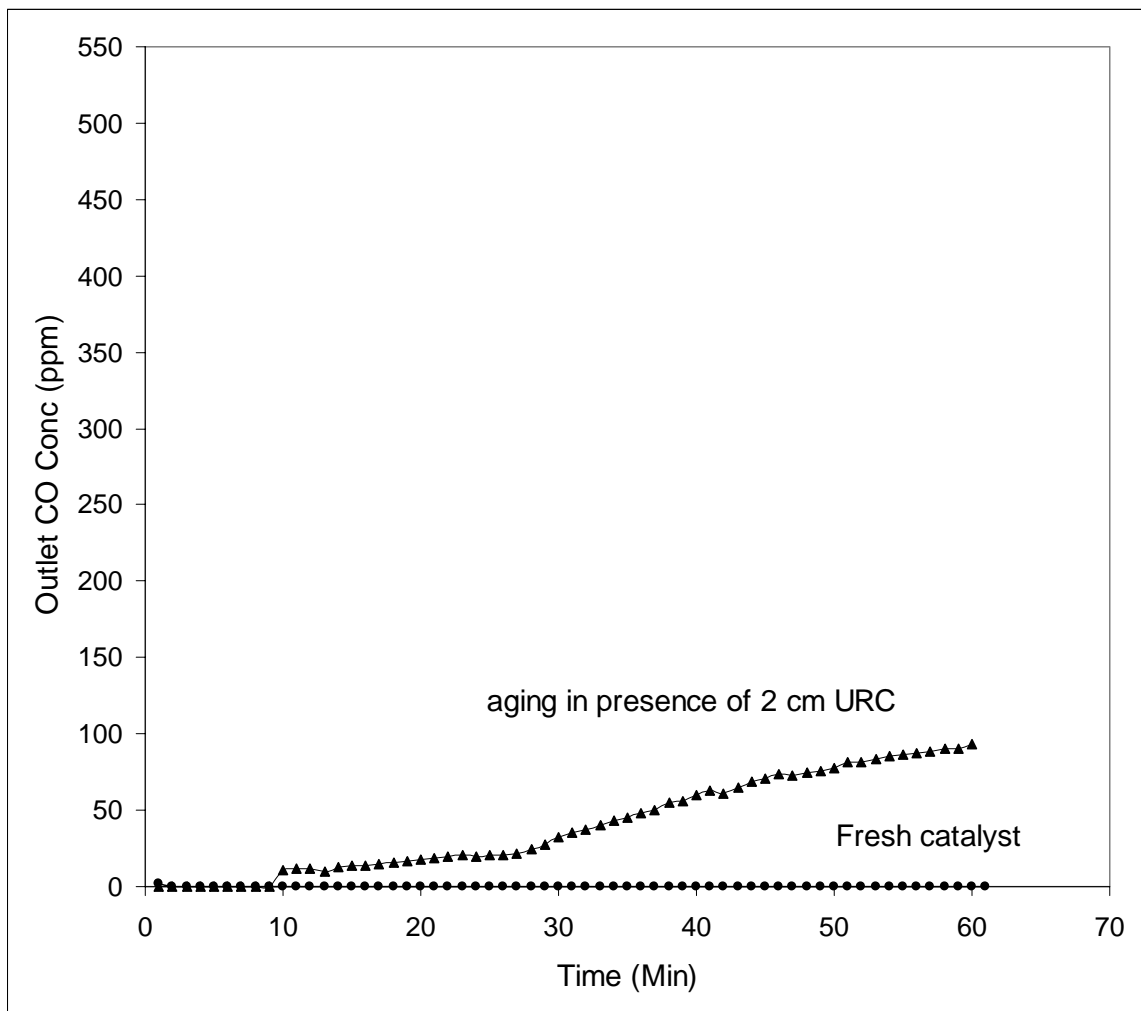
Figure 5.2: Comparison of Catalyst Activity with Aged Catalyst in Presence of URC, at 70^{0}C for 48 hrs

Conditions:

Inlet CO concentration = 3600 ppm

Relative humidity =   90%

Bed cross section =   20.26 cm^2

Figure 5.2 shows the comparison of activity of catalyst aged in presence of URC (universal respirator carbon) to that of fresh catalyst. The aged catalyst shows some deactivation but not significant. The catalyst can still perform well to meet EN 403 standards. The outlet CO concentration after 1 hr was below 100 ppm.
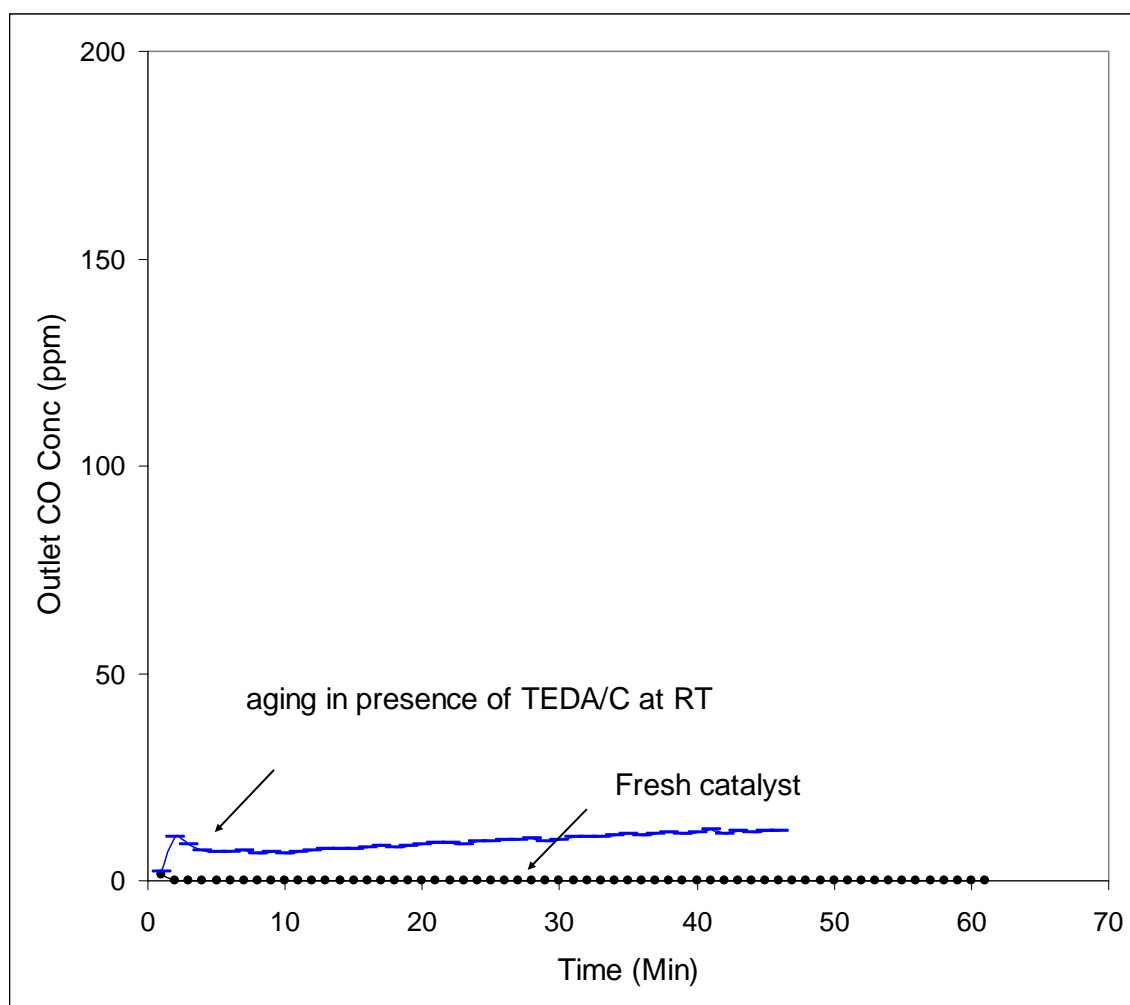
Figure 5.3: Comparison of Catalyst Activity with Aged Catalyst in Presence of ASZM/TEDA, at 22^0C for 48 hrs

Conditions:

Inlet CO concentration = 3600 ppm

Relative humidity =   90%

Bed cross section =   20.26 cm^2

   Figure 5.3 shows comparison of catalyst aged in presence of TEDA/C at room temperature to that of fresh catalyst. The deactivation of catalyst was not significant showing that the catalysts deactivates only when heated in presence of TEDA/C.
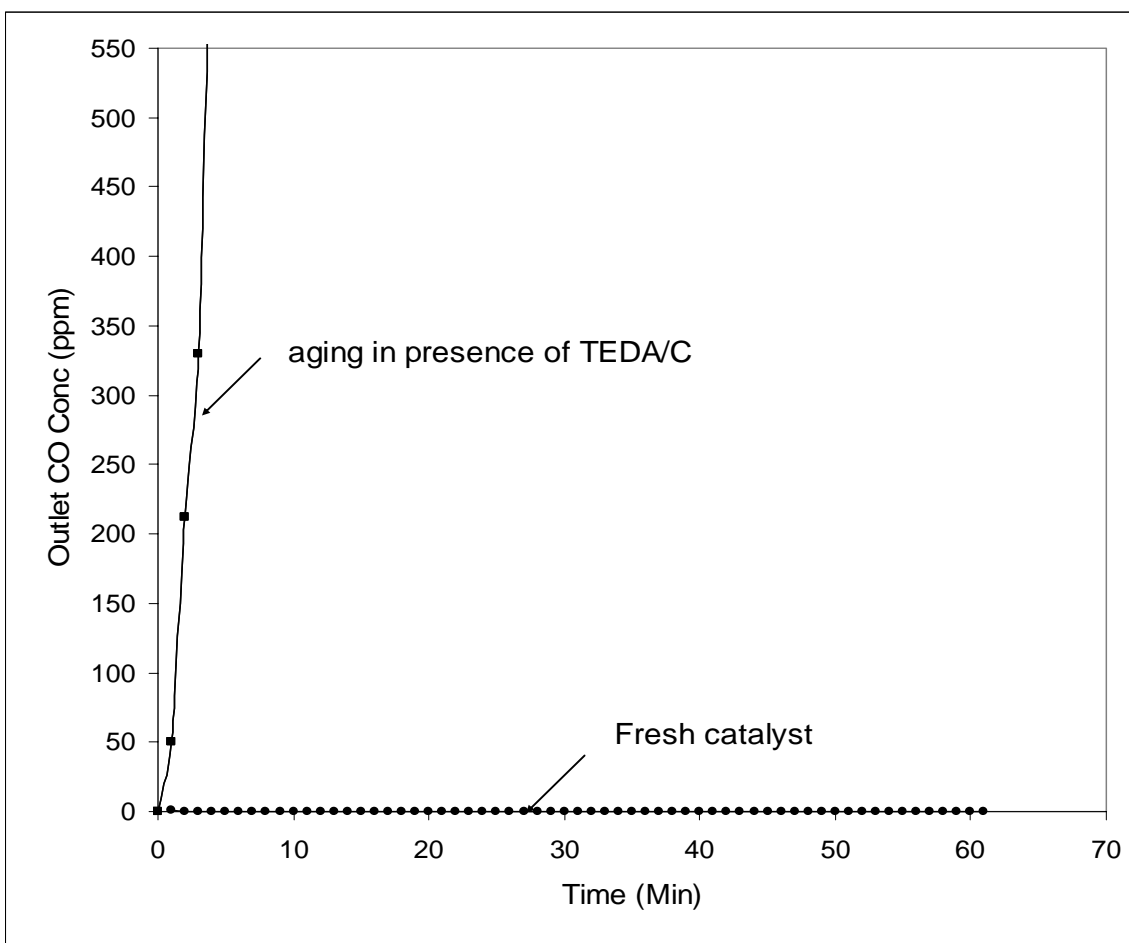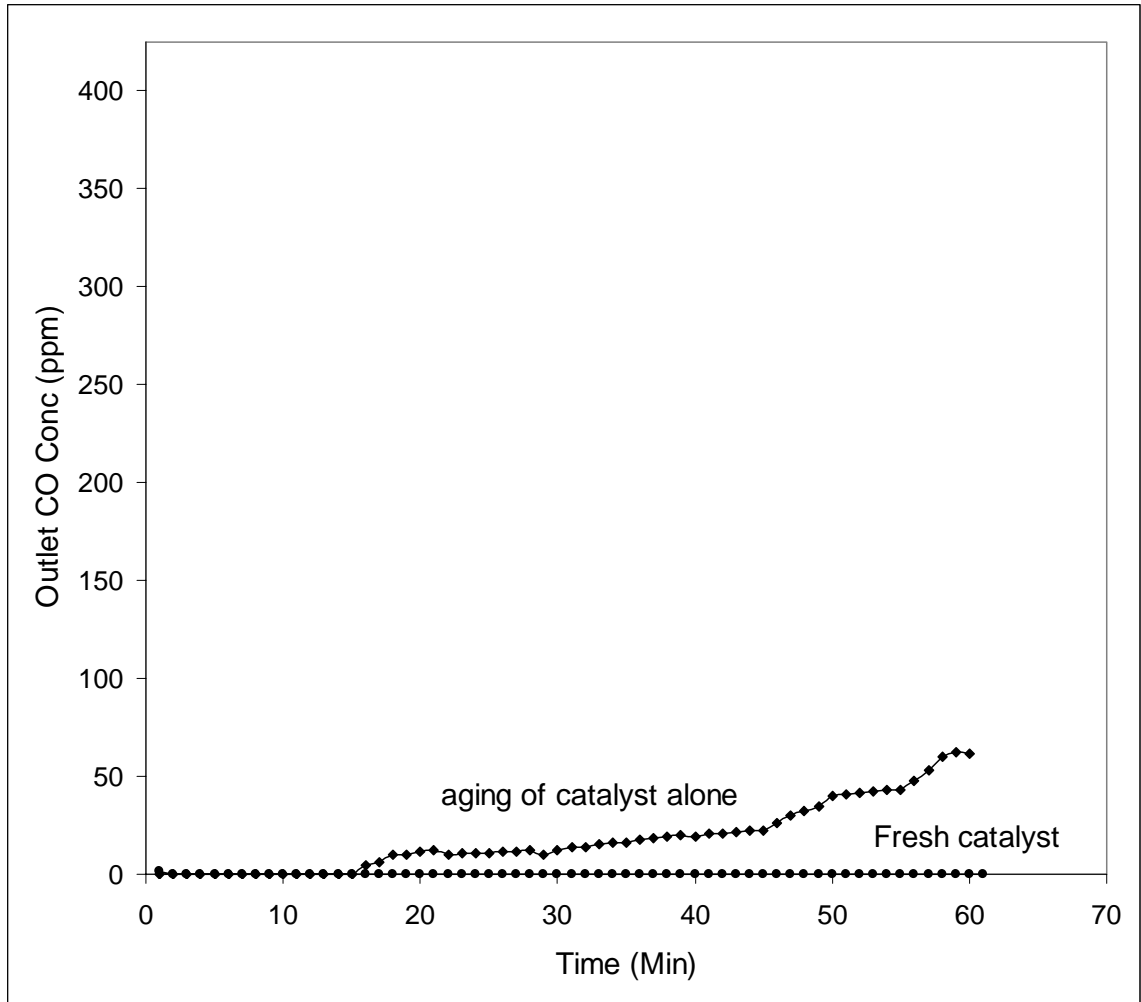

Figure 5.4: Comparison of Fresh Catalyst Activity with Aged Catalyst at 70^{0}C for 48 hrs

Conditions:

Inlet CO concentration = 3600 ppm

Relative humidity =   90%

Bed cross section =   20.26 cm^2

Figure 5.4 shows the comparison of activity of catalyst aged all by itself in presence of air to that of fresh catalyst. The loss in activity is insignificant.

V.2   Pressure Drop Measurements

Pressure drop is a very important parameter in the design of face masks since it directly corresponds to breathing resistance. The total pressure drop permitted by NIOSH under CBRN standards is 70 mm of water at 85 LPM flow rate through the canister. MiniCOT has a pressure drop of 8 mm of water which is extremely low compared to what has been permitted. All the same, this pressure drop is about 4 times lower compared to commercial products.
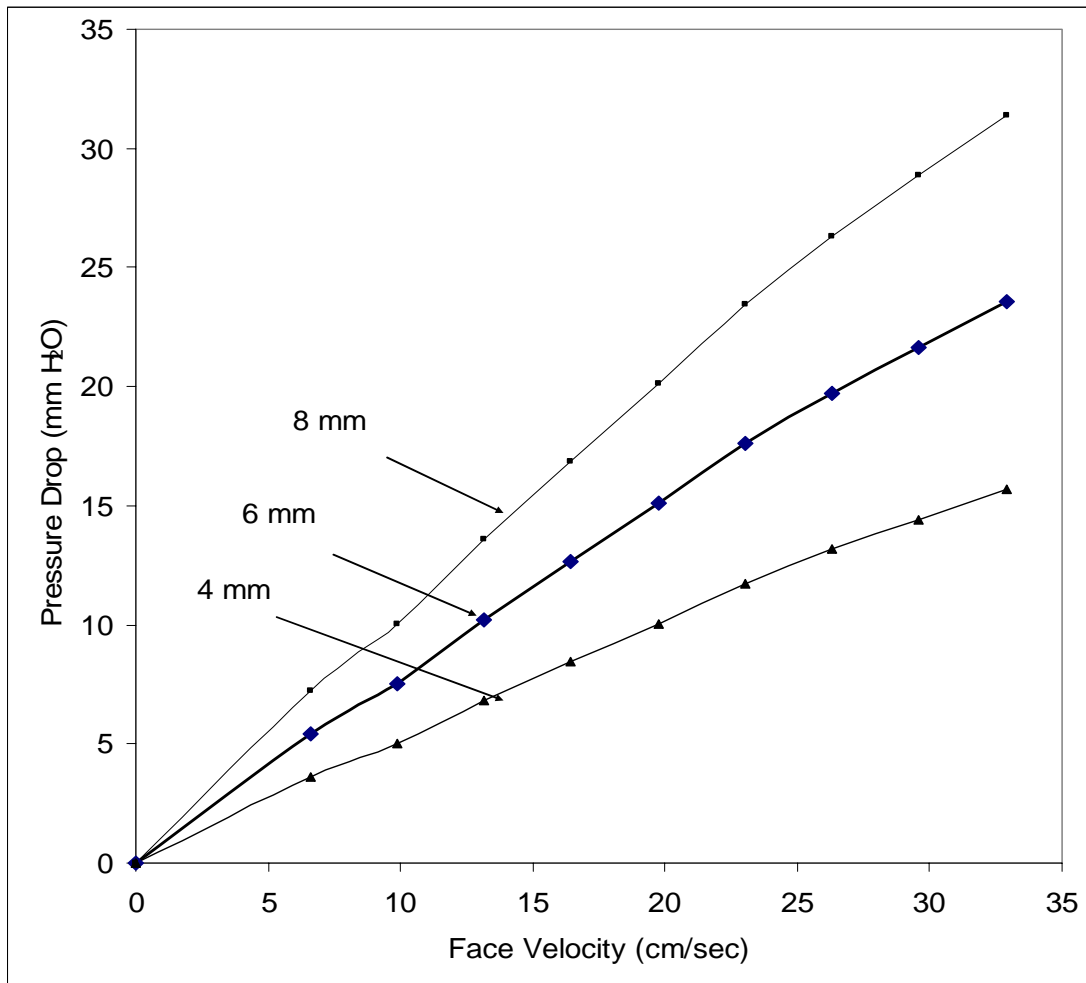
Figure 5.5: Pressure Drop through MiniCOT Catalyst as a Function of Face Velocity for Various Bed Thicknesses

V.3   Process Analysis:

For the sake of technology transfer the catalyst preparation process was divided into different blocks as shown in figure 5.6. Each block then was carefully analyzed for both cost as well as time taken by that particular block and any other challenges that existed. The basis for all the analysis here considered was 4 mm, 85 cm^2 disk.
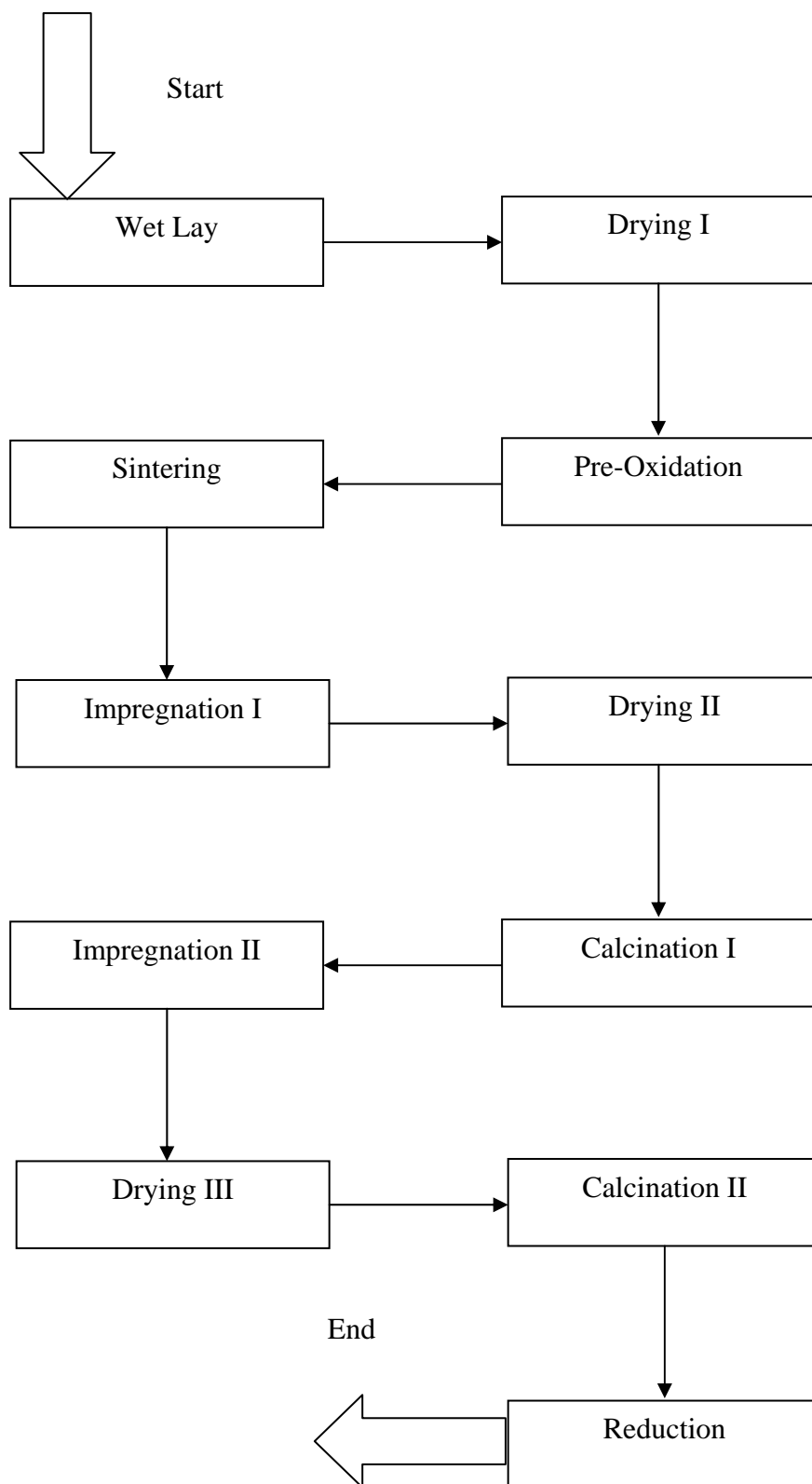
Figure 5.6: Process Flow Diagram of Catalyst Preparation

V.3.1 Wet-lay:

Material take-off (MTO):

Table 5.1 shows the material take-off calculation for wet-lay process stage. The major cost carrying items for this stage are Ni fibers.

Table 5.1: Material Take-off for Wet-lay stage

Material	Quantity (gm)	Cost ($)
4 micron Ni fibers	1.5	0.13
8 micron Ni Fiber	4.5	0.39
Cellulose	2.0	--
Alumina	12	0.01

Time:

Material weighing: 5 minutes

Blending: 10 minutes

Material preparation: 10 minutes

V.3.2 Drying:

Material: product of stage I

Time: 24 hours (@100 ^{0}C)

V.3.3 Pre-oxidation

Material: product of stage II

Time: 30 min.

V.3.4 Sintering

Material: product of stage III

Time:	30 minutes
Furnace start-up time:	8 hrs
Furnace shutdown time:	8 hrs

V.3.5   Impregnation I

Table 5.2 shows the material take-off calculation for impregnation I stage. Cobalt solution adds to the cost of preparation of material in this stage.

Table 5.2: Material Take-off for Impregnation I:

Material	Quantity (gm)	Cost ($)
Sintered preform	17.2 gm	-
Cobalt Solution	19.05 ml (0.28 gm Co)	0.14

Time: 60 minutes

V.3.6: Drying II

Material:	Cobalt impregnated sintered preform
Time:	24 hours (@100 ^{0}C)

V.3.7: Calcination I

Material:	Product of stage VI
Time:	4 hours

V.3.8: Impregnation II

Table 5.3 shows the material take-off calculation for impregnation II stage. Platinum solution adds to the cost of preparation of material in this stage. This has been the most expensive material so far in to the process.

Table 5.3: Material Take-off for Impregnation II:

Material	Quantity (gm)	Cost ($)
Sintered preform(Cobalt impregnated)	17.2 gm	-
Platinum Solution	16.5 gm (0.56 gm Pt)	33.00

Time: 60 minutes

V.3.9: Drying III

Material: platinum impregnated sintered preform

Time: 24 hours (@100 ^{0}C)

V.3.10: Calcination II

Material: Product of stage IX

Time: 4 hours

V.3.11: Reduction

Material: Final catalyst

Time: 3 hours

V.4 Identification of Rate-determining Stages:

The catalyst making process for lab-scale preparation has been documented in chapter 2. For large scale manufacturing, following challenges existed:

1. High cost of making the catalyst

2. Longer batch times

3. Use of Continuous Sintering Furnace

V.4.1 Cost of Catalyst

It was quickly realized that prime cost-driver for catalyst making here is the cost of platinum pre-cursor. (Current recipe: 5 % platinum on Al_2O_3 (Co:Al = 0.34))

Table 5.4 shows the details of cost of platinum solution. The calculations are based on 85 cm^2 disc with 4 mm thickness. This is equivalent to meeting EN403 standards.

Table 5.4: Cost calculations for platinum

Sr. No.	Attribute	Value
1	Area of 6" disk (cm^2)	182.32
2	Alumina for 3X6" disk-2 mm (gm)	12.00
3	Alumina for 85 cm^2, 4 mm layer (gm)	11.19
4	Platinum content (gm)	0.56
	Price of 3.4 % Pt solution ($/ml)	2.00
	Solution required making one prototype (ml)	16.47
	Price of Pt solution for one prototype	33.00

The prime motive in technology transfer as far as cost goes, was to bring this cost down to half as a first milestone. Hence personal communications were initiated with bulk manufacturers of platinum solution. Following modified costing as shown in table 5.5 is possible after getting a response from Johnson Matthey®.

V.4.1.1   Costing of MiniCOT Catalyst for Meeting EN 403 Standards (4 mm Bed Thickness)

Table 5.5 shows the costing of material after Johnson Matthey® response:

Table 5.5: Modified costing of MiniCOT

Sr. No.	Attribute	Value
1	Area of 6" disk (cm^2)	182.32
2	Alumina for 3X6" disk-2 mm (gm)	12.00
3	Alumina for 85 cm^2, 4 mm layer (gm)	11.19
4	Platinum content (gm)	0.56
Johnson Matthey (50 gm/L solution) (50 - 100 Gal range)		
1	Pt bulk price ($/troy ounce)***	856.00
2	Pt bulk price ($/gm)	27.52
3	Fabrication cost* ($/troy ounce)	22.00
4	Fabrication cost ($/gm)	0.71
5	Total cost $/gm of Pt content	28.23
6	**For 4 mm layer ($)**	**15.79**
Johnson Matthey (50 gm/L solution) (higher quantities)		
1	Pt bulk price ($/troy ounce)***	856.00

Sr. No.	Attribute	Value
2	Pt bulk price ($/gm)	27.52
3	Fabrication cost* ($/troy ounce)	15.00
4	Fabrication cost ($/gm)	0.48
5	Total cost $/gm of Pt content	28.00
6	**For 4 mm layer ($)**	**15.67**

Notes:

*Fabrication cost has been defined as a charge that Johnson Matthey® counts to convert a given quantity of platinum into corresponding salt for catalyst preparation purposes.

***: This number can be found real time at www.platinum.matthey.com (changes as bullion price)

V.4.2 Batch Cycle Time Reduction

As seen in the process documented in chapter 2, drying was the highest time consuming process on a laboratory scale. Two different drying cycles together took 48 hours of drying time. Various experiments were performed to reduce this time as much as possible. First set of experiments consisted of cutting the drying time by half. The following table indicates the loss of moisture (weight) comparison of the precursor. It was observed that the weight loss in both drying cycles, viz. 12 hours and 24 hours was exactly same. Hence in conclusion drying time could be reduced in half. Further reduction in drying time could reduce the batch times further as it was the still the slowest step in the process.

The catalyst support was dried for 1.5 hours at 150^0C. The observations on weight (moisture) are detailed in table 5.6.

Table 5.6: Weight Loss Comparison

Reading	Weight (gm)		
	Sample 1	Sample 2	Sample 3
Weight before drying	34.8	33.9	34.45
Weight after drying	29.54	28.8	29.3
Weight loss	5.26	5.1	5.15

Sample 3 was dried in the conventional way, 24 hours at 100^0C. As seen from the table, the total moisture loss in either case remained same. Hence the final drying time reached was 1.5 hours.

V.4.3 Use of Continues Sintering Furnace

In the lab-scale preparation of catalyst; the maximum size of the catalyst that could be obtained was limited by the size of the sintering furnace. The maximum cross-sectional area for one catalyst disc would be 5 cm^2. The end-application demands minimum cross-section on the disk to be 85 cm^2. The continuous sintering furnace was used to sinter multiple disks of 182 cm^2 area each. The results on the final product, that is, the sintered pre-cursor for catalyst preparation, were similar to lab-scale preparation.

V.4.4 Elimination of Stages

Conventional microfibrous carrier preparation process contains 'pre-oxidation step'. The purpose of this stage is to burn the cellulose that has been used as a binder while wet-lay processing of these wires. The pre-oxidation is performed at 400^0C in presence of 5% oxygen for about 30 minutes. Handling of materials become tedious since very fragile material coming out of pre-oxidation stage needs to be carried to sintering furnace. Hence some experiments were performed to check if this stage can be eliminated during the technology transfer process. Few pre-forms were sintered without pre-oxidation. After impregnation and pre-reduction as described previously, these catalysts were tested. Figure 5.7 shows that, there was very little to no change in activity of this catalyst when compared to activity of the catalysts that were prepared out of pre-oxidized preforms. However this needs to be tested for further activity sustenance by performing more demanding tests before finalizing of elimination of pre-oxidation stage.
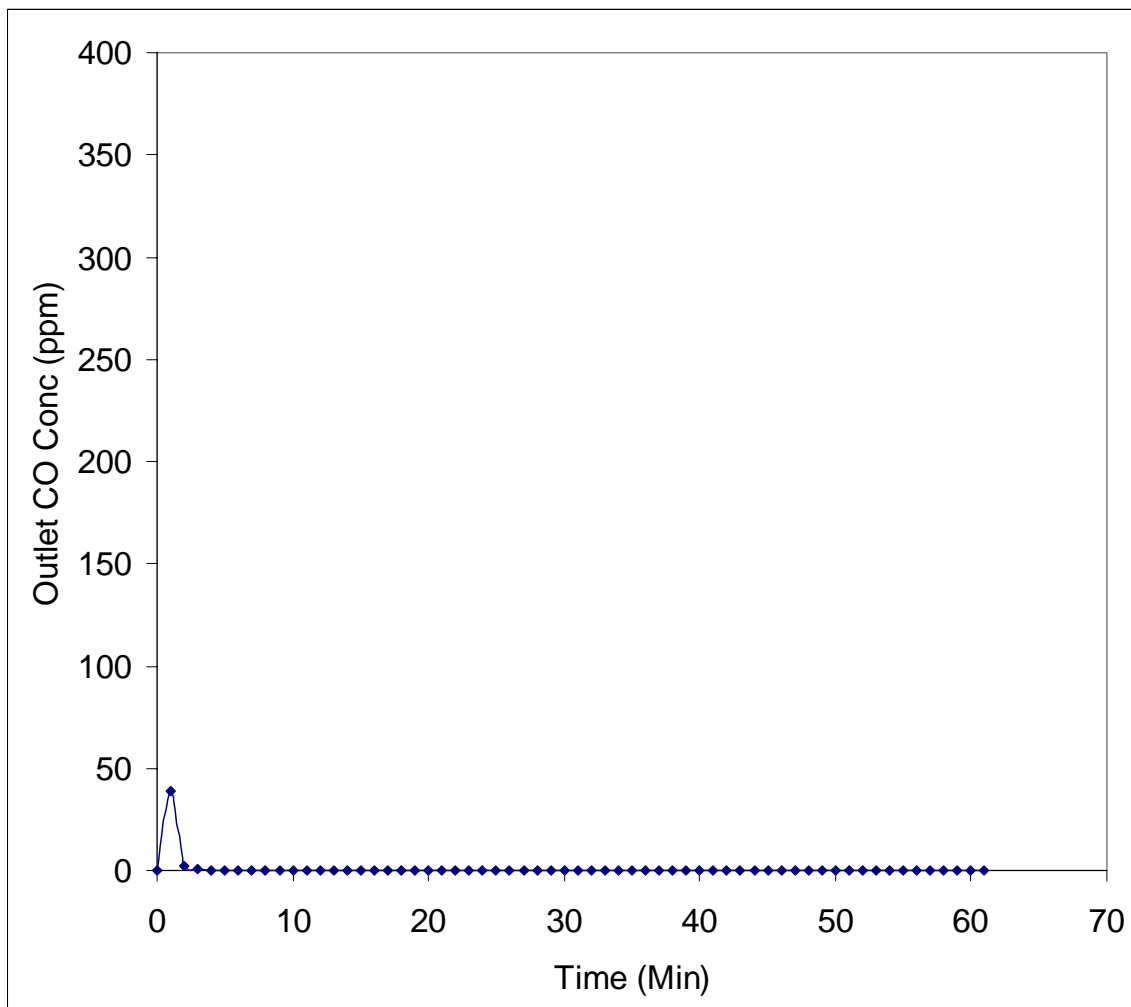
Figure 5.7: Testing of Catalyst after Elimination of Pre-oxidation Stage- Sample I

Conditions:

Standards tested for: EN403

Inlet CO Concentration: 2500 ppm

Relative Humidity: 90 %
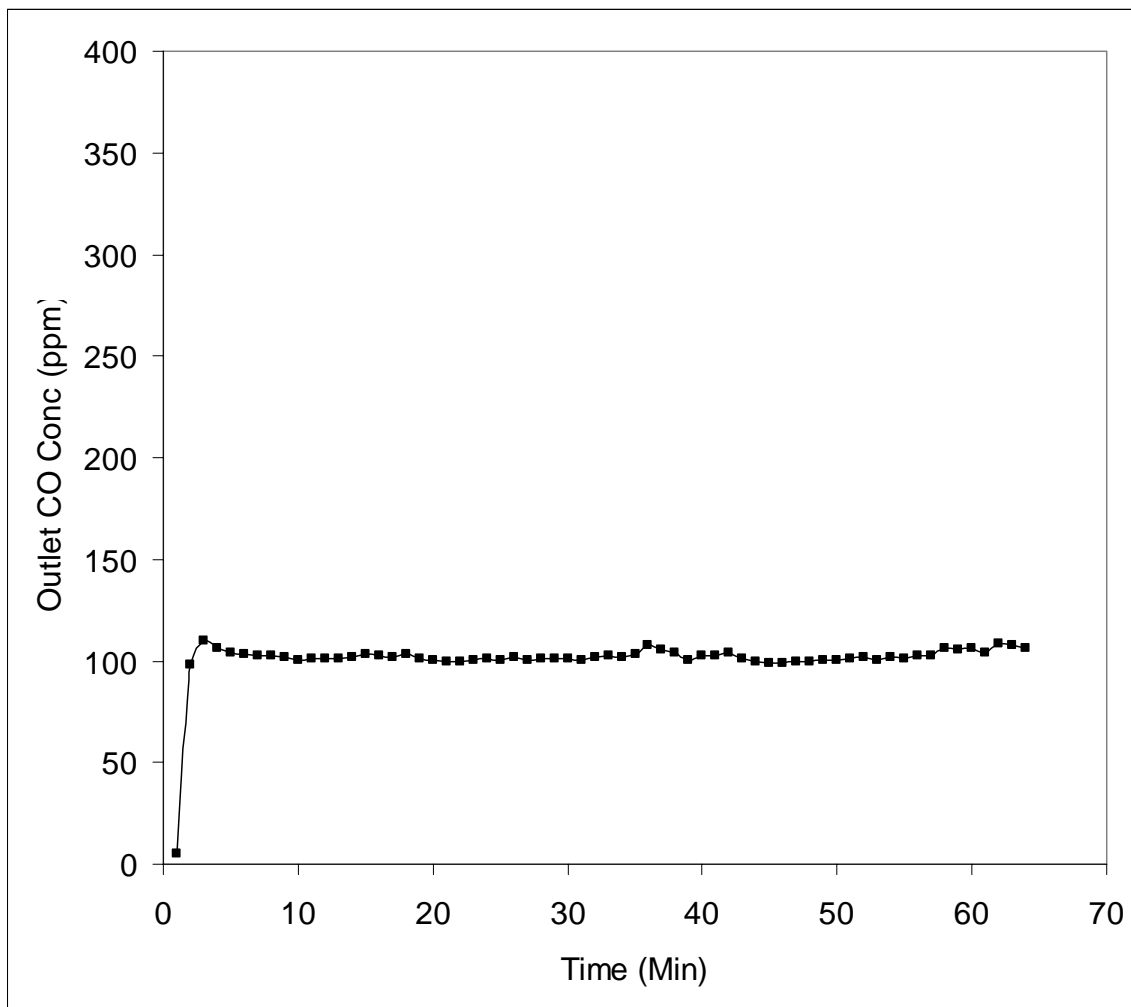
Bed Depth: 4 mm

Figure 5.8: Testing of catalyst after Elimination of Pre-oxidation Stage- Sample II

Conditions:

Standards tested for: EN403

Inlet CO concentration: 2500 ppm

Relative humidity: 90 %

Bed depth: 4 mm

CHAPTER VI

CONCLUSION AND RECOMMENDATIONS FOR FUTURE WORK

This chapter lists the various intermediate conclusions drawn out of the present research work and general future direction for this research project based on current information.

VI.1   Conclusion

This section details the various conclusions drawn our of this research project. The conclusions can generally be divided as following:

1. Catalyst

2. Process

3. Improvement in existing products

4. Technology transfer

VI.1.1 Catalyst

An extensive number of catalysts have been proposed and investigated by many researchers for the low temperature oxidation of carbon monoxide in hydrogen, as described in Chapter I.

VI.1.2 Process

Chapter 3 described catalyst screening, effect of various catalyst making conditions and parameters on the activity of the catalyst. Originally two catalysts were candidates for this reaction but finally cobalt promoted Pt/Al_2O_3 was found to be the most active catalysts over the whole gamut of conditions. A considerable thought has been given to reaction ignition-extinction behavior, which is well known in literature. The benign effect of moisture on the catalyst activity has also been studies in details. The hysteresis maps have been plotted and described in details. A well-known self-sustained oscillations behavior has been observed under pertinent sets of conditions. It has also been observed that, the reactivity of catalyst bed, in microfibrous configuration was much higher compared to packed bed of equivalent particle size.

VI.1.3 Improvement in Existing Products

Chapter IV describes the testing of commercial products and internal bench-marking. Two commercial products were tested in detail, Drager®, Parat C® and Essex® Plus10®. Also relevant analysis of Sundstrom SR77® was done. Following conclusions were reached based on comparison of MiniCOT with commercially available products mainly Parat C® and SR 77®;

i. Order of magnitude reduction in catalyst loading

ii. Four fold reduction in pressure drop

iii. Gas life of canisters > 1 hr

iv. Order of magnitude reduction in bed depth

VI.1.4 Technology Transfer: Cost Issue

The technology transfer process described in chapter V, details how manufacturing cost could be reduced as phase I of the transfer. The platinum cost was reduced by half to $15.67 for scale-up. The time of processes such as drying has been reduces considerably. The microfibrous carriers have been prepared using the continuous belt-furnace to test for effect of scaling-up. Very little change has been observed. Studies have been performed to eliminate the pre-oxidation process so that material handling could be easier. Materials are extremely fragile between pre-oxidation and sintering process. Hence handling becomes an important issue. Pressure drop tests have been performed to test the suitability of this material. As described in chapter V, the pressure drop through the bed of microfibrous material was four times lower than that of equivalent packed bed.

VI.2   Recommendations for Future Work

This section describes in-brief, the general future research direction for this project.

1. Further reduction in catalyst loading

2. Smooth and integrated manufacturing process

3. Alternate carrier materials: primarily polymers

4. Integration of MiniCOT with other sorbents to remove other contaminants from fire gases

5. Packaging

6. Computational fluid dynamic and residence time distribution studies in microfibrous beds

VI.2.1 Further Reduction is Catalyst Loading

As of now, catalyst, primarily platinum metal forms a large fraction of manufacturing cost of the canister. Hence it is very important to lower the loading of platinum to further reduce the cost of material.

VI.2.1.1   Exploitation of Ignition-Extinction Behavior

This can be done by taking advantage of layering characteristics of microfibrous bed. Microfibrous materials can be layered every millimeter with different particle and fiber size.

Smaller catalyst particles can ignite the reaction by increasing the temperature locally since the heat capacity is very low. If front part of the bed can be packed with

extremely small particle size layer, and then increasing the particle size gradually, following advantages can be realized:

i. Front of the bed ignites and hence drives the reaction faster due to temperature rise.

ii. Back part of the bed, having larger particle size structure, can offer resistance to deactivation. The top layer can be deactivated quickly but the inner of the catalyst still remains active.

Thus layering of particles can help not only this reaction, but any reaction that has tendency to show multiplicity behavior.

VI.2.1.2   Modeling of Ignition-Extinction Phenomenon

Considerable work has been done by various researchers on modeling of ignition-extinction behavior and hysteresis. This body of literature can be further utilized to come-up with a suitable model for promoted platinum/alumina catalyst. This model can also be helpful in predicting layering of various particle sizes.

VI.2.1.3   Analytical & Surface Chemistry Studies

A qualitative reaction model could be proposed with the help of surface chemistry. The enhancement of reaction rate due to moisture could be further studied to quantify the effect.

Analysis should also be performed to study catalyst structure and quantitatively find out catalyst structure. Preliminary results from SEM/EDS are shows in appendix D.

VI.2.2 Smooth and Integrated Manufacturing Processes

The various manufacturing processes involved can be further smoothened out and integrated. This would mainly consist of customizing available set-up. The customization shall consist of making trays that can hold optimum number of catalyst disks. The whole tray then can be moved from stage to stage. The efficiency at the impregnation stage should be improved to minimize losses. Other ideas for integrating the process could be grabbed from bench-marking against processes of current extrudate manufacturers.

VI.2.3 Customizing Process to Fit Available Hardware

As described under catalyst preparation section in Chapter II, the current process incorporates calcination at 400^0C for about 4 hours. However the existing equipment that Intramicron® has possession of is convective ovens that can heat only upto 300^0C. Hence catalysts were prepared at these conditions. Following figures show the comparison of catalyst activity with calcination temperature of 300^0C to the conventionally prepared catalyst. It can be observed that, the activity of the catalyst remains same.

VI.2.4 Alternate Carrier Material

The current fiber material used for making MiniCOT is nickel. This can be replaced with polymer, a material which is a much cheaper option. Following sets of experiments should be performed in order to test the suitability of polymer materials for this application.

i. Preparing catalyst as powder:

Catalyst needs to be prepared in the powder form before entrapping it into polymer fibers as catalyst needs to pass through calcination process at 400^0C. Polymer fibers are temperature intolerant about $120 – 130^0$C.

ii. Testing catalyst activity for water tolerance:

The wet-lay process used for making catalyst carriers consists of preparing the material in deep water column. Hence catalyst activity tests need to be performed after dipping the catalyst in water and drying.

iii. Catalyst reduction at lower temperature:

The catalyst pre-reduction process needs to be performed at a temperature lower than 120^0C. If catalyst does not activate enough, sets (ii) could be repeated for pre-reduced catalyst.

VI.2.5 Integration of MiniCOT with Other Sorbents

As stated in various standards already, the canister should be capable of removing a lot of other contaminants viz., HCl, HCN, Propenal, NH_3, cyclohexane, phosgene etc. For example the requirements for EN 403 are listed in Table 6.1.

Table 6.1: Other gas requirements for EN403

Test Agent	Test gas Conc. In air (ppm)	Breakthrough Conc. (ppm)
Propenal (acrolein)	100	10.5
Hydrogen Chloride (HCl)	1000	5
Hydrogen Cyanide	400	10

All the gases listed in the table above could be removed using carbon sorbents. Universal Respirator Carbon (URC) entrapped in polymer microfibrous materials can be a good candidate material for Propenal, HCl and HCN removal.

A layer of this material can be placed up-front of MiniCOT to remove these contaminants. Some of the ageing studies have already been performed (reported in Technology transfer Chapter) in presence of URC. More extensive tests could be performed in this direction to make an integrated microfibrous canister.

VI.2.6 Packaging

The packaging issues need to be resolved as these materials may not be used for few years and they should still be active. The shelf-life for existing commercial canisters is about seven years. MiniCOT in integrated fashion should be able to offer a similar shelf-life.

VI.2.7 Computational fluid dynamic and residence time distribution studies in microfibrous beds

As described in chapter 3, the activity of the catalyst observed in microfibrous configuration is much higher compared to packed bed configuration for the same particle size. This needs to be studied further to explain the behavior. Computational fluid dynamic studies and residence time distribution studies can be useful tools to explain this. A simple tracer study where the inlet tracer is a delta function and monitoring the outlet tracer concentration as a function of time can throw some light on flow patterns within micro-fibrous bed. This phenomenon can also be modeled using models, such as

dispersion model to further explain the behavior. Simple heat transfer experiments can also be performed to compare rates of heat transfer of different geometries.

VI.2.8 Heat Transfer Experiments

Simple heat transfer experiments can be performed to monitor the radial rise of temperature inside a microfibrous bed. At time t = 0, increase the temperature of the reactor wall to a higher value and then monitor the center temperature. A profile of temperature as a function of time and radius can be compared with that of packed bed to find out the difference between the rates of heat transfers. Same set of experiments can be performed for axial heat transfer. This phenomenon can also be modeled in terms of various resistances.

REFERENCES

[1.1]   S. Yoon, S. Macdonald, R. G. Parrish, *Journal of American Medical Association,* 279, 685-687(1998).

[1.2]   S. Katz, G. McCaa, A. Barth, *Bureau of Mines Bulletin* 14, 1924

[1.3]   D. Parker, G. McCaa, E. Denny, *Bureau of Mines Handbook,*139 (1923)

[1.4]   S.Katz, *Industrial and Engineering Chemistry* 6 555-557(1925)

[1.5]   EN 403, European Standards for Testing of Respiratory Protective Devices, EN 403: 1993

[1.6]   CBRN, NIOSH Standards 2003

[1.7]   ANSI/ISEA 110-2003 ANSI Standards 2003

[1.8]   A. Lamb, W. Bray, J. Frazer, *Ind. Eng .Chem.,* 12, 213-221 (1920)

[1.9]   J. Almquist, W. Bray, *J. Am. Chem. Soc.,* 45 2305-2322 (1923)

[1.10]   A. Lamb, W. Vail, *J. Am. Chem. Soc*, 47 123 – 142 (1925)

[1.11]   J. Frazer, *Ind. Eng. Chem.,* 32 405-411 (1931)

[1.12]   M. Brittan, H, Bliss, C. Walker, *AIChE J.,* 16(2), 305-314 (1970)

[1.13]   S. Veprek, D. Cocke, S. Kehl, H. Oswald *J. Catal.,* 100 250-263 (1986)

[1.14]   T. Rogers, C. Piggot, W. Bahlke, J. Jennings, *J. Am. Chem. Soc.,* 43(9) 1973-1982 (1921)

[1.15]   S. Imamura, H. Sawada, K. Uemura, S. Ishida, *J. Catal.,* 109, 198-205 (1988)

[1.16] J. Musick, F. Williams, *NRL Report 8353,* 1979

[1.17] G. Gürdag, T. Hahn, *App. Cat. A General,* 192 51-55 (2000)

[1.18] A. Benton, T. Williams, *J. Phys. Chem.,* 30, 1487-1496 (1926)

[1.19] C. Engelder, L. Miller, *J. Am. Chem. Soc,* 27, 1345-1353 (1927)

[1.20] M. Haruta, S. Tsubota, T. Kobayashi, H. Kageyama, M. Genet, B. Delmon, *J. Catal.*, 144, 175-192(1993)

[1.21] M Haruta, T Takase, T. Kobayashi, S Stubota, *Cat Sci Tech* Vol I, pg 331 (1991)

[1.22] T Kobayashi, M Haruta, H Sano, M Nakane, *Sensors and Actuators* 13, 339 (1988)

[1.23] N Funazaki, Y Asano, S Yamashita, T Kobayashi Haruta M, *Sensors and Actuators,* 13-14, 536 (1993)

[1.24] H Sato, E Tsuchida, *Trans. IEICE* E73 (9) 1525 (1990)

[1.25] A. Tripathi, N Gupta, U Chatterji, M Iyer, *Indian J. Technol.* 30 (2), 107 (1992)

[1.26] M. Haruta, N. Yamada, T. Kobayashi, S. Iijima, *J. Catal.,* 115, 301-309 (1989)

[1.27] J. Jia, J. Kondo, K. Domen, K. Tamatu, *J. Phys Chem, B* 105, 3017-3022 (2001)

[1.28] J. Grunwaldt, A. Baiker, *J. Phys Chem, B* 103, 1002-1012 (1999)

[1.29] J. Jansson, M. Skoglundh, E. Fridell, P. Thormahlen, *Topics in Catalysis* 16/17, (1-4), 385-389 (2001)

[1.30] C. Costello, M. Kung, H. Oh, Y. Wang, H. Kung, *App. Cat. A: General,* 232, 159-168 (2002)

[1.31] M. Date, Y. Ichihashi, T. Yamashita, A. Chiorino, F. Boccuzzii, M. Haruta, *Catal. Today,* 72, 89-94 (2002)

[1.32] S. Gardner, G. Hoflund, *Langmuir*, 7, 2135-2139 (1991)

[1.33] G Hoflund, S. Gardner, D. Schryer, B Upchurch, E Kielin, *React. Kinet. Catal. Letters,* 58(1), 19-26 (1996)

[1.34] G. Dong, J. Wang, Y. Gao, S. Chen, *Catalysis Letters,* 58, 37-41 (1999)

[1.35] E. Gulari, C. Guldur, S. Srivvanvit, S. Osuwan, *Applied Catalysis A: General* 182, 147-163 (1999)

[1.36] J. Lin, J. Chen, C. Hsiao, Y. Kang, B Wan, *Applied Catalysis B: Environmental* 36, 19-29 (2002)

[1.37] G. Hoflund, *Catalysis Letters* 31, 133-141 (1995)

[1.38] A. Toroncrona, M. Skoglundh, P. Thormahlen, E. Fridell, E. Jobson, *Appl. Catal. B.,* 14, 131(1997)

[1.39] P. Thormhalen, M. Skoglundh, E. Fridell, B. Andersson, *J. Catal.* 188, 300-310 (1999)

[1.40] Y. Mergler, A Aalst, J. delft, B. Nieuwenhuys, *Applied Catalysis B: Environmental* 10, 19-29 (1996)

[1.41] M. Fuller, M. Warwick, *J. Catal.,* 34, 445-453 (1974)

[1.42] S. Imamura, S. Yoshie, Y. One, *J. Catal.,* 115, 258-264 (1989)

[1.43] S.H. Oh, C. Eickel, *J. Catal.*, 112, 543-555 (1988)

[1.44] C. Satterfiend, *Heterogeneous Catalysis in Practice*, 1st, McGraw Hill Company, 1980

[1.45] J.R. Anderson, *Structure of Metallic Catalysts*, Academic, New York, 1975

[1.46] D. Cahela, B. Tatarchuk, *Catal. Today,* 69, 33-39 (2001)

[1.47] M. Meffert, Ph D Dissertation, Auburn Univeristy, Auburn, AL 1998

[1.48] C Marion, D Cahela, S Ahn, B Tatarchuk, *J Power Sources,* 47, 297-302 (1994)

[1.49] D Harris, D Cahela, B Tatarchuk, *Composites Part A,* 32, 1117-1126 (2001)

[1.50] D. Kohler, J Zabasjja, F. Rose, B Tatarchuk, *J Electrochem Soc* 137 (6), 1750-1757 (1990)

[1.51] E. Luna, B. Tatarchuk, *AIChE Annual Conference,* Austin TX, (2004)

[1.52] Y. Lu, B. Chang, B. Tatarchuk, *ASM International Conference,* Columbus OH, (2004)

[3.1]   R. Aris, *The mathematical Theory of Diffusion and Reaction in Permeable Catalysis,* Clarendon, Oxford, (1975)

[3.2]   S. Elnashaie, J. Yates, *Chem. Eng. Sci.,* 28, 515 (1973)

[3.3]   T. Matsuura, M. Kato, *Chem. Eng. Sci.,* 11, 171(1967)

[3.4]   M. G. Slinko, M. M. Slinko, *Catal. Rev. – Sci. Eng.,* 17, 119 (1978)

[3.5]   M.P. Harold, D. Luss, *Ind. Eng. Chem. Res.* 26, 2099-2106 (1987)

[3.6]   R.K. Herz, S.P. Marin, *J. Catal.,* 65, 281 (1980)

[3.7]   M. Harold, M. Garske, *J. Catal., 2*7, 524 (1991)

[3.8]   V. Zhdanov, B. Kasemo, *J. Catal.*, 220(2) 478-485 (2003)

[3.9]   R. Jaree, H. Hudgins, P. Budman, V. Silveston, M. Menzinger, *Ind. Eng. Chem. Res.,* 42 1662 (2003)

[3.10] V. Bykov, G. Yablonskii, V. Elokhin, *Surf. Sci.*, 107(1), L334-L338 (1981)

[3.11] L. Abramova, S. Baranov, .A. Dulov, *Kinetics and Catalysis* 44(6), 862-864 (2003)

[3.12] D. Haaland, F. Williams, *J. Catal.*, 76, 450 (1982)

[3.13] A. Salanov, V. Savchenko,*Kinetics and Catalysis* 26(5), 1136-1142 (1985)

[3.14] G. Lavin, W. Jackson, *J. Am. Chem. Soc.,* 53, 383-384 (1931)

[3.15] K. Allers, H. Pfnur, P. Feulner, D. Menzel, *J. Chem. Phys.,* 100(5), 3985 (1994)

[3.16] J. Bergeld, B. Kasemo, D. Chakarov, *Surface Science,* 495, L815-L820 (2001)

[3.17] X. Gong, P. Hu, R. Raval, *J. Chem. Phys.,* 119(12), 6324-6334 (2003)

[3.18] R. Lagos, T. Simoes, A. Godoy, *Physica A,* 257, 401-407 (1998)

[3.19] E. McCarthy, J. Zahradnik, G. Kuckzynski, J. Carberry, *J. Catal.,* 39, 29-35 (1975)

[3.20] J. Turner, B. Sales, M. Maple, *Surface Science,* 109(3), 591-604 (1981)

[3.21] N. Collins, S. Sundaresan, Y. Chabal, *Surface Science,* 180(1), 136-152 (1987)

[3.22] S. Ladas, R. Imbihl, G. Ertl, *Surface Sci.,* 197, 153 (1988)

[3.23] P. Tsai, M. Maple, R. Herz, *J. Catal.,* 113, 453-465 (1988)

[3.24] R. Imbihl, S. Ladas, R. Ertl, *Surface Sci.,* 215, L307-L315 (1989)

[4.1] Personal Communication, Dr. Lars Ronner, Sundstrom Corp., (lars.ronner@srsafety.se)

APPENDICES

Appendix A: QRAE® datalog sample

1. Screen shot of ProRAE suite®

2. Above File in the text format:

```
Instrument: QRAE+ (PGM2000)                          Serial Number:
408301
User ID: 00000001              Site ID: 00000001
Data Points: 47               Data Type: Avg          Sample Period: 60
sec
Last Calibration Time: 10/25/2004 11:14
========================================================================
=============
Gas Type:                       CO(ppm)     H2S(ppm)      OXY(%)
NONE
High Alarm Levels:               1500.0        250.0       -----      -
----
Low Alarm Levels:                1435.0        200.0       -----      -
----
========================================================================
=============
Line#         Date   Time       CO(ppm)     H2S(ppm)      OXY(%)
NONE
```

```
==========================================================================
============
   1  03/08/2005 14:59          38.9          0.0       -----        -
----
   2  03/08/2005 15:00           2.2          0.0       -----        -
----
   3  03/08/2005 15:01           0.6          0.0       -----        -
----
   4  03/08/2005 15:02           0.3          0.0       -----        -
----
   5  03/08/2005 15:03           0.2          0.0       -----        -
----
   6  03/08/2005 15:04           0.1          0.0       -----        -
----
   7  03/08/2005 15:05           0.1          0.0       -----        -
----
   8  03/08/2005 15:06           0.0          0.0       -----        -
----
   9  03/08/2005 15:07           0.0          0.0       -----        -
----
  10  03/08/2005 15:08           0.0          0.0       -----        -
----
  11  03/08/2005 15:09           0.0          0.0       -----        -
----
  12  03/08/2005 15:10           0.0          0.0       -----        -
----
  13  03/08/2005 15:11           0.0          0.0       -----        -
----
  14  03/08/2005 15:12           0.0          0.0       -----        -
----
  15  03/08/2005 15:13           0.0          0.0       -----        -
----
  16  03/08/2005 15:14           0.0          0.0       -----        -
----
  17  03/08/2005 15:15           0.0          0.0       -----        -
----
  18  03/08/2005 15:16           0.0          0.0       -----        -
----
  19  03/08/2005 15:17           0.0          0.0       -----        -
----
  20  03/08/2005 15:18           0.0          0.0       -----        -
----
  21  03/08/2005 15:19           0.0          0.0       -----        -
----
  22  03/08/2005 15:20           0.0          0.0       -----        -
----
  23  03/08/2005 15:21           0.0          0.0       -----        -
----
  24  03/08/2005 15:22           0.0          0.0       -----        -
----
  25  03/08/2005 15:23           0.0          0.0       -----        -
----
  26  03/08/2005 15:24           0.0          0.0       -----        -
----
```

27	03/08/2005 15:25	0.0	0.0	-----	- ----
28	03/08/2005 15:26	0.0	0.0	-----	- ----
29	03/08/2005 15:27	0.0	0.0	-----	- ----
30	03/08/2005 15:28	0.0	0.0	-----	- ----
31	03/08/2005 15:29	0.0	0.0	-----	- ----
32	03/08/2005 15:30	0.0	0.0	-----	- ----
33	03/08/2005 15:31	0.0	0.0	-----	- ----
34	03/08/2005 15:32	0.0	0.0	-----	- ----
35	03/08/2005 15:33	0.0	0.0	-----	- ----
36	03/08/2005 15:34	0.0	0.0	-----	- ----
37	03/08/2005 15:35	0.0	0.0	-----	- ----
38	03/08/2005 15:36	0.0	0.0	-----	- ----
39	03/08/2005 15:37	0.0	0.0	-----	- ----
40	03/08/2005 15:38	0.0	0.0	-----	- ----
41	03/08/2005 15:39	0.0	0.0	-----	- ----
42	03/08/2005 15:40	0.0	0.0	-----	- ----
43	03/08/2005 15:41	0.0	0.0	-----	- ----
44	03/08/2005 15:42	0.0	0.0	-----	- ----
45	03/08/2005 15:43	0.0	0.0	-----	- ----
46	03/08/2005 15:44	0.0	0.0	-----	- ----
47	03/08/2005 15:45	0.2	0.0	-----	- ----

3. Data Exported to MS Excel®:

Instrument: QRAE+ (PGM2000)   Serial Number: 408301
User ID: 00000001   Site ID: 00000001
Data Points: 47   Data Type: Avg   Sample Period: 60 sec
Last Calibration Time: 10/25/2004 11:14
===
==
Gas Type: CO(ppm)
                                                               H2S(ppm)
High Alarm Levels: 1500   250
Low Alarm Levels: 1435   200
===
==

Line#	Date	Time	CO(ppm)	Alarm	H2S(ppm)	Alarm

===
==

Line#	Date	Time	CO(ppm)	Alarm	H2S(ppm)	Alarm
1	3/8/2005	14:59	38.9		0	
2	3/8/2005	15:00	2.2		0	
3	3/8/2005	15:01	0.6		0	
4	3/8/2005	15:02	0.3		0	
5	3/8/2005	15:03	0.2		0	
6	3/8/2005	15:04	0.1		0	
7	3/8/2005	15:05	0.1		0	
8	3/8/2005	15:06	0		0	
9	3/8/2005	15:07	0		0	
10	3/8/2005	15:08	0		0	
11	3/8/2005	15:09	0		0	
12	3/8/2005	15:10	0		0	
13	3/8/2005	15:11	0		0	
14	3/8/2005	15:12	0		0	
15	3/8/2005	15:13	0		0	
16	3/8/2005	15:14	0		0	
17	3/8/2005	15:15	0		0	
18	3/8/2005	15:16	0		0	
19	3/8/2005	15:17	0		0	
20	3/8/2005	15:18	0		0	
21	3/8/2005	15:19	0		0	
22	3/8/2005	15:20	0		0	
23	3/8/2005	15:21	0		0	
24	3/8/2005	15:22	0		0	
25	3/8/2005	15:23	0		0	
26	3/8/2005	15:24	0		0	
27	3/8/2005	15:25	0		0	
28	3/8/2005	15:26	0		0	
29	3/8/2005	15:27	0		0	
30	3/8/2005	15:28	0		0	
31	3/8/2005	15:29	0		0	
32	3/8/2005	15:30	0		0	

33	3/8/2005 15:31	0	0
34	3/8/2005 15:32	0	0
35	3/8/2005 15:33	0	0
36	3/8/2005 15:34	0	0
37	3/8/2005 15:35	0	0
38	3/8/2005 15:36	0	0
39	3/8/2005 15:37	0	0
40	3/8/2005 15:38	0	0
41	3/8/2005 15:39	0	0
42	3/8/2005 15:40	0	0
43	3/8/2005 15:41	0	0
44	3/8/2005 15:42	0	0
45	3/8/2005 15:43	0	0
46	3/8/2005 15:44	0	0
47	3/8/2005 15:45	0.2	0

Appendix B

Results of Tests Performed according to Various Proposed Standards

Catalyst testing for CBRN General and Specific Category:

Following are the different test condition for CBRN general and specific category.

-     Inlet CO Concentration: 3600 ppm (General), 6000 ppm (Specific)

-     Outlet CO Concentration: $\leq$ 500 ppm (time weighted average

    over 5 minutes, c*t = 2013 ppm.min)

-     Relative Humidity: 89 – 95%

-     Temperature: $25 \pm 2.5\ ^0C$ & $0 \pm 2.5\ ^0C$

-     Inlet Flow Rate: 64 ± 10 LPM

-     Time: 15, 30, 45 and/or 60 minutes

-     Pressure Drop: $\leq$ 70 mm of H_2O (Entire canister)

Service Life Testing

-     100 ± 10 LPM inlet flow rate , 5 minutes minimum lifetime at $25 \pm 2.5\ ^0C$ (Other

    conditions same as above)

Inspired Air Temperature Test:

-     Inlet CO Conc. = 1200 ppm

-     Flow Rate = 40 LPM

-     Outlet Conc. < 10 ppm

-     Temperature Measured at face-piece $< 46^0C$ (Dry Bulb)
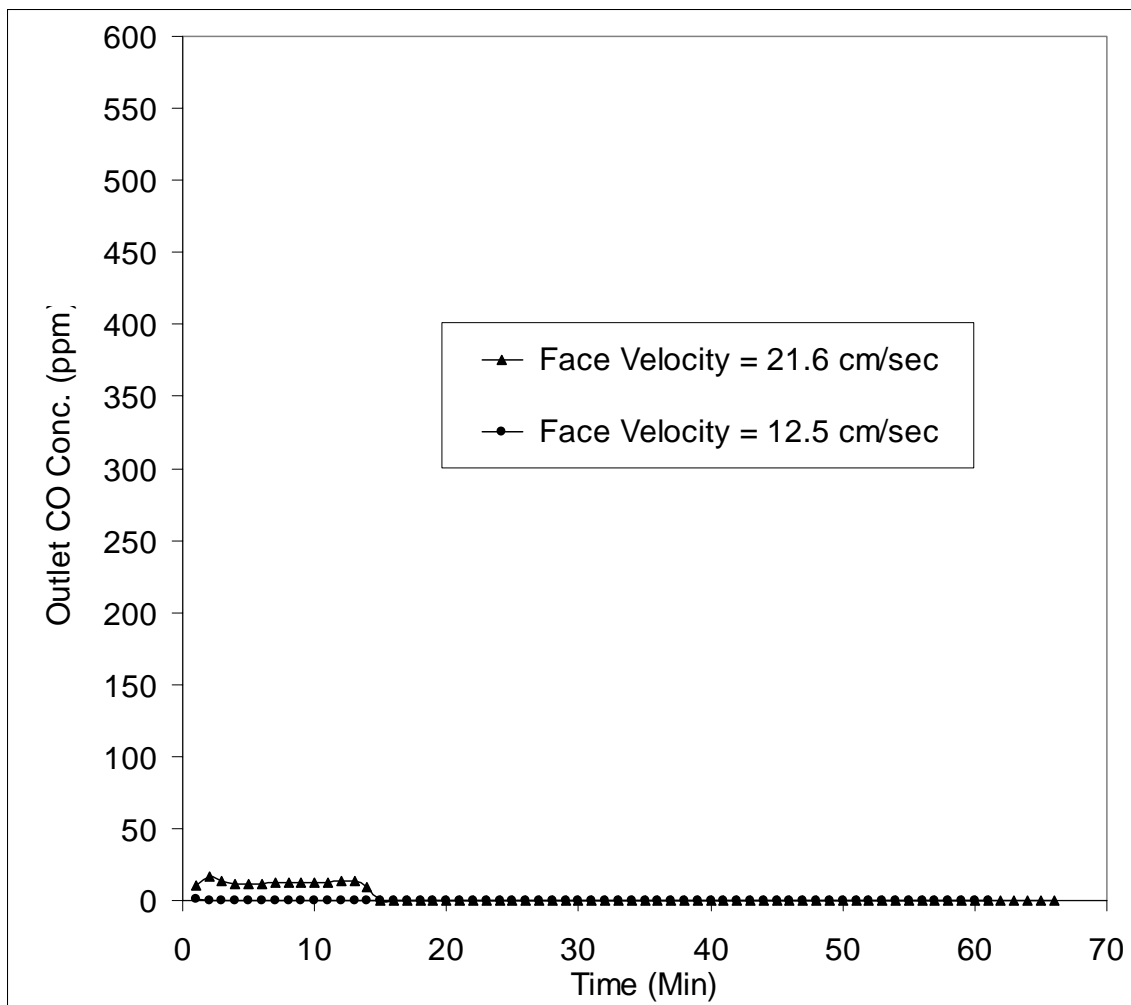
Figure A3.1: Catalyst testing for CBRN general category

Test Conditions:

Inlet CO Concentration=   3600 ppm

Bed Depth=   4 mm
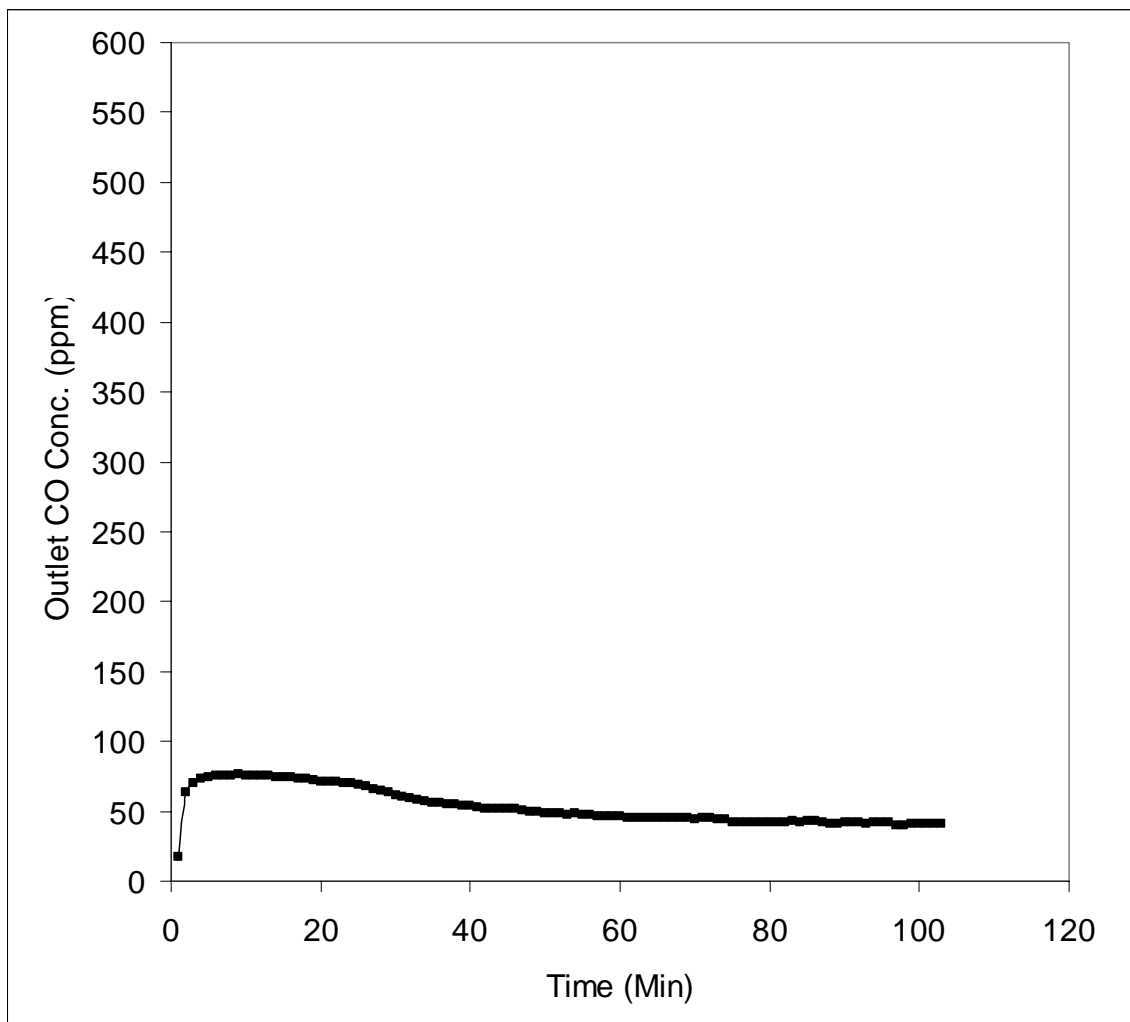
Relative humidity=   90%

Temperature= 22^0C

Figure A3.2: Catalyst testing for CBRN general category at 0^0C

Test Conditions:

Inlet CO Concentration=   3600 ppm

Bed Depth=   6 mm

Relative humidity=   90%

Temperature= 0^0C

Face velocity=   12.5 cm/sec
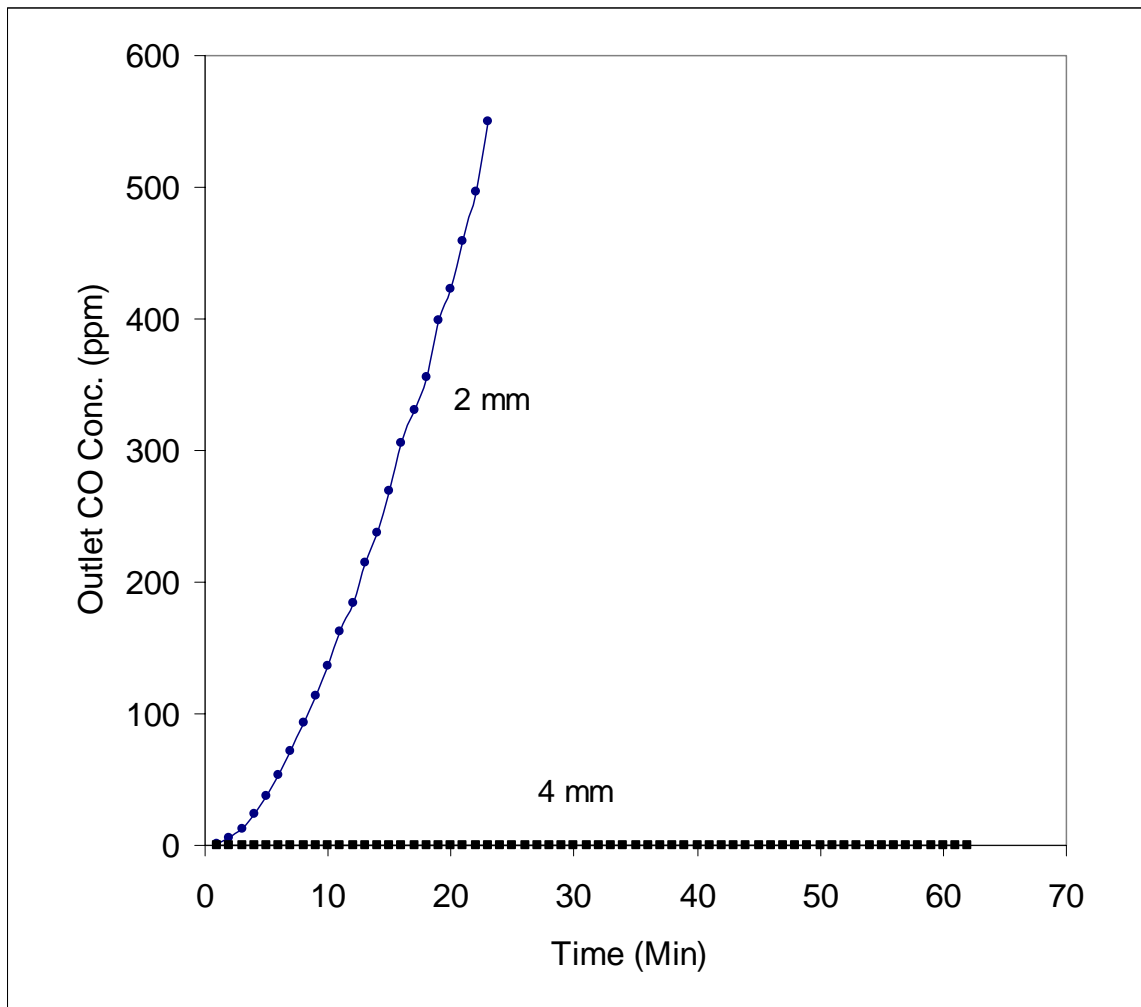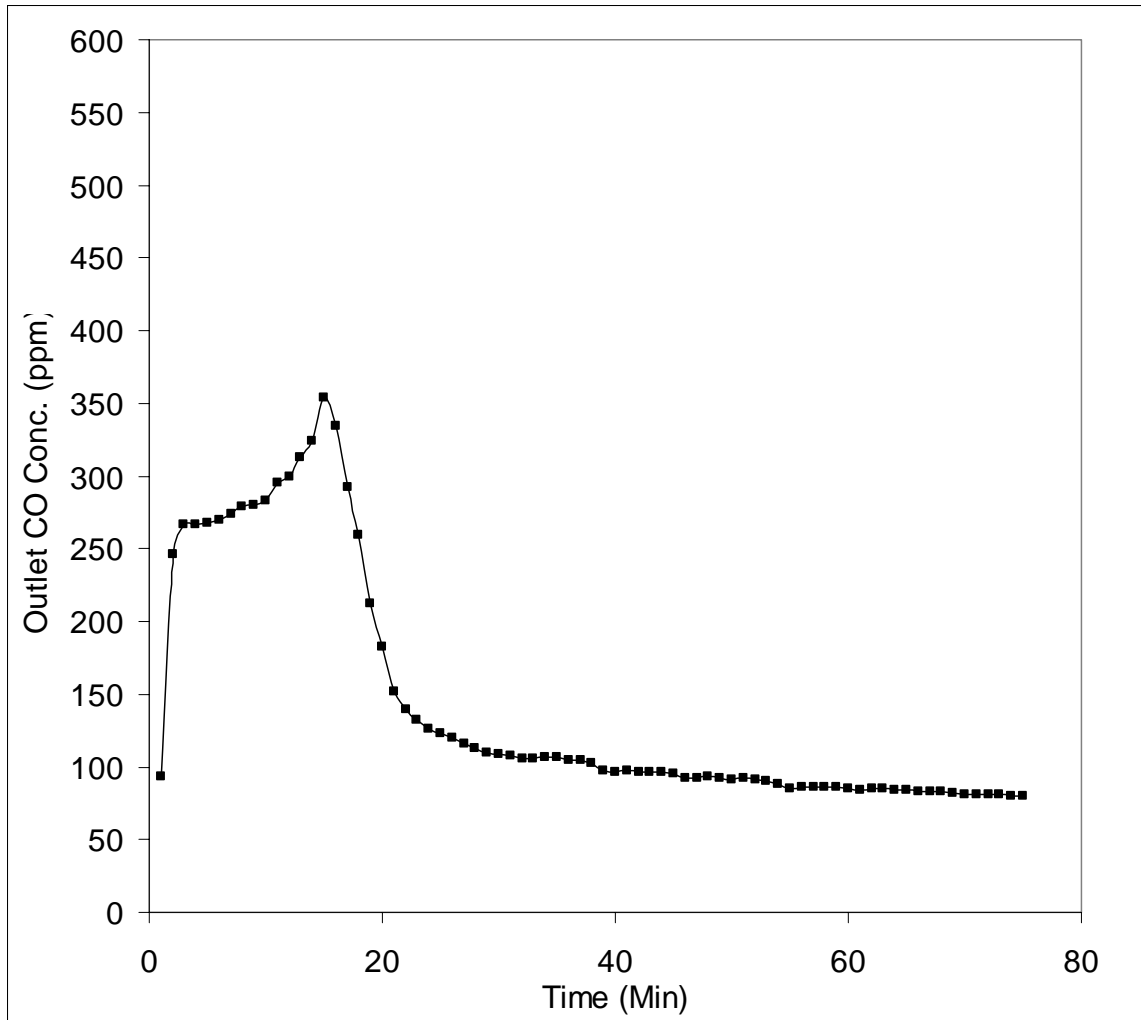
**CBRN Specific Category:**

Figure A3.3: Catalyst testing for CBRN specific category at 22^0C

Test Conditions:

Inlet CO Concentration=   6000 ppm

Relative humidity=   90%

Temperature= 22^0C

Face Velocity=   12.5 cm/sec

Figure A3.4: CBRN Specific Category at 0^0C

Test Conditions:

Inlet CO Concentration=   3600 ppm

Bed Depth=   6 mm

Relative humidity=   90%

Temperature= 0^0C

Face velocity=   12.5 cm/sec

Inspired Air Temperature Test:
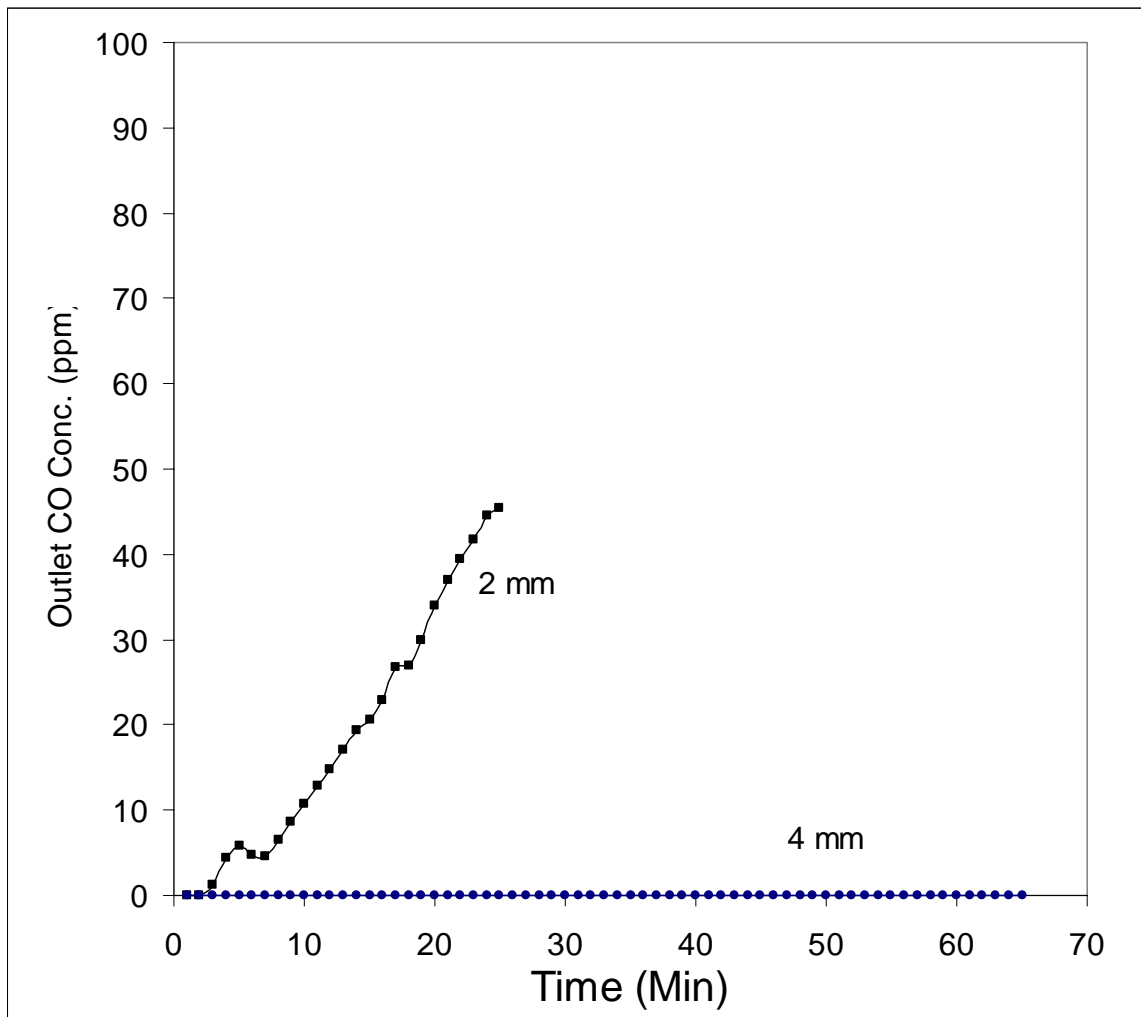
Figure A3.5: CBRN general and specific inspired air temperature test

Test Conditions:

Inlet CO Concentration=   1200 ppm

Relative humidity=   90%

Temperature= 22^0C

Face velocity=   7.8 cm/sec

ANSI 110-2003 # 6 and #7 tests:

- Inlet CO Concentration: 3000 ± 90 ppm (#6), 5000 ± 150 ppm (#7)

- Outlet CO Concentration   ≤200 ppm

- Relative Humidity: 87 ± 3%

- Temperature: 27 ± 2 0C (#6 & #7), 0 ± 2 0C (#7)

- Inlet Flow Rate: 100 ± 0.5 LPM

- Time: 15 minutes
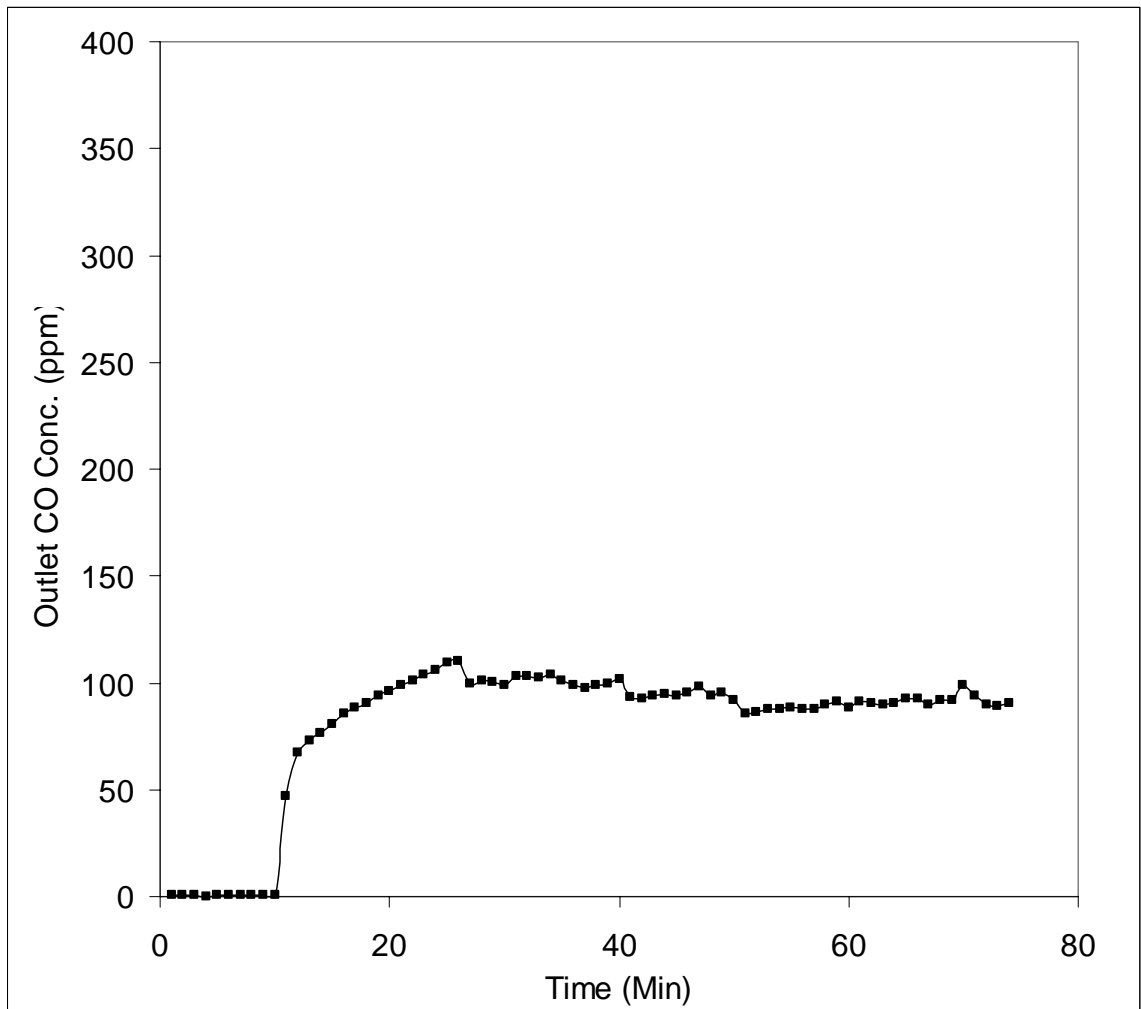
Figure A3.6: catalyst testing for ANSI #6

Test Conditions:

Inlet CO Concentration=   3000 ppm

Bed depth=   4 mm

Relative humidity=   90%

Temperature= 22^0C

Face velocity=   19.5 cm/sec

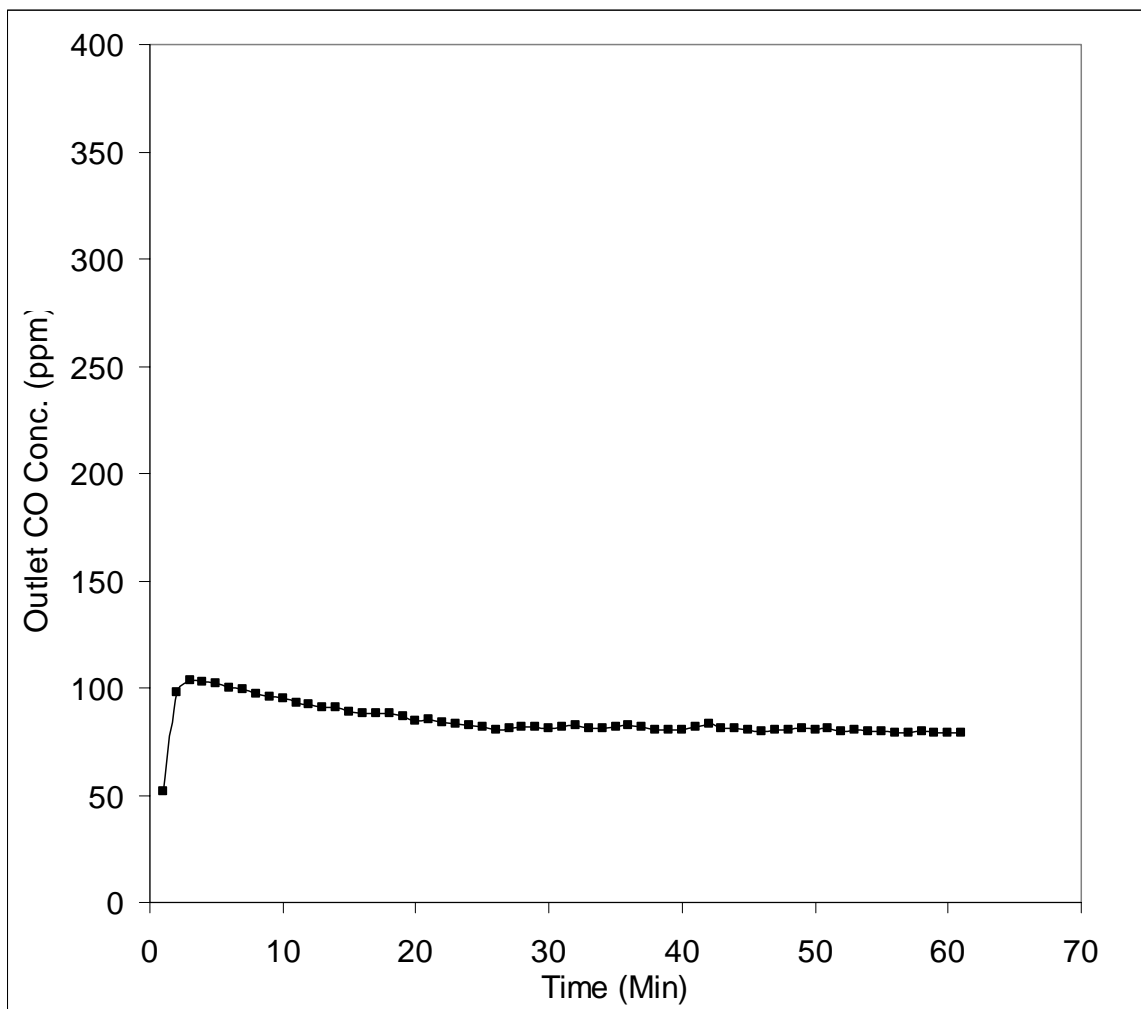Figure A3.7: Test for ANSI #7

Test Conditions:

Inlet CO Concentration=   5150 ppm

Bed depth=   6 mm

Relative humidity=   90%

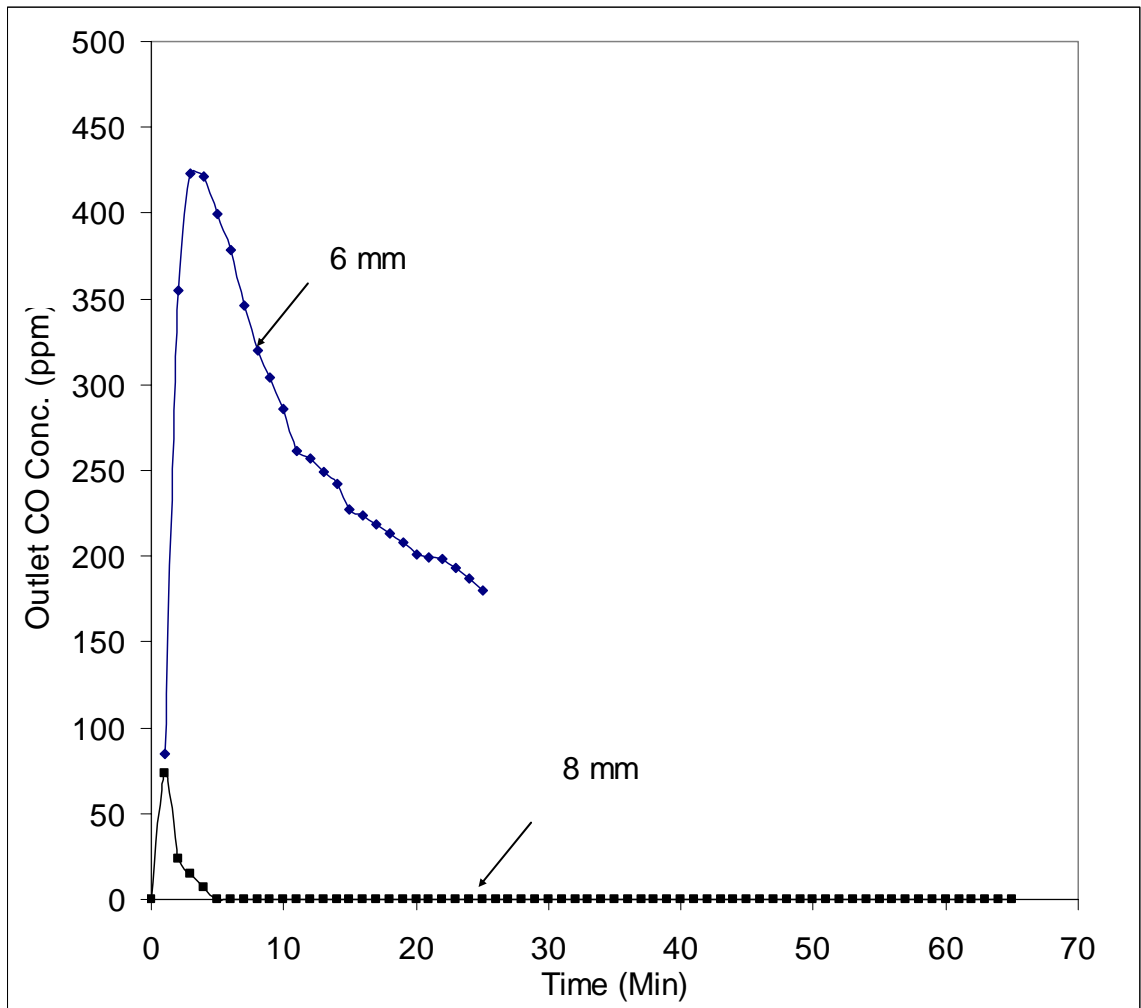Temperature= 22^0C

Face velocity=   19.5 cm/sec

Figure A3.8: Test for ANSI #7 at 0^0C

Test Conditions:

Inlet CO Concentration=   3600 ppm

Relative humidity=   90%

Temperature= 0^0C

Face velocity=   19.5 cm/sec

Experimental Results with Heat Capacity added upstream of the Bed:

Some key tests were repeated with 2 cm bed of carbon 12X30 particles upstream of the
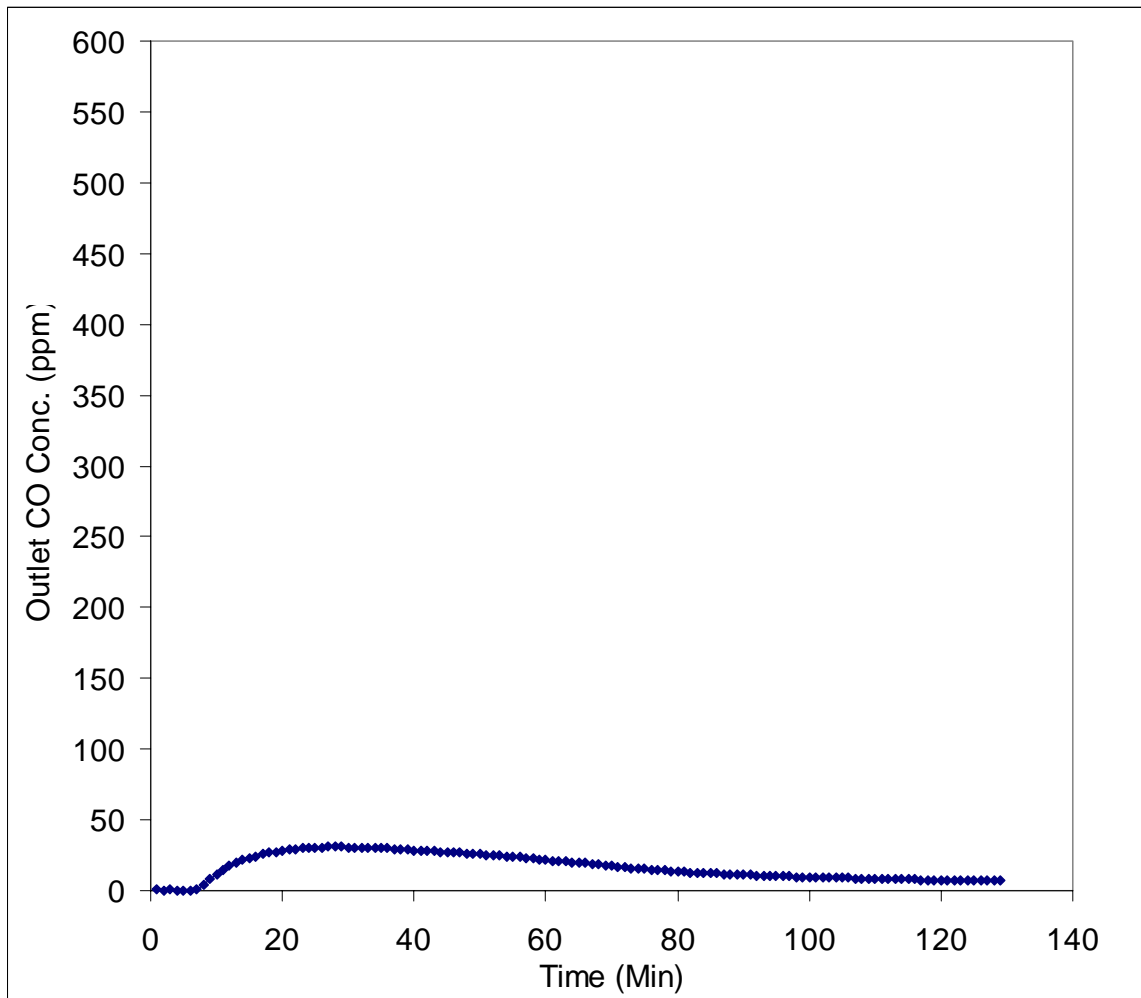
microfibrous entrapped CO oxidation catalyst.

Figure A3.9: CBRN general category at 0^0C

Test Conditions:

Inlet CO Concentration=   3600 ppm

Bed depth=   4 mm

Relative humidity=   90%

Temperature= 0^0C

Face velocity=   12.5 cm/sec

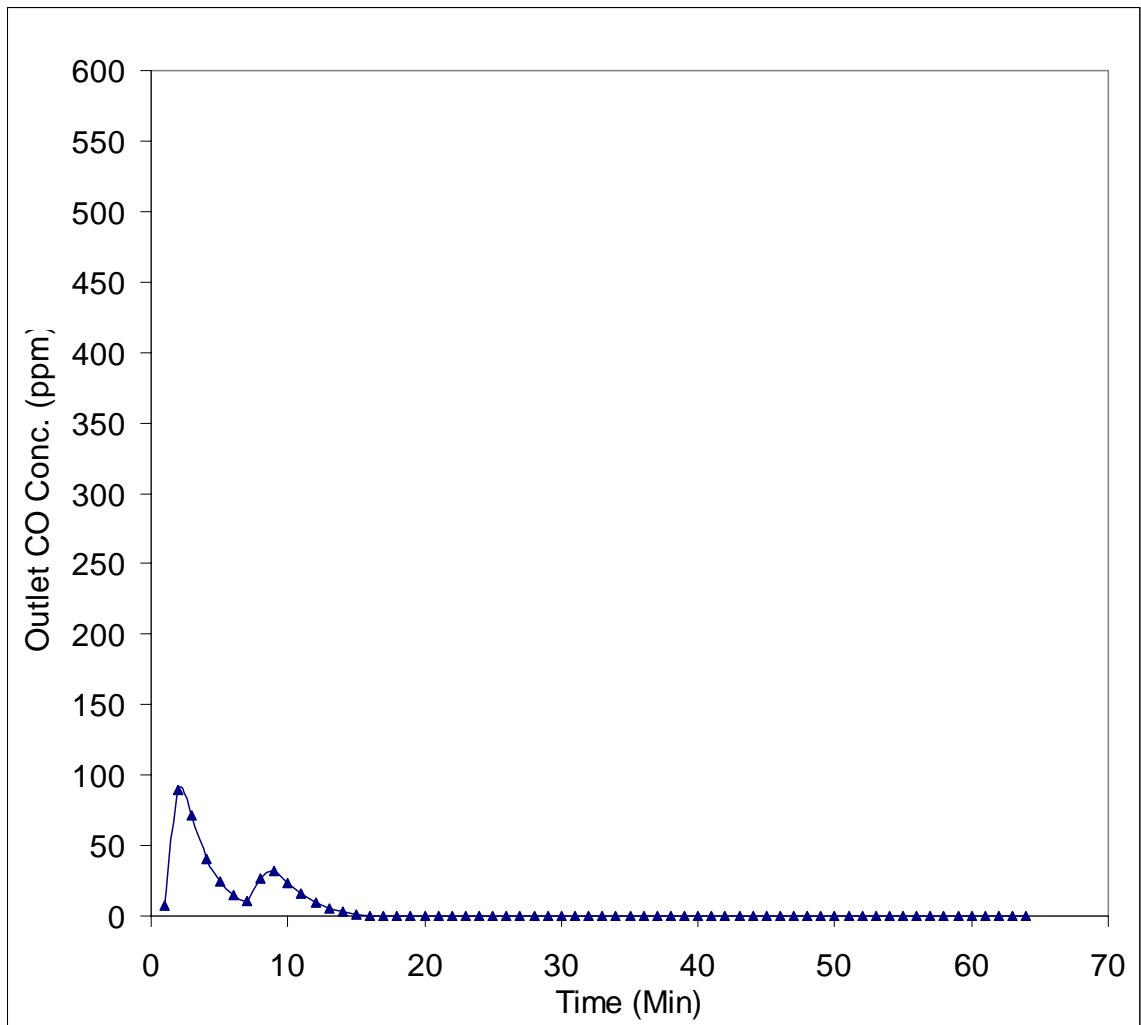

Figure A3.10: CBRN specific category

Test Conditions:

Inlet CO Concentration=   6000 ppm

Bed depth=   6 mm

Relative humidity=   90%

Temperature= 0^0C
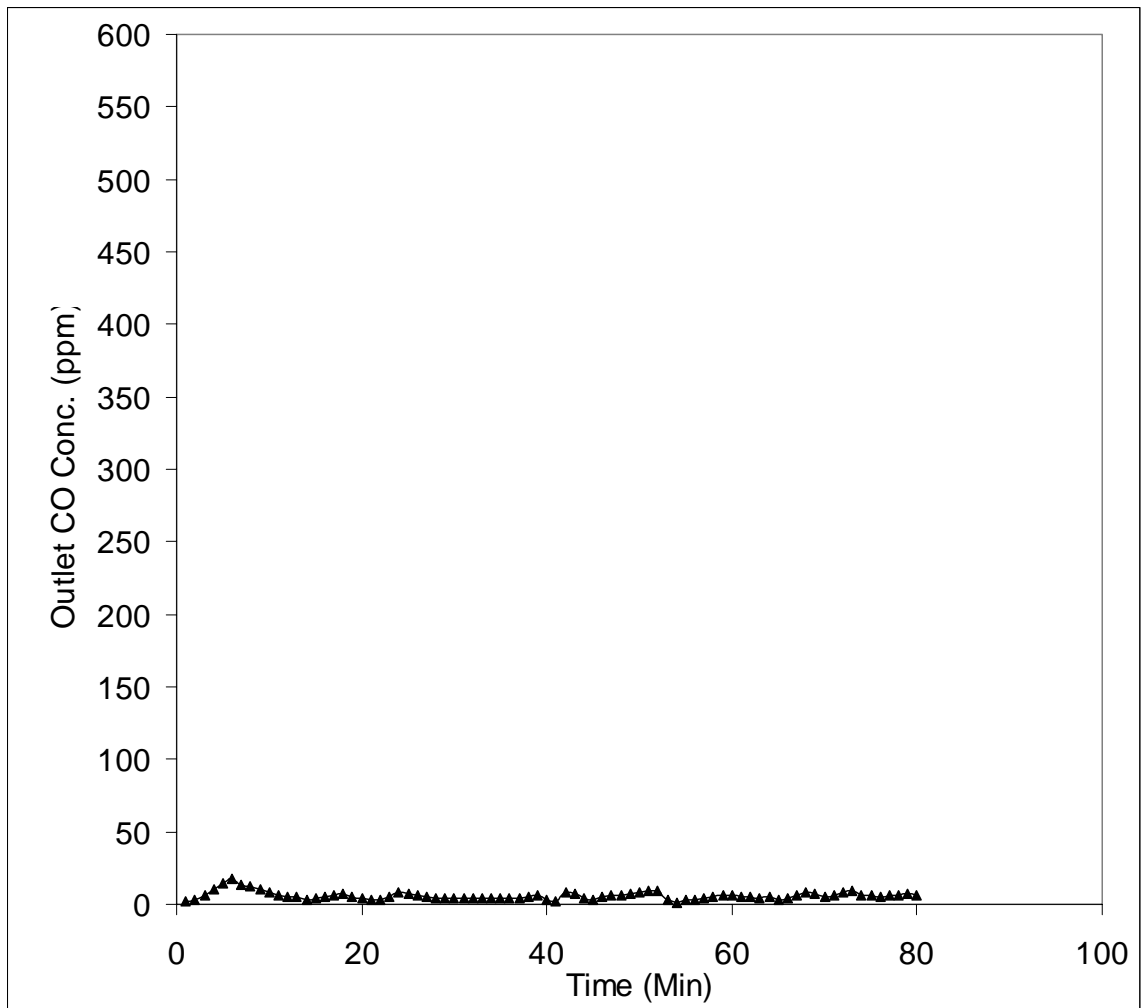
Face velocity=   21.5 cm/sec

Figure A3.11: CBRN General Category

Test Conditions:

Inlet CO Concentration=   3600 ppm

Bed depth=   4 mm

Relative humidity=   90%

Temperature= 22^0C

Face velocity=   12.5 cm/sec
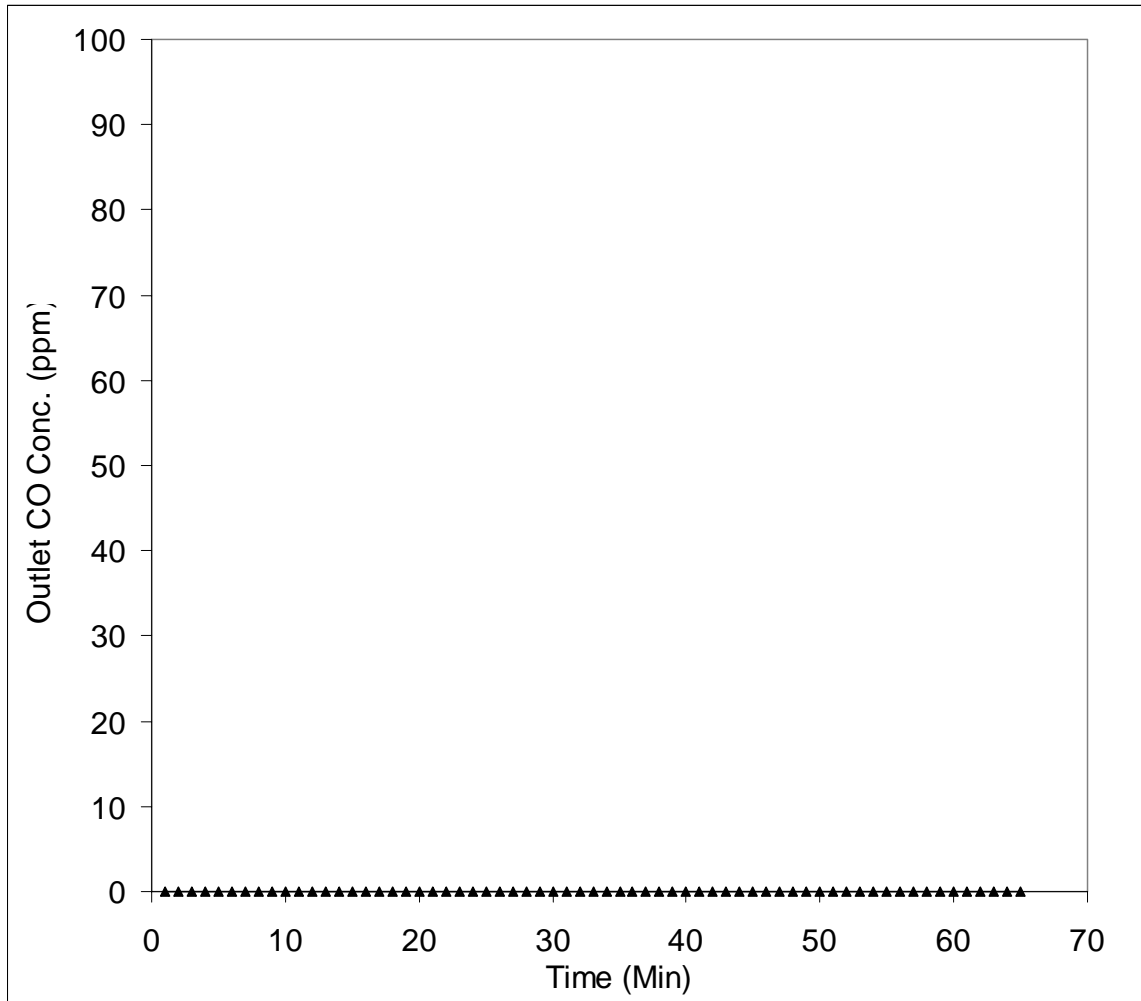
Figure A3.12: Inspired air temperature test with packed bed of sorbents

Test Conditions:

Inlet CO Concentration=   1200 ppm

Bed depth=   4 mm

Relative humidity=   90%

Temperature= 22^0C

Face velocity=   7.8cm/sec

Appendix C

## Adiabatic Flame Temperature Calculation

Definition:

When an exothermic reaction is carried out in adiabatic mode, all the heat generated in the reaction goes to raise the temperature inside the reactor. This temperature is referred to as, adiabatic flame temperature.

Adiabatic flame temperature of a reaction can be evaluated by solving following equation:

$$\sum_{out} n_i H_i(T_{ad}) = -n_f \Delta H_R + \sum_{in} n_i H_i(T_{feed}) \quad \ldots\ldots\ldots\ldots (0)$$

Reaction:

$CO + 0.5O_2 \rightarrow CO_2$
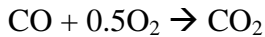
$$\Delta H_R = -282 \ \text{kJ/mol} \quad \ldots\ldots\ldots\ldots\ldots\ldots\ldots\ldots (1)$$

Sample Calculation:

Inlet CO Concentration = 3600 ppm

Basis:

Inlet CO Conc =   1 mole

Inlet O_2 Conc =   19 moles

Inlet N_2 Conc =   258 moles

Tref =   298 K (same as feed temperature)

Heat in:

$$\Delta H_{in} = \sum m C_p(T_{in} - T_{ref}) \quad \ldots\ldots\ldots\ldots\ldots\ldots (2)$$

Heat Out:

$$\Delta H_{out} = \sum mC_p \left(T_{ad} - T_{ref} \right) \dots\dots\dots\dots\dots\dots\dots \text{ (3)}$$

Equations (1), (2) and (3) when substituted in equation (0), can be solved for Tad,

adiabatic flame temperature.

Heat capacities for various components of the reaction can be found in Perry's

Handbook.

$C_{pCO2} = 0.03611 + 4.233*10^{-5}*T_{ad}$

$C_{pO2} = 0.02910 + 1.158*10^{-5}*T_{ad}$

$C_{pN2} = 0.02900 + 0.2199*10^{-5}*T_{ad}$

Substituting these expressions in equations (2) and (3) and simplifying yields:

$T_{ad} = 332$ K

Appendix D

Preliminary Results from SEM/EDS

This section gives the Scanning Electron Microscope (SEM) and SEM/ Energy Dispersive Spectrometer (EDS) information of the microfiber composite catalyst. Figures 3.21 (a & b) and 3.22 (a & b) show the SEM images of the microfiber composite catalyst perform i.e. silica support material entrapped into the Microfibrous mesh. Figures 3.21 a & b are the SEM images of the perform after Wet lay and before sintering. Figures 3.22 a & b are the SEM images of the perform after sintering.

As shown in the figure 3.21 b, the silica particles are properly entrapped into the mesh of cellulose and nickel fibers. Figure 3.22 b, shows that the cellulose after pre-oxidation and sintering is removed from the mesh and only nickel fibers are left.
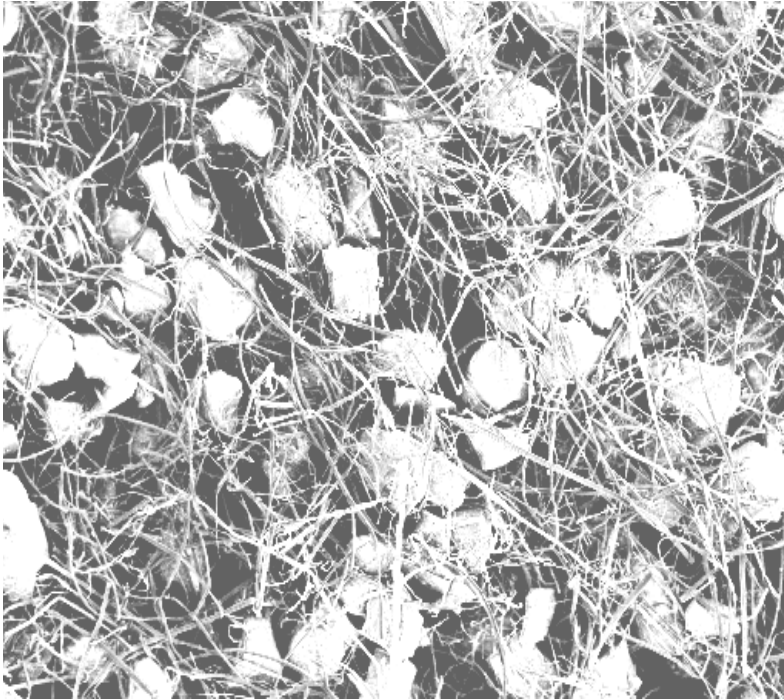
Figure 3.21 a: SEM image of microfiber entrapped Silica particles at magnification level

of 37 (before sintering).

8 µm Ni Fiber
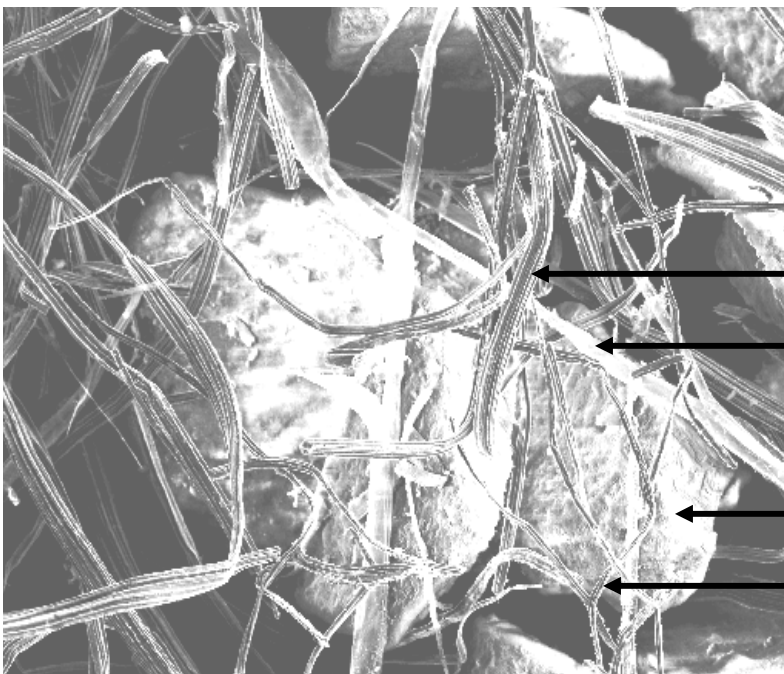
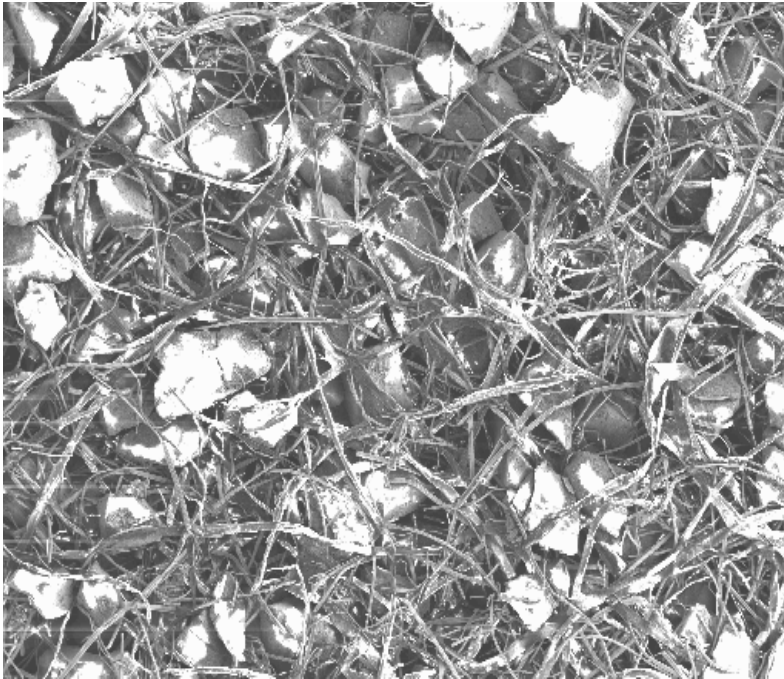Cellulose Fiber

Silica Particle

4 µm Ni Fiber

Figure 3.21 b: SEM image of microfiber entrapped Silica particles at magnification level of 200 (before sintering).

Figure 3.22 a: SEM image of microfiber entrapped Silica particles at magnification level of 37 (After sintering).
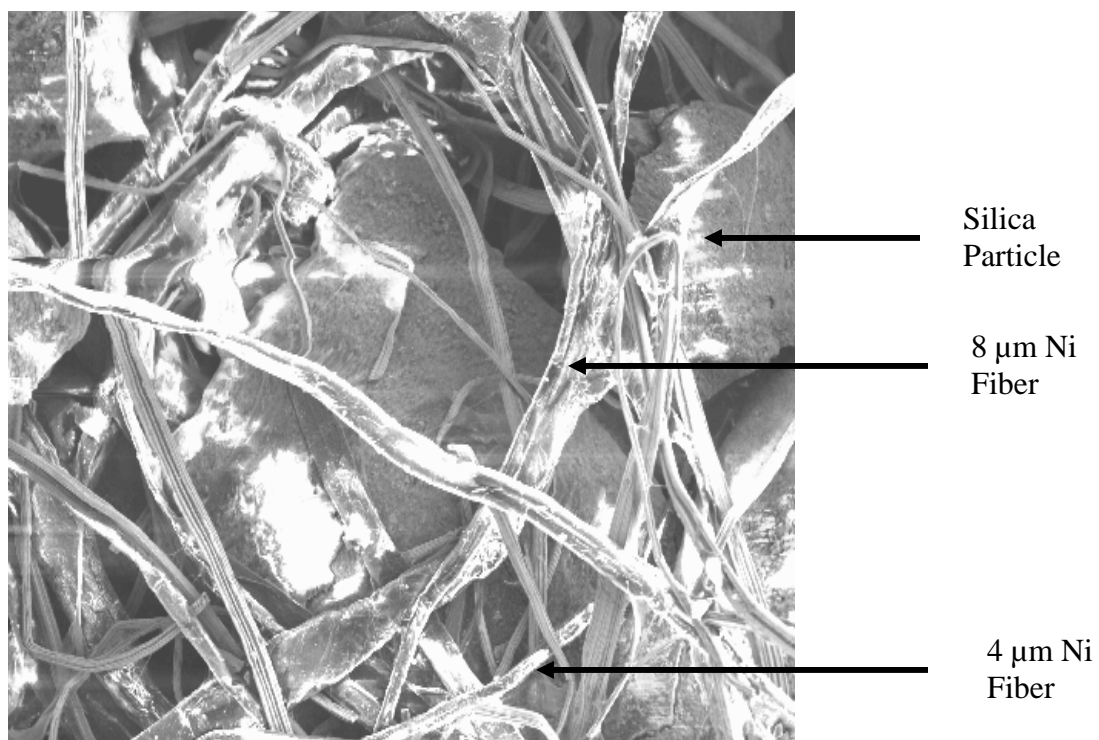
Silica
Particle

8 µm Ni
Fiber

4 µm Ni
Fiber

Figure 3.22 b: SEM image of microfiber entrapped Silica particles at magnification level

of 200 (after sintering).

SEM/EDS of the catalyst for quantification:
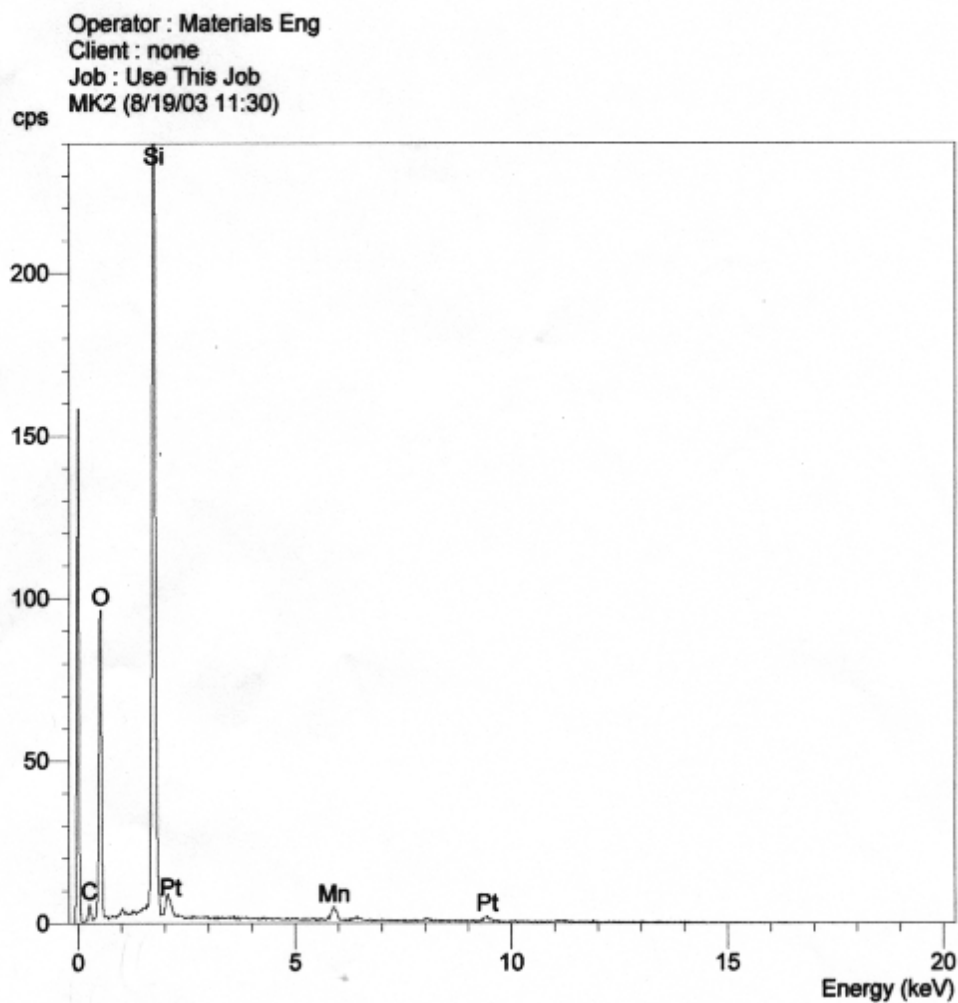
Figure 3.23 shows the EDS spectrum of Pt/Mn/SiO2 catalyst.

Figure 3.23: EDS spectrum of Pt/Mn/SiO$_2$ catalyst

As seen in figure, there is one peak corresponding to each element present in the catalyst. Based on the spectrum table 3.7 gives the quantification of various elements present in the catalyst.

Table 3.7: Quantification of Pt/Mn/SiO2 catalyst based on EDS spectrum:

Sr. No.	Element	Wt %	Atomic %
1	Si	34.45	24.73
2	O	58.73	74.02
3	Mn	2.07	0.76
4	Pt	4.74	0.49

The weight % of platinum shown by EDS is in good agreement with the calculated weight (5.1%). The atomic ratio of Mn:Si (0.03) is also in good agreement with the calculated atomic ratio (0.025).

Table 5-1. Quantification of Pt-Co/Al$_2$O$_3$ catalyst based on the EDS spectrum.

Sr. No.	Element	Wt %	Atomic %
1	Al	41.87	31.01
2	O	51.05	67.53
3	Co	3.02	1.04
4	Pt	4.06	0.42

The weight % of Pt obtained by EDS is in good agreement with the calculated weight (4.7wt%) during the incipient-wetness impregnation process. The atomic ratio of Co:Al (0.034:1) is also in good agreement with the calculated atomic ratio (0.04:1).
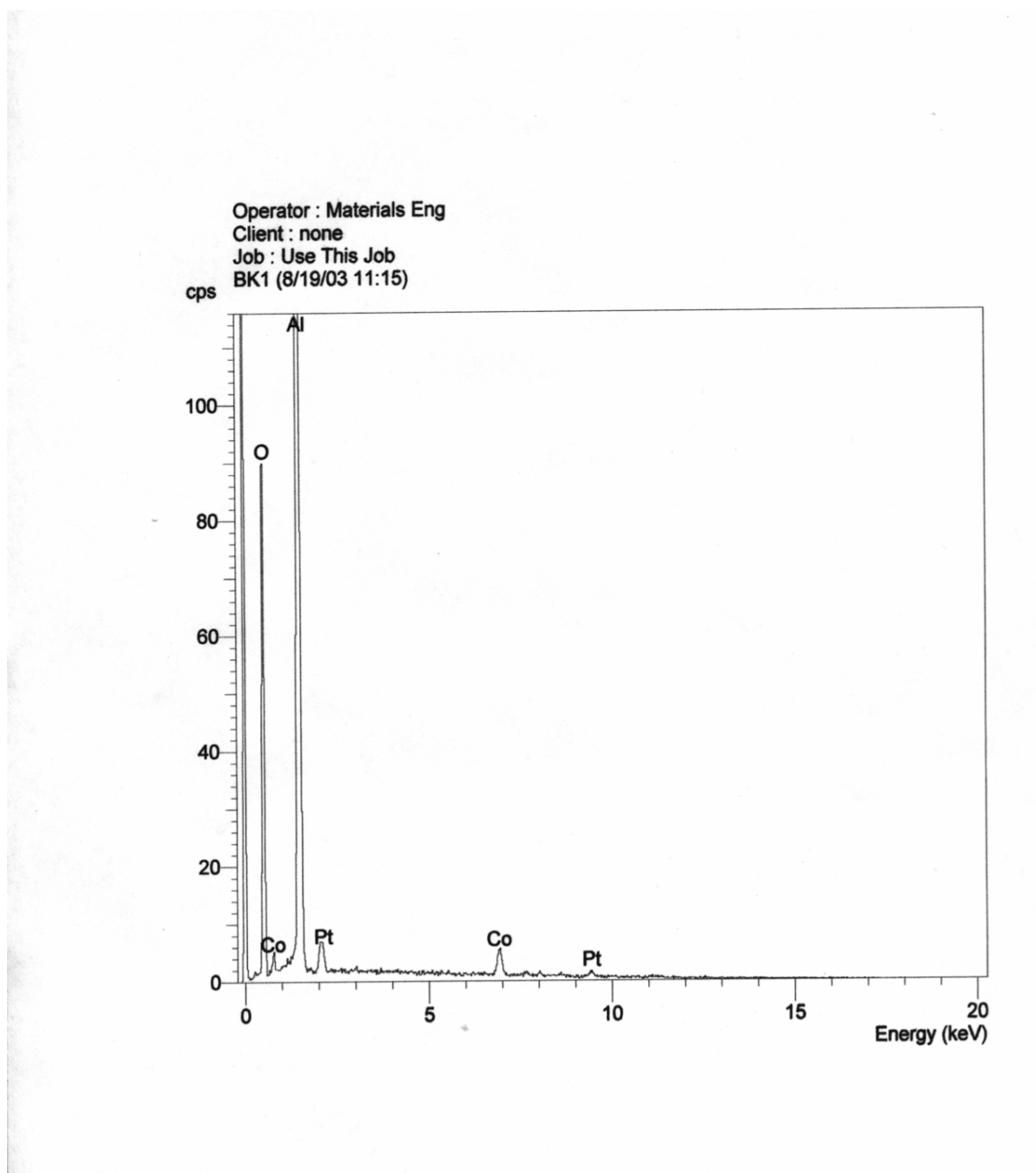

Figure 3.24: EDS spectrum of Pt/Co/Al$_2$O$_3$ catalyst